FLUOROCARBON POST-ETCH RESIDUE REMOVAL USING RADICAL ANION CHEMISTRY

A Thesis
Presented to the
Academic Faculty

by

Christopher L. Timmons

In Partial Fulfillment of the
Requirements of the degree
Doctor of Philosophy in Chemical Engineering

Georgia Institute of Technology
November 2004

FLUOROCARBON POST-ETCH RESIDUE REMOVAL USING RADICAL ANION CHEMISTRY

Approved:

Dr. Dennis Hess, Chairman
School of Biomolecular & Chemical Engineering
Georgia Institute of Technology

Dr. Carson Meredith
School of Biomolecular & Chemical Engineering
Georgia Institute of Technology

Dr. Paul Kohl
School of Biomolecular & Chemical Engineering
Georgia Institute of Technology

Dr. Joseph Schork
School of Biomolecular & Chemical Engineering
Georgia Institute of Technology

Dr. Charles Liotta
School of Biomolecular & Chemical Engineering
and School of Chemistry and Biochemistry
Georgia Institute of Technology

Date Approved:

November 22, 2004

ACKNOWLEDGEMENTS

I would like to gratefully acknowledge my thesis advisor, Professor Dennis Hess, for his guidance, enthusiasm and support during my studies. He has instilled in me an appreciation for science and creativity in research that I hope is reflected in this work.

I would also like to thank my committee members, Dr. Charles Liotta, Dr. Paul Kohl, Dr. Carson Meredith and Dr. Joseph Schork, for their insightful suggestions, feedback and critique of my work. The generous use of equipment and training provided by the research groups of Dr. Paul Kohl, Dr. Cliff Henderson, Dr. Lawrence Bottomley, Dr, Jiri Janata, Dr. Charles Eckert, and Dr. Jack Winnick were essential for my success throughout my research.

I wish to thank the current and past members of my research group for providing a stimulating and fun environment including Dr. Galit Levitin, Dr. Satya Myneni, Dr. Matthew Spuller, Dr. Jie Diao, Ingu Song, Gelareh Shakourian, Qian Luo, Sudeep Vaswani and Prabhakar Tamirisa. I am indebted to Galit and Satya for advice, technical discussions and support. I have enjoyed their close friendship. I also appreciate the numerous samples processed by Jie and Sudeep. I will miss the countless conversations where I learned about different backgrounds and cultures as well as learned much about myself.

I appreciate the friendship and support from the many friends I have made here; there are too many to list. I would especially like to thank Chris Moore and Cody Berger and their

families for helping me keep my sanity during this journey. Both were always selfless, honest and loyal and I could not ask for better friends. I also appreciate the friendships of Matt Spuller, Beckie Jones and Hollie Kelleher. I wish to thank my parents for their advice and support, both emotional and financial, throughout graduate school. They are responsible for the person I am today. I would also like to thank the MiRC and CHBE staff, especially Gloria Beale, Rod Sefton and Scott Fowler.

Finally, I would like to thank my wife, to whom I dedicate this accomplishment, for her never ending support, patience and motivation. I could not have done it without her.

Partial finanical support for this project was provided by Air Products and Chemicals, Inc. and the GAANN fellowship (provided through Professor Peter Hesketh).

TABLE OF CONTENTS

LIST OF TABLES

LIST OF FIGURES

CHAPTER 1

INTRODUCTION

1.1 Integrated Circuit Scaling

The monolithic solid state transistor has had a profound impact on technology of the second half of the 20th century. The solid state transistor, which is the building block of the integrated circuit (IC), can be found in nearly every facet of industrialized society. Examples of societal progress empowered by electronics include improvements in the following fields: medical diagnostics, prevention and treatment; manufacturing and automation; communication; education and safety. Of course, modern conveniences such as mobile phones, pocket computers and wireless devices are also based on integrated circuits. The transistor is essentially a voltage-controlled electrical switch, which replaced the need for the vacuum tube in electronics.

Several key discoveries were important to enable IC manufacturing as it is known today. Bardeen, Brattain and Shockley collaborated to invent the first solid state transistor using germanium, gold and plastic in 1947 at Bell Labs.[1,2] These discrete transistors initially competed with vacuum tubes as amplifiers in AM radios. An equally important invention was simultaneously made by Noyce of Fairchild semiconductor and Kilby of Texas Instruments in 1958 who fabricated and connected (integrated) multiple transistors on a single substrate. Integration dramatically reduced the size of circuits and enabled more complexity compared to those based on discrete components. Other important inventions

include the first transistor on silicon (Teal at Texas Instruments in 1954), the metal oxide semiconductor field effect transistor - MOSFET (Kahng at Bell Labs, 1960) and the planar transistor (Kilby at Fairchild and Noyce at Texas Instruments, 1959).

The ability to fabricate multiple transistors on a single substrate substantially lowered the cost of manufacturing and enabled more complex ICs. Integrated circuits were also more reliable and reproducible. Miniaturization of the transistor reduced manufacturing costs, enabled more capabilities and improved transistor speed. These benefits eventually lead to a dramatic rate of miniaturization of electronic devices and circuits beginning with widespread commercialization in the 1960s. The miniaturization of transistor dimensions has continued at an astounding pace. In 1965, Gordon Moore predicted that the number of transistors on an integrated circuit (IC) would double every 18 to 24 months.[3] For over 35 years, the exponential rate of increased transistor density on a chip has been realized and is likely to continue for at least another decade. Moore's prediction is compared with actual number of transistors on Intel processors in Figure 1.1.

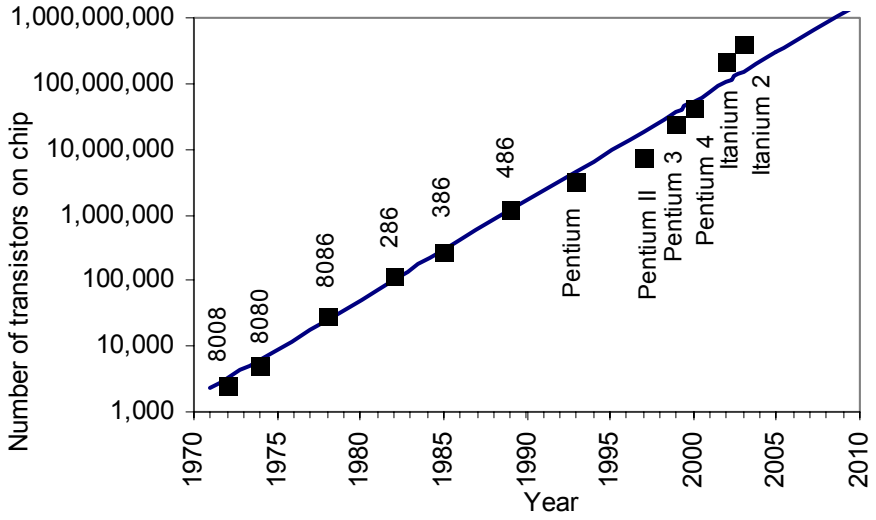

Figure 1.1. Number of transistors on Intel Processors and their year of introduction. The line represents a rate of doubling transistors per chip every 24 months.[4]

Transistor device speed inversely scales with feature size resulting in a corresponding exponential increase in computing power of the IC. Over the 35 years, process scaling limitations have been overcome with process improvements with little change in the transistor materials although there are exceptions such as copper and polysilicon integration. As transistor and device features continue to shrink from millimeter and micron scales to the nanometer scale, features are becoming so small that material physics, instead of processing, can potentially limit the size of transistors. For example, a thin dielectric film called the gate oxide must become thinner than 4-5 atomic layers to continue the rate of scaling; however, at lower thicknesses, electron tunneling through the oxide results in unacceptable rates of leakage current and power consumption. Printed dimension sizes of the smallest transistor feature (gate stack) for the current generation of transistors is 35-40 nm and wiring line widths are as small as 90 nm.[4] To continue

scaling IC dimensions, new materials with improved properties must replace conventional materials.

1.2 New Material Integration

As scaling continues, transistor switching speed will no longer dictate IC performance. Instead, the wiring that connects transistors (interconnects) will soon limit overall IC speed.[4,5] Similar to the gate oxide, the dielectric property of silicon dioxide, which electrically isolates interconnect wires, is limiting the rate of scaling. Continued reduction of the wiring dimensions will result in degraded performance due to capacitive coupling. To prevent this from occurring, chip manufacturers, IC tool-makers, academic researchers and international consortia are searching for new materials with superior material properties that can be integrated into the IC manufacturing process. For interconnect dielectrics, the desired material must have a lower dielectric constant than silicon dioxide. These are termed 'low-k' materials. A material with a lower dielectric constant will reduce the capacitive coupling between neighboring interconnects as the spacing is scaled down.

Integration of a new material into an IC requires complete evaluation of all manufacturing processes that are associated with the deposition, patterning and cleaning of the material as well as processing following material introduction. Cleaning processes are particularly sensitive to material incompatibility due to the use of aggressive chemicals and the variety of different IC materials. With IC yield targets as high as 95%, effective cleaning is as important as any other IC process. Furthermore, cleaning

processes account for up to 25% of processes and are utilized for particulate/contaminant removal, surface preparation and photoresist/etch residue removal.[6] A particular class of cleaning, required after plasma etching, is post-etch residue removal which accounts for up to 30% of the cleaning processes.[6] Conventional cleaning technology utilizes multiple steps including oxygen plasma ashing and liquid-based solvent or semi-aqueous stripping chemicals.

Shrinking feature sizes and integration of new materials require constant improvement to current cleaning technology. The lack of clear leader for replacement of silicon dioxide as the interconnect dielectric makes development of new cleaning chemistries particularly challenging. Likely low-k candidates for next generation ICs are organic doped silicon dioxide materials. The organic doping reduces the dielectric constant of the material by reducing the material polarizability. An advantage of silicon dioxide-based materials is that they can be patterned similarly to conventional silicon dioxide using fluorocarbon-based plasma etching. Fluorocarbon residues formed during plasma etching are effectively removed (cleaned) by oxidative processing such as oxygen plasmas or liquid strippers. Unfortunately, these conventional cleaning processes have shown selective depletion of organic components from new low-k materials or even complete removal. This removal or selective depletion degrades the physical and electrical properties of the dielectric to unacceptable levels.[7] Current industry requirements demand less than 2.5% dimension loss and less than 2% change in dielectric constant after cleaning processing.[9] This dissertation is aimed at developing and understanding new chemistries capable of

fluorocarbon post-plasma etch residue removal while maintaining compatibility with new silicon dioxide-based low-k materials.

1.3 Dissertation Overview

New chemistries for cleaning fluorocarbon post-plasma etch residue from organic containing low-k materials have been evaluated and studied. When integrated, low-k material replacements such as silicon dioxide-doped or siloxane-based materials will be patterned using conventional fluorocarbon plasma etching. In order to achieve anisotropic patterning, a fluorocarbon residue is deposited on the surface of the features and must be removed prior to subsequent processing steps. Incomplete removal of this residue can result in problems such as poor electrical contact, poor film adhesion and poorly controlled feature dimensions. Conventional cleaning processes use oxidative chemistries, such as hydrogen peroxide-based or oxygen plasma-based processes for removal of fluorocarbon residues. Unfortunately, these oxidative processes oxidize the organic components and silicon-carbon bonds in the low-k materials. Modification or etching of the low-k materials results in increased dielectric constant, reduced mechanical strength and poor control of reproducibility and film thickness. In order to integrate these low-k materials, new cleaning chemistries must be found that can effectively remove the residues without modifying the materials. One of the major difficulties is identifying chemistries that are capable of interacting with the relatively inert fluorocarbon residue.

The following chapter details the background literature relevant to IC fabrication, cleaning and low-k materials. Chapter 3 covers the materials and experimental

techniques utilized throughout this dissertation. Chapter 4 details characterization of 'model' residue films to determine the effect of the plasma etching environment on the chemical nature of the film. A reductive chemical process, based on sodium naphthalene radical anions, is found to be capable of modifying the residue, which is subsequently removed by aqueous ozone. Although ozone is typically assumed to be an oxidative process, by using specific process conditions, the unselective oxidizing strength can be minimized. Sodium naphthalene radical anions penetrate rapidly through the model residue enabling treatment of typical residues in less than ten seconds. Unfortunately, sodium is a contaminant and any sodium-based process is incompatible with IC processing. In Chapter 5, two methods are evaluated for generation of sodium-free radical anions. An ion-exchange chemical reaction is shown to be unsuccessful at stabilizing the anion while precipitating a sodium salt. Radical anions generated electrochemically are more stable and lack sodium, achieving IC process compatibility. In addition, electrochemical generation and degradation effects are characterized. In Chapter 6, the 'model' etch residues are demonstrated to be unsuitable for studying electrochemically generated radical anions due to incompatibility with solvents. The model etch residue and other surfaces are analyzed using the Owens/Wendt technique which enables prediction of solvent interaction or wetting. This evaluation method may aid in the formulation of new cleaning chemistries. In addition, the cleaning effectiveness of electrochemically generated radical anions are evaluated using industrial residues and the removal mechanism is invesitgated. Chapter 7 includes evaluation of semiconductor compatibility of this cleaning process with several low-k materials as well

as issues regarding process integration. The final chapter includes a summary and suggested future work.

CHAPTER 2

BACKGROUND AND LITERATURE REVIEW

2.1 Integrated Circuit Overview

2.1.1 Back-end-of-line integrated circuit fabrication

Integrated circuit fabrication steps are split into two segments where similar processing occurs. Front-end-of-line (FEOL) processing includes fabrication from the transistor level to the first metal layer. After the first metal layer, processing is termed back-end-of-line (BEOL) where fabrication of the remaining levels of wiring occurs. Wiring is necessary to connect groups of transistors into gates, which form the basis of computer logic. Up to eight levels of planar wiring are used to connect transistors using metal lines or interconnects. A cross section of an integrated circuit is shown in Figure 2.1. Planar wiring is fabricated using alternating levels of interconnect and via levels. Interconnect levels are used for lateral or planar wiring, while via layers are used to vertically connect interconnect layers.

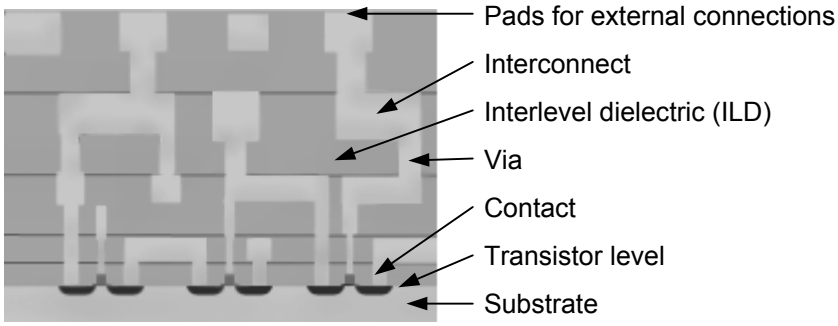

Figure 2.1. Diagram of transistor and interconnect wiring. Features not necessarily to scale

Each metal wire is insulated by an interlevel dielectric (ILD) material. Silicon dioxide is the conventional ILD material because of its ease of integration and history of use; however, replacement materials, which offer improved electrical performance, are being actively researched. These materials, termed 'low-dielectric constant' or 'low-k', reduce the capacitance between neighboring lines enabling more reliable and faster transmission of signals. In addition, integration of low-k materials also allows continued shrinking of features without degradation of electrical performance. Integration of these materials are discussed in more detail in the following sections.

Beginning in the mid-90s, copper replaced aluminum as the standard conductor used for interconnects in state of the art ICs. The advantages of copper are primarily its higher conductivity and superior electromigration resistance compared to aluminum. Replacement of aluminum with copper interconnects allows the continued scaling down and performance improvement of ICs.

The process for fabrication of copper interconnects used in BEOL processing is termed 'Damascene', named after a similar inlay process developed in the ancient city of Damascus. Because copper cannot be effectively plasma etched, a direct patterning process, like aluminum processing, is impossible. Damascene processing is illustrated in the final two steps of BEOL via processing shown in Figure 2.2.

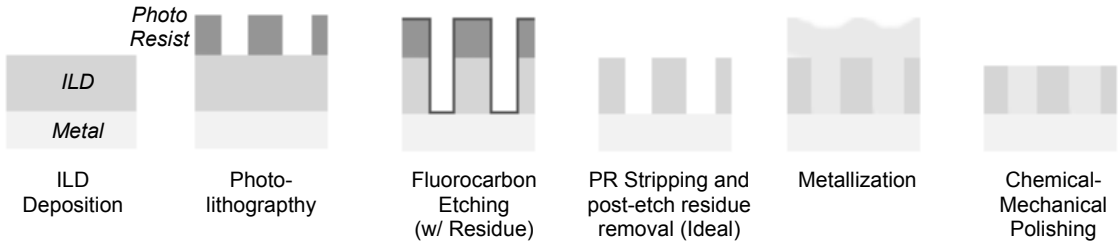

Figure 2.2. A cross section of BEOL via processing after each step.

For complete via processing, the first step is planar deposition of the ILD followed by photolithographic patterning using a radiation sensitive polymer (photoresist or PR). Selective exposure to radiation using a mask modifies the polymer chemistry and enables dissolution in an aqueous base. The photoresist layer is patterned leaving the features (interconnects or vias) defined by the area where the ILD is exposed. Anisotropic plasma etching removes the exposed ILD material creating trenches or holes for the interconnect or via. The chemistry of the plasma etching process is determined by the ILD material. For silicon dioxide or silicon dioxide-based low-k materials, etching using a fluorocarbon plasma is the most efficient and robust. As a result of the fluorocarbon plasma etching process, a fluorocarbon residue is deposited on all exposed surfaces. The next step is cleaning or removal of the photoresist and the fluorocarbon residue. This cleaning process can require up to four separate steps. The trenches formed in the ILD material are filled with copper material using electroplating. Finally, a chemical-mechanical polishing process planarizes the surface resulting in the copper features inlayed into the ILD layer. The process is repeated for each subsequent layer of wiring. A more advanced process, termed 'dual-Damascene', can be used to pattern both the interconnect and via layer at the same time.

2.1.2 Drivers in the semiconductor industry and low-k material integration

The semiconductor manufacturing industry is driven by a desire to increase performance and reduce the cost of manufacturing each chip. Cost and performance generally scale with the number of devices on the IC, thus, driving the miniaturization or scaling of devices. Smaller features and devices permit smaller ICs to be fabricated increasing IC density on wafers. Assuming that 'per wafer' processing costs remain roughly constant, the cost per IC decreases. Shrinking features also improves performance yielding more valuable ICs. If IC dimensions are constant, more transistors can be incorporated, improving the IC capabilities.

The number of transistors on an IC, which is proportional to performance, has approximately doubled every 18-24 months since the commercial manufacturing of the first ICs. This staggering rate of improvement has never been achieved in any other industry for such an extended period of time. An international consortium of semiconductor manufacturers has developed the International Technology Roadmap for Semiconductors (ITRS) that dictates the pace of improvements and scaling. This ensures compatibility between the equipment and material providers and the manufacturing companies.

Continued improvements in device performance over the next ten years cannot be achieved through device scaling alone.[8] As dictated by the ITRS, incorporation of new materials is necessary to continue scaling at the current rate.[9] Integration of copper interconnects is all but complete and is common-place in state of the art fabrication

facilities. Scaling down the gate oxide thickness improves the speed of device switching and reduces power consumption; however, new required thicknesses are approaching less than four to five atomic layers or less. At this point, the material no longer behaves with bulk properties and processing challenges are immense. To continue scaling, the gate oxide layer material must be replaced with a new material with a higher dielectric constant. A search for a high-k material that can be successfully integrated into the fabrication process is ongoing.

To improve performance in the BEOL, low-k materials are expected to replace silicon dioxide as the ILD material.[10] The reduction of the dielectric constant of the ILD reduces interference or 'cross-talk' between interconnects. This allows either high frequency signal propagation or closer packing of interconnects while maintaining comparable signal loss.

Replacement ILD materials can be divided into two categories. Primarily organic low-k dielectrics include fluorocarbon polymers, hydrocarbon polymers and porous polymers. Specific candidates include amorphous fluorocarbon, BCB (benzocyclobutene), SiLK (Dow proprietary organic) and poly(arylene) ether. Fluorocarbon-based plasma etching is generally not acceptable for processing organic materials; therefore, they are not discussed further. The other class of materials are inorganic or organic-doped inorganic materials. In the remainder of this paper, low-k dielectrics will refer to this class of inorganic low-k materials. These materials are generally silicon dioxide doped with one or a combination of fluorine (FSG – fluorine-doped silicon glass), a hydrocarbon

(SiCOH) or a fluorocarbon. The doping of these molecules reduces the dielectric constant of the hybrid material, yet the material still retains the processability of silicon dioxide. The structure varies depending on the material and the deposition method. Plasma deposited low-k materials are amorphous without a clear bonding configuration. Other hybrid materials are more structured and contain silicon-oxygen backbones or cages with organic or hydrogen side groups such as MSQ (methyl silsesquioxane) or HSQ (hydrogen silsesquioxane). These porous materials are deposited by spin coating. Because silicon dioxide remains the primary constituent, etching is fairly similar to pure silicon dioxide, although the porosity can be problematic with cleaning and mechanical processing.

Only fluorinated silicate glass (FSG) or fluorine-doped silicon dioxide has been reported in commercial fabrication lines.[11,12] The dielectric constant of FSG (3.7) is an improvement over silicon dioxide (3.9) and there are relatively few integration issues because the material behaves similarly to the conventional material..

This research focuses on developing and understanding new cleaning processes for BEOL processing. Flourocarbon plasma etching is effective at patterning silicon dioxide-based and siloxane-based low-k ILD materials; therefore, cleaning of fluorocarbon residues will continue to be relevant in the foreseeable future.[13,14,15,16] The incorporation of new materials into the semiconductor processing offers many integration challenges, especially cleaning and residue removal processing. Adding difficulty is the fact that,

because of integration challenges there is not a clear leader for a replacement ILD material.

2.2 Fluorocarbon Residue Generation During Plasma Etching

2.2.1 Principles of plasma etching

Plasma generation for patterning purposes takes place under vacuum conditions, typically between 1 and 100 mTorr.[17] Gases are fed into the plasma chamber at controlled rates and the pressure is maintained using specially designed vacuum pumps. To ignite and sustain the plasma, an alternating-current electric field in the RF or microwave range is generated inside the chamber. Depending on the type of etching chamber, the field is generated capacitively across parallel plates or inductively with a coil. The electric field causes dissociation of etch feed gases, generating free electrons, ions and radical neutrals. Continuous collisions between electrons, ions and neutral species form the plasma environment. Differences in mobility between the electrons and the ions result in preferential loss of electrons to surfaces in contact with the plasma. This loss creates a voltage difference between the plasma and the surfaces which is dropped primarily across a thin charge imbalance region near the surface termed the sheath. This electric field accelerates ions towards all contacted surfaces including the bottom electrode where the sample is typically located. This is termed ion bombardment on the sample. In addition, the sample is exposed to the reactive species in the atmosphere. The ion energy, ion flux, ion dissociation and reactive species concentrations can be controlled by the specific plasma parameters such as pressure, bias, power and etch gas.[17]

Reactive ion etching (RIE) is a specific type of plasma reactor configuration which etches by a synergistic combination of ion bombardment, reactive etch molecules and radicals.[17] Ion bombardment removes material by physical bombardment as well as provides energy to the surface to activate or break bonds. This enables surface reactions with otherwise unreactive gas molecules or radicals to produce volatile products which are pumped from the chamber. Increasing the negative bias on the sample electrode increases ion bombardment. Anisotropic or directional etching is achieved by plasma deposition of a film on feature sidewalls during etching. By control of the reactive species in the plasma atmosphere, a film can be deposited on all exposed surfaces; however, ion bombardment and physical ion sputtering remove the material on the bottoms and tops of features. The film on the sidewall prevents lateral etching by blocking exposure to reactive species. Plasma processes must be tuned to control the relative deposition and etch rate in order to achieve an anisotropic process. This process is depicted in Figure 2.3.

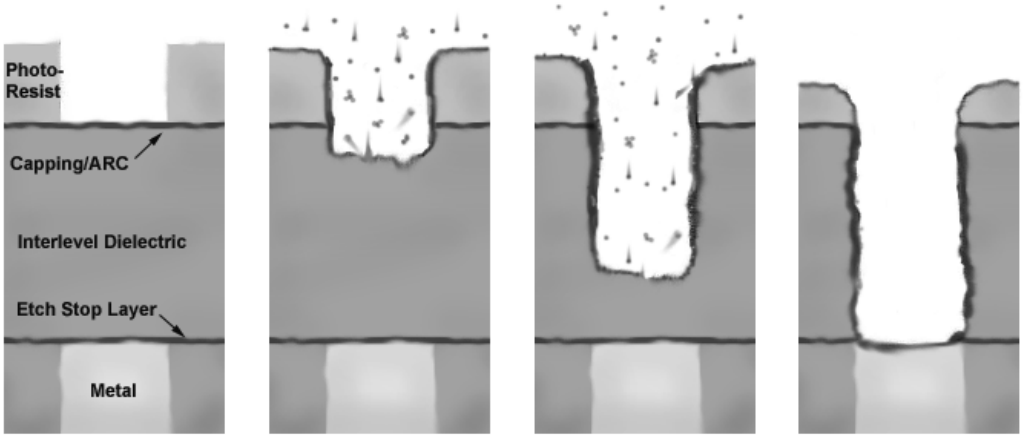

Figure 2.3. Schematic illustration of reactive ion etching of a feature.

2.2.2 Fluorocarbon plasma etching of silicon dioxide

Fluorocarbon-based RIE is used for anisotropic etching of silicon, silicon dioxide and silicon dioxide-based materials.[18,20,23,24] Fluorine-based plasma chemistries etch silicon and silicon dioxide by the spontaneous reaction of silicon and fluorine radicals forming SiF_4 as a volatile etch product. Ion bombardment aids in breaking the strong silicon-oxygen bond in silicon dioxide as well as delivering energy and heating the surface. Process control and selectivity is achieved by deposition of a fluorocarbon film which can selectively inhibit etching. Under appropriate RIE etching conditions, fluorocarbon plasmas will selectively etch silicon dioxide over silicon or silicon nitride because of this layer.[18] CF_x radicals formed in the plasma result in the spontaneous fluorocarbon deposition on all surfaces including the sidewall of structures.[19] Liberation of oxygen radicals from the silicon dioxide remove or at least thin the fluorocarbon layer by the formation of CO and COF_2.[18,23] Oxygen can also be added to the plasma feedgas for the same effect. This competing reaction allows the fluorocarbon layer to remain thin enough to enable species to diffuse through the underlying surface and react with the target material. Researchers have observed an inversely proportional relationship between etch rate and fluorocarbon layer thickness independent of the surface material.[18,23] A thicker fluorocarbon layer lowers the etch rate of the underlying material by reducing diffusion of reactants and reducing the effect of ion. For all known fluorocarbon etching conditions, a steady state fluorocarbon is present on the surface and etching occurs by transport of reactants and products through the film.

Ion bombardment also plays a role in controlling the etch process. Without significant ion bombardment, the majority of fluorocarbon etching chemistries will only deposit

material, even on silicon dioxide. Ion bombardment is important because it reduces the fluorocarbon thickness by physical sputtering, enhances reaction rates, and aids in diffusion of reactants through the layer.[31] With fluorocarbon films of less than 10 angstroms, energetic ions can bombard the underlying surface.[20] This results in bond breakage, temperature increase and aids transport of reactants through the fluorocarbon film. Reactive radicals and gas molecules also diffuse through the fluorocarbon layers and participate in reactions. As the layer becomes thicker, the energy that impinging ions deliver to the surface is reduced and the diffusion rate through the film decreases. This results in tilting the balance of etching and deposition towards deposition. Further evidence of the requirement of ion bombardment is the lack of etching on the sidewall of structures which are exposed to only reactive radicals. Without ion bombardment, the deposition on the sidewall prevents any lateral etching thus enabling anisotropy.[17] Deposition parameters of the inhibitive fluorocarbon layer plays an important role in controlling the etch process. Figure 2.4 demonstrates the relevant processes occuring during anisotropic plasma etching. During the etch process, the photoresist layer is exposed to heavy ion bombardment as well as radiation. This results in the formation of a hardened carbonaceous crust on the surface of the photoresist. In addition, the radiation and ion bombardment can partially cross-link the photoresist layer.

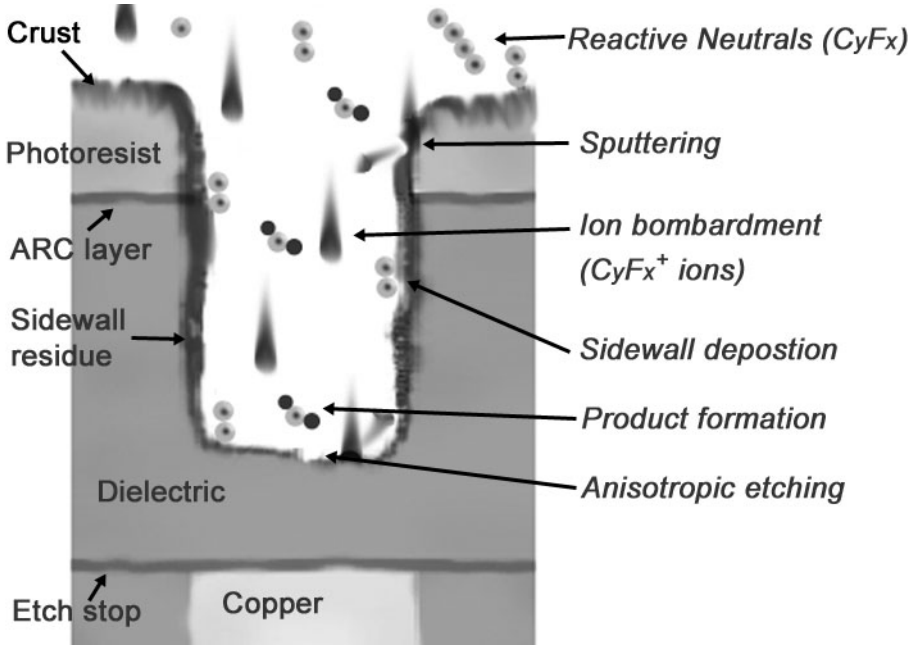

Figure 2.4. Schematic of molecular processes occurring during anisotropic fluorocarbon etching. (molecules not to scale)

2.2.3 Fluorocarbon post-etch residue characterization

Both the chemical composition and the thickness of the fluorocarbon layer are important to the plasma etching process. Recent work has linked the fluorine content of the residue to the etch rate during processes where fluorocarbon films of less than 10 angstroms are generated.[20] It is believed that fluorine in the residue is the primary supplier of fluorine in the production of volatile SiF_4. Reaction and transport of fluorine from the fluorocarbon film to the silicon dioxide interface is aided by ion bombardment and was found to be a function of ion energy. There is recent trend of choosing higher-carbon containing fluorocarbon feedgasses such as cyclic-C_4F_8, C_4F_6 and C_3F_6 because deposited layers with a higher-carbon content generate a more etch resistant fluorocarbon film.[21,22] Processes using these gases may etch slower due to less fluorine in the film, but the

comparison is confounded because these processes deposit films at an increased rate. While particular deposited films has been characterized, fundamental understanding between the chemistry of the film and the etching process is lacking. The composition and bonding to the substrate is also expected to be important to removal processes, although there has been no substantial work completed to understand the link.

Fluorocarbon etch residues have been characterized by both X-ray photoelectron spectroscopy (XPS) and spectroscopic ellipsometry. Researchers have made in-situ ellipsometry measurements of the steady state fluorocarbon film.37 Depending on the process conditions, measurements indicate thicknesses ranging between 5-30 angstroms when etching silicon dioxide.[23] The film reaches this steady state thickness after 15 seconds of plasma exposure.[24] High resolution XPS measurements can detect the amounts of each of the following carbon fluorine bonding configurations: CF_3, CF_2, CF, CCF, and CC/CH. From the relative amounts, a degree of crosslinking can be calculated based on the number of cross-linking moieties (CCF, CF) over the total number of carbon-containing moieties.[25] This assumes that there is little branching in the polymeric residue which is expected with plasma deposited films. Uncrosslinked residues are likely to dissolve or swell at more appreciable rates, but offer less resistance to plasma etching. The fluorine to carbon ratio in the residue and the presence of Si-F or C-F, common at the residue interface, can also be determined by XPS.[26] These are the standard techniques used to investigate etch residues.

Standard etch process evaluation metrics such as etch rate, selectivity and anisotropy all relate to the deposition characteristics of the fluorocarbon layer. The deposition characteristics, however, rely on virtually all etch process parameters such as reactor configuration, etch gases, power, sample bias, pressure and even sample location.17 Traditional etch gases include CF_4/H_2 and CHF_3; however, researchers are currently investigating many alternative gases. Etch gas possibilities include saturated, unsaturated, linear and cyclic fluorocarbons with 2 to 5 carbons.[21,22,27] Etch recipes sometimes include additives such as oxygen and argon. Oxygen addition to the feedgas increases the etch rate of the fluorocarbon film and argon addition increases ion bombardment energy. Addition of these feedgases give researchers valuable control over etch process characteristics. The high power and high plasma density settings of new etch systems result in significant fragmentation and ionization of the fluorocarbon etch gases and thus high ion flux. These tools increase the etching rate, but are more likely to cause plasma damage to samples.

2.2.4 Fluorocarbon post-etch residue generation while etching low-k materials

The importance of the substrate becomes apparent during the study of fluorocarbon etching of silicon dioxide-based low-k materials.[14,15,16] Using standard fluorocarbon plasma recipes, methyl-doped silicon dioxide etches relatively similarly to silicon dioxide. The organic components etch by formation of volatile products (CO, CO_2, H_2O, H_2) as a result of oxidation by reactive oxygen species. Oxygen species originate from either the silicon dioxide surface or from addition to the etch feedgas. The etch process, however, is still dependent upon the composition of the low-k material. Because of the additional organic component in methyl-doped-silicon dioxide, fluorocarbon layers

deposited at a faster rate. To demonstrate the effect of oxygen in the substrate, methyl-doped silicon was etched using a recipe known to etch methyl-doped silicon dioxide.[14] The lack of oxygen in the substrate resulted in a sharp increase in the fluorocarbon deposition rate. While many of the low-k etch characteristics are investigated, only a single study was found that examines the composition of the fluorocarbon film formed during etching.[14] The chemical composition of the fluorocarbon film appeared mainly dependent on the feedgas and closely resembled films formed during silicon dioxide etching.

Fluorocarbon etching of porous silicon dioxide or porous siloxane polymers is also possible.[15,16,28] Although etch rates of porous silicon dioxide were faster than its dense counterpart, rates normalized by material density were lower.[28] This reduced etch rate effect was attributed to fluorocarbon film pore filling. Unfortunately, the chemical composition of the fluorocarbon residue was not examined. Post etch cleaning and drying of porous low-k materials is a particular challenge and is discussed in Section 2.4.2.

2.3 Fluorocarbon Residue Removal

2.3.1 Conventional fluorocarbon cleaning techniques

The removal of the fluorocarbon residues following an etching process is essential for subsequent processing steps. Fluorocarbon residue remaining at the bottom of the via or contact can reduce or prevent electrical contact with underlying layer. Because incomplete removal at this location can result in device failure, fluorocarbon cleaning at

the bottom of contacts to the source and drain was the focus of the majority of early cleaning research.[29,30,31,37] With decreasing feature size, removal of residue on the sidewall is also becoming important. Aggressive chemicals tend to etch both the ILD and the residue which increases the printed critical dimension of the feature.[32] Because of the low surface energy of fluorocarbon materials, residue remaining on either the sidewall or bottom of the trench can cause adhesion problems with subsequent layers.[34] The low surface energy of the fluorocarbon residue also hinders wetting of the small features. In addition, contaminates, such as copper or barrier metals can become embedded in the residues. [33] Diffusion of these contaminants into surrounding materials and degrade physical and electrical properties. Clearly, complete residue removal on both the sidewall and bottom of the feature is desired.

The most comprehensive and common silicon surface clean in the IC industry for the last 30 years is the RCA clean or some modification thereof. This process consists of SC-1, dHF and SC-2 cleaning steps. The SC-1 (standard clean-1) or APM step is an aqueous mixture of ammonium hydroxide and hydrogen peroxide heated to 60 °C. The dilute-HF is a 50:1 mixture of deionized water (DIW) and hydrofluoric acid.[34] The SC-2 step is an aqueous mixture of hydrochloric acid and hydrogen peroxide heated to 60 °C. The SC-1 or APM step strongly oxidative and removes organic contamination from the surface by oxidation. On silicon, this step also causes the growth a thin oxide that captures metallic contamination on the surface. Dilute HF etches a thin layer of silicon dioxide from the surface. This helps remove embedded metallic contamination or any contamination on the surface of the oxide. The final step (SC-2) also removes metallic and other ionic

contamination from the wafer. The RCA clean is effective for removing both polymeric and metallic contamination from silicon or silicon dioxide. Wafers are sequentially dipped in each cleaning solution in a temperature controlled tank. Industrially, 25-100 wafers are exposed simultaneously, however, single wafer baths or spray tools are currently being evaluated for improved performance and repeatability.[32]

Over the last two decades, researchers have investigated alternative liquid treatments such as hydrofluoric, nitric, sulfuric and chromic acids with and without an oxidizer.[29,35] It is unclear if any of these methods actually attack fluorocarbon residues, however, nearly all of them attack silicon dioxide and/or oxidize silicon. Similar to the RCA clean, the likely mechanism of cleaning is undercutting the underlying material, although some oxidative attack of the residue may also occur. Evaluation of removal mechanisms is often difficult to assess. Furthermore, much of work focused on silicon surfaces at the bottom of contacts, not on BEOL processing. Restoring the properties of the underlying plasma-damaged silicon as well as residue removal is important. Many of these treatments, including the original RCA clean, are too aggressive for current geometries and incompatible with metal at the bottom of the trench. Problems such as metal oxidation and dimension loss has required new cleaning technologies for BEOL cleaning.

For BEOL cleaning, a variety of liquid and plasma-based cleaning processes have been investigated for post-etch residue removal. Dilute versions of the RCA clean and acid cleans as well as mixtures of sulfuric acid and hydrogen peroxide (SPM) can be effective at residue removal. These solutions are still fairly aggressive oxidizing agents and must

tailored for specific processes to ensure selectivity. In addition, the chemical inertness and crosslinking of the fluorocarbon residues implies that the dominant liquid chemical cleaning mechanism is undercutting of the layers beneath the heavily fluorinated layer.[34] For example, semi-aqueous fluorine-based chemistries, which are currently the most popular cleaning agent, etch the underlying silicon dioxide resulting in film lift-off. Because the material is generally removed by an undercutting mechanism rather than a chemical attack, it is common to experience inconsistent and incomplete residue removal. Hydroxylamine chemistry can be used for residue removal; however, higher temperatures and long process times are often required. Copper compatibility is also questionable. Furthermore, thicker or higher fluorine content films, required for high aspect ratio etching, may pose challenges to conventional wet cleaning that uses an remove residue by undercutting an underlying material.

Attempts to remove the residue by plasma processes have been successful in the past. Because the residue is primarily organic, oxygen plasma (ashing) or oxygen RIE is very common for residue removal.[35] Other plasma chemistries such as NF_3/Ar and hydrogen have also shown success at residue removal at the bottom of features.[36,37] Ion bombardment is effective at activating the surface by breaking bonds enabling reactions between the residue and radicals, ions or gas molecules. The sidewall of the residue, which experiences little ion bombardment, is typically resistant to attack by reactive radicals. Research has shown that even hydrogen or oxygen radicals can not displace fluorine in fluorocarbons without the aid of ion bombardment for activation, making sidewall removal difficult.[38] Oxygen plasma are also unable to remove inorganic

components of residues because their oxidation, unlike organic residues, results in the formation of an involatile material. With the requirement of complete residue removal, a process based solely on plasma treatments seems unlikely. Both plasma and liquid chemical-based cleaning solutions that rely on an oxidation mechanism for residue removal will likely be incompatible with organic containing low-k materials.

2.3.2 Low-k cleaning compatibility

The primary issue with low-k cleaning processes is chemical compatibility. Because of the presence of the organic component in all low-k materials, oxidative cleaning processes will etch or deplete the organic material from the film degrading both the physical and electrical properties.[39] This has been demonstrated with oxygen plasma exposure to doped silicon dioxide low-k materials. [40,41,42,43,44] Oxygen radicals in the plasma environment depleted the organic material by oxidizing Si-C and Si-H bonds leaving stoichiometric silicon dioxide. The depth of penetration has been measured to greater than 300 angstroms using typical ashing recipes. Reducing hydrogen/nitrogen or hydrogen/helium plasmas for photoresist stripping is an alternative to oxygen ashing.[43] It may be more compatible for photoresist stripping; however, its compatibility with low-k materials is still being investigated and the effectiveness on etch residues is still unknown.[45] While hydrogen/nitrogen plasma processes appear to be a possible replacement, plasma damage and ineffective sidewall residue removal are still problematic. Industrially, plasma-based cleaning is rarely completely effective alone and is, therefore, used in conjunction with liquid processing.

Porosity in low-k materials adds a level of complexity to cleaning processing; however, porous materials are the only materials capable of reaching ultra low-k levels (<~2.5). Pores can either be isolated or connected. As pores size increases, and the amount of porosity increases, connected pores become unavoidable. Connected pores permit access to the entire bulk layer to gas and liquid phase cleaning solutions. In these cases, selectivity of the cleaning solutions is critical because such a large amount of surface area is exposed. Drying of porous materials is also particularly challenging. Moisture absorption reduces the effective dielectric constant and must be avoided. In addition, water and other high surface tension liquids can cause pore collapse when evaporated from the material. Discussed in the next section, super-critical fluid processing is the leading candidate to overcome these issues and replace of conventional wet cleaning.

2.3.3 Emerging BEOL cleaning technologies

The incorporation of new materials, decrease in feature size and reduction of chemical usage has driven an increasing focus on new cleaning technologies in the past decade. Aggressive oxidative approaches for BEOL cleaning have been phased out because of copper oxidation issues. Discussed previously, plasma-based oxidative cleaning processes, are incompatible with organic containing low-k materials. Because of decreasing feature sizes and tighter dimensional requirements, cleaning treatments that appreciably etch the ILD as a mechanism to clean are becoming less acceptable.

Hydrogen/nitrogen-based plasmas appears to be the front runner as a photoresist stripper and residue cleaner method for low-k materials.[46,47] These plasmas are less reactive with silicon dioxide-based organic materials than oxygen plasmas; however, carbon depletion

and dielectric constant shifts have been observed as a result of exposure.[48] Compatibility with fluorine containing ILD materials is unlikely because of the reducing ability and formation of hydrogen fluoride. Plasma cleaning is limited due because of the anisotropic nature of ion bombardment and subsequent plasma damage to dielectric or underlying films.

Another promising cleaning approach is the use of environmentally friendly super or sub-critical fluids based on carbon dioxide.[49,50,51,52] The fluids are produced by application of pressure and temperature beyond the critical point of carbon dioxide (31 °C, 1100 psi). Except for fluorous and silicone materials, supercritical carbon dioxide fluids have little solvating power and are inert to typical semiconductor materials. This fluid does have a density close to that of liquids, but with a fraction of the surface tension. High surface tension liquids can cause pore collapse and is believed to prohibit wetting and drying of small features.[53,54] This problem can be alleviated with supercritical carbon dioxide processing. To improve solubility, specific chemicals are added to the fluids. These mixtures have been reasonably successful at photoresist and residue removal.[50,51] In principle, these additivies, as well as the carbon dioxide, can be easily be separated, recovered and recycled by reducing the pressure of the fluid. If successful, this will reduce the use of chemicals and deionized water. In addition, carbon dioxide-based fluids should not require a rinsing or drying step.

There are some challenges that must be overcome with supercritical fluid processing. The effect of additives on the cleaning chemistry and on the fluid are not well

understood. Although the equipment is cluster-tool compatible, high pressure equipment is still expensive and not well standardized compared to conventional wet processing tools. For industrial acceptance, developed cleaning processes must be as robust and effective as previous methods. Processing time requirements for single wafer cleaning will also be difficult to meet with current processes. Drying tools, based on supercritical carbon dioxide, are currently available.

New liquid-based cleaning methods include dilute versions of the RCA clean, SPM or other oxidizing chemistry. Although oxidative damage to low-k materials can be reduced with dilution, the cleaning effectiveness is also lowered. Often, these dilute solutions are not robust and must be tailored for specific types of residues. Semi-aqueous cleaners which are solutions of organics with aqueous fluorine ions, are currently the most popular and clean by undercutting of silicon dioxide under the residues. The organic aids in dissolution of the residue and drying. It seems unlikely that aqueous or semi-aqueous cleaners will be compatible with porous ILDs. The use of ozone as an oxidizing agent is also becoming very popular, although it use is targeted more for FEOL cleaning. These applications are discussed in Section 2.6.2.

2.4 Radical Anion Chemistry

2.4.1 Surface modification of fluorocarbon surfaces

Residues formed during fluorocarbon plasma etching are inert to most chemical reactions because of the strength of the carbon-fluorine bond. These residues are somewhat similar to surfaces of polytetrafluoroethylene (PTFE) polymers. A large body of research

covering surface modification and reactions with PTFE surfaces exists and can be used for insight into cleaning of fluorocarbon residues. While the goals of surface modification and cleaning are different, the goal of causing a reaction with an inert fluorocarbon surface is shared.

A major difference between PTFE and plasma deposited fluorocarbon residues is the crosslinking or CF and CCF moieties. In addition to the strength of the carbon-fluorine bond, PTFE is inert because of the tight packing of CF_2 chains which sterically hinder reactive species access to the carbon backbone.[55] XPS analysis of residues indicate the presence of a significant amount of CF_3, CF and CCF moieties in fluorocarbon etch residues.[18,20] These bonds are more susceptible to attack than CF_2; however, activating even a tertiary carbon-fluorine bond is still difficult.

The carbon-fluorine bond is the strongest observed in organic chemical structures.[56] Since fluorine is the strongest reducing agent, alkane C-F bonds are generally resistant to SN_1 or SN_2 reaction schemes under standard conditions. Reactions with oxidizing or reducing agents such as peroxides or halogen gases require extreme processing temperatures, typically above 600 °C.[55,56] Alkane C-F bonds are even resistant to attack by hydrogen radicals.[55] Researchers have observed that tertiary C-F bonds are more reactive than secondary or primary due to reduced electrostatic shielding from the fluorine.[57] Over the last two decades, however, several types of reactions requiring only mild reaction conditions have been demonstrated.

Researchers have observed selective and unselective defluorination of perfluorocarbons when exposed to sodium and organic radicals. Examples include naphthalene and benzophenone radical anions.[58] Organometallic radical ions, such as sodium dicarbonyl(cyclopentadienyl)ferrate, are also known to selectively reduce tertiary C-F bonds.[59] Cobaltocene (Cp_2Co) is another organometallic reagent that is reactive towards fluorocarbons.[60] While these techniques seems promising, use of these reagents or reaction schemes are prohibitive because they must be confined to highly controlled environments. Cobaltocene is explosive upon exposure to air as well as highly toxic. Other catalytic pathways for defluorination have been found using organometallic components; however, the complexity of the reaction components and conditions or reaction times are currently prohibitive and not practical for IC manufacturing integration.

As mentioned previously, an area of related research is surface modification of PTFE for adhesion promotion. The method of surface modification is fluorine abstraction or defluorination of the surface. Techniques commonly used for PTFE surface modification can be categorized as liquid chemical, plasma, and gamma and UV irradiation.[79,61,62] Plasma approaches have been investigated thoroughly and are effective for PTFE modification, but require the energy from ion bombardment.[63] For microelectronic applications, residue deposited on the feature sidewalls is not exposed to significant ion bombardment. UV radiation exposure processes are prohibitively slow and gamma irradiation would cause damage to the IC.[61] Only the liquid-based chemical treatments are practical and can be easily integrated. These methods include surface treatment by

aromatic radical anions, solvated electrons and alkali molten salts.[79,56,64] Generally, solvated electrons for surface modification have been generated in liquid ammonia which is not very practical for commercial integration due to the low temperature required and associated safety hazards.[65] Naphthalene radical anions formed by sodium metal in THF or diglyme are relatively mild are is the most common commercial methods for PTFE surface modification.[56,66]

Researchers have speculated on the defluorination mechanism of the radical anion reaction with PTFE surfaces.[79,56,58] The generally accepted mechanism for sodium naphthalene radical anion reaction with PTFE is shown is Figure 2.6. Driven by the electron deficiency of the carbon backbone due to the electron-withdrawling fluorine, the radical electron is transferred from the anion to the backbone. Excess electrons on the PTFE chain cause instabilities enabling the sodium cation to and form NaF. The naphthalene is regenerated and available to be reused if more sodium metal is present to regenerate the radical anion. Free electrons on the carbon backbone collapse into double or triple bonds, crosslink with other chains, react with components or become hydrolyzed upon exposure to air. The reduction from CF_2 to CF to C is a stepwise reduction with the second abstraction being slower than the first.[67]

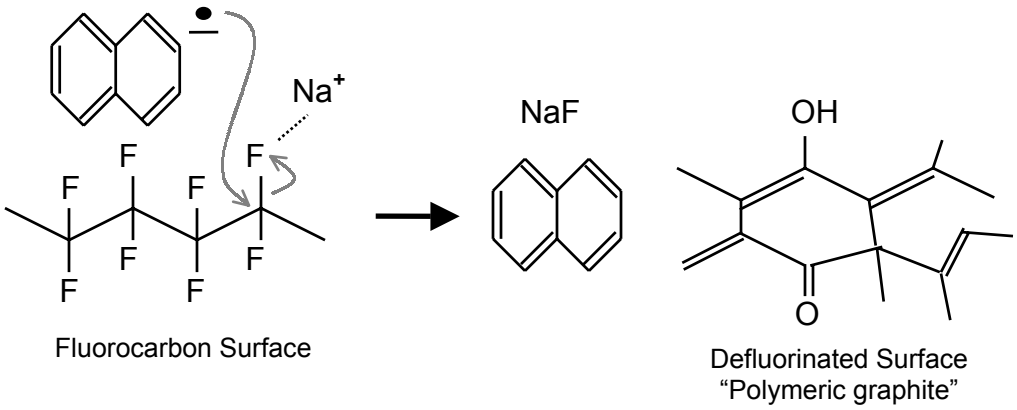

Figure 2.6. Mechanism of radical anion attack of a fluorocarbon surface.

McCarthy has completed the most comprehensive study of the modified or defluorinated PTFE surface after radical anion treatments.[67] Radical anions based on benzoin were generated using potassium tert-butoxide in dimethylsulfoxide (DMSO). Penetration depth of the reaction was measured over the range of several hours and 3.5 days. The initial rate is approximately 35 nm/hr, but slows to 8.3 nm/hr after 12 hours. The benzoin radical anion is significantly less reactive with PTFE surfaces than the naphthalene radical anion, although the defluorinated surfaces appear chemically similar. Ketyl, carboxyl and hydroxyl groups are observed on the surface by XPS analysis; however, it is difficult to discriminate these groups. After treatments of 8 hrs, the surface becomes brittle due to the crosslinking. Analysis by solid state ^{13}C NMR (nuclear magnetic resonance) and FT-Raman revealed the presence of single, double and triple carbon-carbon bonds, although noise in the data prevented quantization. A degree of unsaturation as high as 26% of carbon-carbon bonds has been reported elsewhere.[68] Incorporation of hydrogen was also detected in the defluorinated layer using ^{13}C CPMAS (cross polarization magic angle spinning) NMR. Using deuterated solvents and reactants,

the likely source of hydrogen was found to be the solvent (DMSO). Oxidation of the defluorinated film by exposure to ambient conditions over two weeks was also observed. The pictoral representation of the defluorinated surface demonstrating the different functionalities is shown in Figure 2.7. Later in the work, the modified layer is removed using an aggressive oxidation process ($KClO_4/H_2SO_4$ for 2 hours) and the surface is functionalized using a variety of chemical techniques.

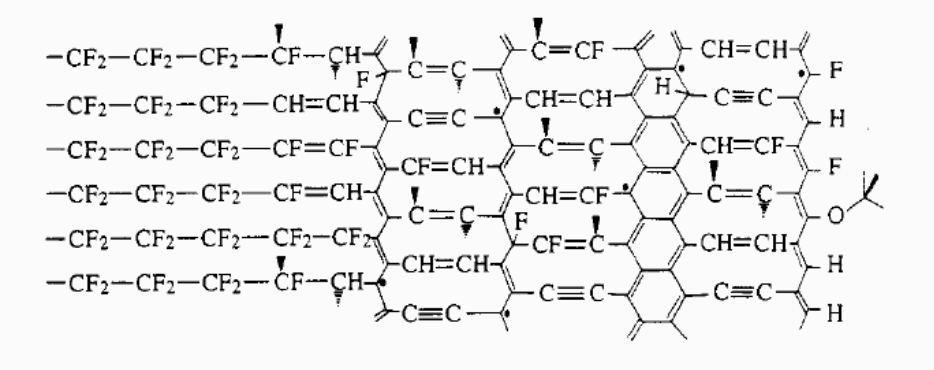

Figure 2.7. Pictoral representation of PTFE surface after radical anion defluorination from McCarthy et al.[67]

The rate of penetration of the defluorination reaction into surfaces has been measured using several different techniques. McCarthy utilized precise weighing with a microbalance before and after radical anion treatments.[67] Another method examined cross sections of PTFE plaques using SEM and X-Ray fluoresence to determine penetration depths which were reported on the order of microns.[69] Other authors only report that reaction depths were greater than XPS measurement depths.[70] These methods require at least several microns of reaction penetration for accurate measurements. No reliable method to measure shallow penetration depths (10-50 nanometers) was identified.

Kinetic studies identify the naphthalene radical anion defluorination reaction as second order with respect to the naphthalene suggesting two radical anions must be at the surface at one time for the reaction to occur.[79] Kinetic data was collected by measuring the rate of product formation (sodium fluoride) and the reaction product, at various exposure times by fluorine NMR The reaction was determined to be second order; however, determination of a rate constant is not possible with the information provided.[79] Replacement of naphthalene with alternate organic radicals such as anthracene, biphenyl or benzophenone results in significant reduction in the rate by greater than 97%.[79] The results are not completely understood, but are likely related to the increase in stability of the resulting radical anions and the lower reduction potential of the anion.

McCarthy and others have also demonstrated dehalogenation of other polymers including polyvinyldifluoride, polyvinyl chloride, polyvinyl dichloride, polychlorotrifluoroethylene.[70,71] The rate and completeness of dehalogenation was found to be proportional to the strength of electron withdrawling-character of the halogens on the backbone. Although, dehalogenation was observed, the degree of structural changes was not as significant as those detected in PTFE. This also suggested that sodium naphthalene solutions will be inert to nonpolar or low polarity polymers.

Except for a single patent, all surface modification of halopolymers has been performed using alkali-metal generated radical anions. US patent 5,800,858 details a process to generate radical anions electrochemically for surface modification of PTFE.[72] Electrochemical generation of anthracene radical anions and subsequent modification of

PTFE surfaces is investigated. Although the electrochemical generation technique is demonstrated, little scientific understanding of the penetration or kinetic rate is established. Furthermore, cleaning applications of fluorocarbon residues is not mentioned.

2.4.2 Background on radical anion chemistry

Radical anions were first discovered in the laboratory in the 1867 by Berthelot by combining potassium and naphthalene.[73] Later, Schlenk began the first in-depth studies of radical anions.[74,75] Early researchers believed that the metal formed a bond with the naphthalene, thus generating a neutral radical; however, this view was disproven by the stability in more polar solvents compared to nonpolar.[76] It was also demonstrated that the solution was conductive which further suggests that an ionic pair is formed.

In general, radical anions are formed by electron transfer from a source to a neutral molecule. The electron source can be an alkali metal or an electrode in an electrochemical setup. The reaction requires a slightly to moderately-polar aprotic solvent to solvate the ion pair. The most common procedure for generating radical anions is addition of sodium metal to a solution of naphthalene dissolved in tetrahydrofuran (THF) or diglyme. The resulting radical anion is a lewis base which makes them extremely reactive with water and oxygen. Typical molecules for forming radical anions are polycyclic aromatic hydrocarbons (PAH) or aromatic containing molecules; however, forming radical anions with a variety of other aromatic-containing molecules is possible.[77]

Thermodynamically, any molecule can be converted into a radical anion; however, practical limitations, such as the potential window of electrochemistry, prevent formation. A molecular orbital must be available for a molecule to accept an extra single electron. The lowest energy unoccupied molecular orbitals (LUMO) of stable molecules are typically antibonding orbitals.[78] Conventional techniques such as alkali metals or electrochemistry cannot supply enough potential or energy to transfer a single electron into sigma (single bond) antibonding orbitals; however, pi (double bond) antibonding molecular orbitals are lower energy. Conjugation reduces the antibonding orbital energy level even further, which allows transfer and occupation by a radical electron by conventional means noted earlier.[78] Because conjugation reduces the potential required to form radical anions, polycyclic aromatic hydrocarbons (PAH) make good molecules for the formation of radical anions. Additionally, incorporation of non-reactive electronegative moieties, such as a carbonyl group, further reduces the energy of pi antibonding orbitals in the molecule. The single electron density of radical naphthalene is shown in Figure 2.8.

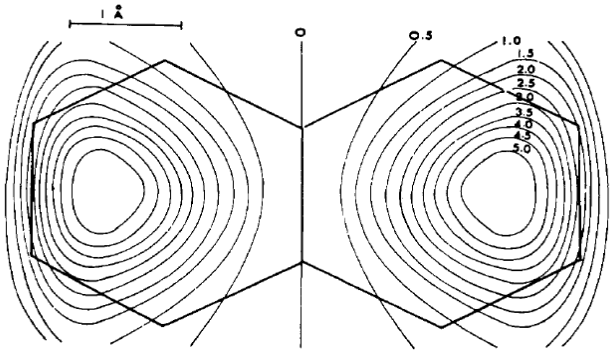

Figure 2.8. Single electron density of radical anion naphthalene. Lines show electron density in units of 10^{-3}.[76]

The energy level of the radical electron is related to the energy or potential required to transfer the electron into the orbital. The chemical reduction of PAHs has been studied extensively and good correlations are observed with several chemical properties such as gas-phase electron affinity and calculated LUMO energies.[76] The reduction potential of the radical anion is also related to the reaction kinetics with fluoropolymers. For example, radical naphthalene (E_{red} = -2.6 vs SCE) reacts 50 times faster with a fluorocarbon surface than radical anthracene (E_{red} = -2.0 vs SCE).[79] Higher reduction potentials, however, can also lead to unwanted side reactions. The reduction potentials for common radical anions is shown in Table 2.1.

Table 2.1. Reduction potentials of common radical anions.[80]

Radical anion	E_{red} (V vs SCE)
Biphenyl	-2.80
Naphthalene	-2.60
Pyrene	-2.10
Anthracene	-1.98
Tetracene	-1.58

In solution, radical anions must have a counter-ion to maintain neutrality and stability. The counter-ion and the nature of the ion pair can affect the reactivity of the radical anion. The nature of the ion pair is dependent on the radical anion, counter ion, solvent and temperature. Radical anion ion pairs can be described as tight or contact, loosely solvent separated or free ion pairs.[76,81,82,83,84,85] Techniques such as NMR, EPR, visible spectroscopy and conductance measurements have given insight into the nature of the association. While exceptions exist, tighter ion pairs tend to occur with smaller anions (naphthalene, anthracene, biphenyl) and smaller counter ions (lithium) where the charge

density is more localized.[76] In addition, less polar solvents (tetrahydrofuran and dioxane) and higher temperatures also promote tighter pairs. Radical anions generated in strongly interacting solvents, such as glymes, can chelate and strongly polar solvents, such as hexamethylphosphoramide (HMPA), tend to allow loose or free ion pairs. The nature of the ion pair of radical anions is important for reactions. Generally reaction kinetics and pathways favor separated pairs, although some reactions are faster with tight ion pairs.[76] Relevant to this work, the room-temperature system of sodium naphthalene radical anion in THF is generally regarded as having tight ion pairs. For room temperature naphthalene radical anion in dimethylformamide, the pairs are solvent or loosely seperated.[86]

Radical ions absorb in the ultra-violet and visible range. The relatively strong absorption (molar absorbtivity ~ 1600-3000 $cm^{-1}M^{-1}$) for radical anions allow convenient monitoring of their existence and decay either visually or quantitatively.[87] Radical anions typically have absorption maxima detectable in UV-visible region. Naphthalene radical anion in THF has absorption maxim at the following wavelengths: 368, 437, 466, 775 nm.[76] The decay of many radical anions in DMF has been catalogued although naphthalene is omitted.

Radical anions primarily participate in two types of reactions: proton abstraction and electron transfer.[76] The mechanism and reaction of proton abstraction between naphthalene and water is demonstrated in Figure 2.9.[88] The radical anion deprotonates the water molecule forming a radical hydronaphthalene. This intermediate is further

reduced by another radical naphthalene and forms an even stronger base. This base then abstracts another proton forming dihydronaphthalene. The initial reaction was found to be first order with respect to water and naphthalene radical anion. The measured reaction rate constant at room temperature was 2 x 10^4 $M^{-1}s^{-1}$.[88] The second protonation was found to be kinetically faster than the first. This reaction is commonly used to dry organic solvents; potassium metal and biphenyl are added to the solvent which react with the dissolved water.[89]. The presence of radical biphenyl, indicated by a blue color, verifies that the solvent is dry. A similar reaction mechanism occurs between radical anions and other protic molecules.[76]

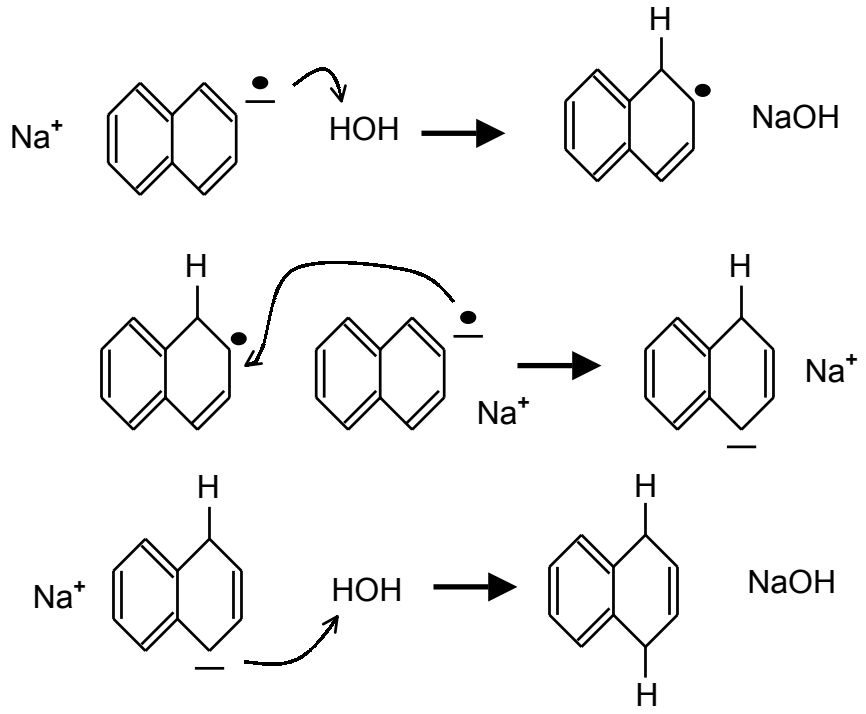

Figure 2.9. Mechanism of sodium naphthalene deprotonation of water.

Radical anions are also commonly used in electron transfer reactions or reactions that are initiated by electron transfer. Radical naphthalene and biphenyl have reduction potentials

close to that of sodium making them powerful reducing agents.[76] Alkane hydrocarbons are generally resistant to reduction. With alkene hydrocarbons, participation in polymerization, dimerization or addition reactions are common and depend on the molecular geometry.[76] Reactions with alkynes include proton abstraction and formation of ions in solution leading to variety of products. Radical anions are also reactive with CO_2 forming carboxylic acids and can be used to initiate 'living' polymer systems.

Dehalogenation reactions by radical anions have been studied extensively.[76,80,90,91] The two reaction pathways for the dehalogenation by a radical anion are detailed by Equations 2.1-2.4. The reaction begins by electron transfer to carbon bonded to the halogen and is driven by the electron deficiency created by the electronegative halogen. This is followed by rapid expulsion of the halogen. The alkyl radical can combine with another radical or be converted to a carbanion by gaining another electron. The carbanion rapidly deprotonates the first hydrocarbon available. The pathways depend on the reduction potential and concentration of radical anion, the electronegativity of the halogen and sterric effects.

$$R—X + A\bullet \rightarrow R\bullet + X^- + A \qquad (2.1)$$

$$R\bullet + R\bullet \rightarrow R—R \qquad (2.2)$$

$$R\bullet + A\bullet \rightarrow R– + A \qquad (2.3)$$

$$R^- + R—X \rightarrow RH + RH_{n-1} + X^- \qquad (2.4)$$

The kinetic rate of dehalogenation has been found be vary linearly with the reduction potential of the radical anion using n-hexyl-halides.[80] Additionally, the rate of reaction increased with decreasing electronegativity of the halogen due to the reduced bond strength. Only naphthalene and biphenyl were capable of reacting with alkylfluoride molecules. Pseudo first order rate constants varied between 2.2×10^{8} $M^{-1}s^{-1}$ to 2×10^{-4} $M^{-1}s^{-1}$ with fluoroalkyl reactions constants at the low end.[80]

This dehalogenation reaction is applicable to the cleavage of carbon-fluorine bonds which are the strongest in organic chemistry. This process is generally unselective and can be performed at room-temperature conditions. Because the radical anions are in solution, surfaces can easily be treated and dehalogenated. This is covered in Section 2.5.3.

2.4.3 Generation techniques for radical anions

Solutions of radical anions can be generated by reduction with alkali metals or by electrochemical reduction. Radical anions can be made by addition of an alkali metal to a solution of PAH in an appropriate solvent. These solutions can be stable for months if stored in a dry, oxygen free environment. Lithium and sodium are commonly used as reducing agents. Potassium and barium have also been reported.[92] Solvents must be aprotic and polar to stabilize the ions. Common solvents used for alkali metal generation include tetrahydrofuran, glymes and dimethoxyethane (DME). For sodium naphthalene, the equilibrium concentration of radicals is dependent on the solvent.[93] The reaction proceeds to completion in DME, methylethoxyethane, diglyme. In THF, the reaction

proceeds to 85% completion. This property is very sensitive to the structure of the solvent implying the importance of geometrical interactions with the ions.

Radical anions can also be generated electrochemically using standard electrochemical cells and equipment.[77,94] Typical setups use either platinum or mercury pool working electrodes because of the high negative potential required. Again, aprotic polar solvents are required. Common solvents are dimethylformamide (DMF), dimethylsulfoxide (DMSO), acetonitrile and 2-methyltetrahydrofuran. Any soluble electrolyte able to withstand the required reduction potential can be used. Typical electrolytes include alkylammonium salts such tetrabutylammonium iodide or tetrabutylammonium tetrafluoroborate. Generally, the two most common research topics conducted on electrochemically generated radical anions are chemical or physical property analysis and their participation in a reactions, typically dehalogenation. For these applications, low concentrations, often less than 5 mM, are required. For substantial surface defluorination and possibly cleaning, concentrations of at least 50 to 100 mM may be necessary. Stability of radical anions at these significantly higher concentrations is unknown. Another issue with electrochemical generation is the high negative potentials that are required for naphthalene reduction. At these potentials, the solvent or electrolyte may also be reduced.

2.5 Aqueous Ozone

2.5.1 Chemistry of aqueous ozone

In this research, aqueous ozone is used as a selective oxidant to remove fluorocarbon residues after they have been modified with a radical anion treatment. This treatment, in conjunction with a 'model' residue film, has been used to investigate the radical anion penetration rate. For cleaning actual residues, this second step may be necessary for particular thicker residues. Since typical aqueous ozone treatments react with organic materials, the process must be modified using additives to prevent degradation of organic containing low-k materials.

The use of ozone in semiconductor cleaning processes has been studied extensively over the past decade. Ozone is attractive because its degradation products are strong oxidants and is more environmentally friendly than other oxidative treatments used in IC manufacturing. Traditionally, organic residues are removed by oxidation in solutions of ammonium hydroxide/hydrogen peroxide or sulfuric acid/hydrogen peroxide. Large baths of these solutions at high temperatures are dangerous, demand frequent replenishment or replacement and create costly disposal concerns.[95] In some instances, commercialized aqueous ozone processing tools have already replaced these baths.[96]

With an oxidation potential of 2.07 V (vs SCE), ozone is considered a strong oxidant and is thermodynamically capable of oxidizing a variety of organic molecules. For the majority of organic molecules, however, the kinetic rates of direct oxidation by ozone are so small that they can be considered insignificant.[98] The most common reaction with reasonably fast kinetics occurs between ozone and carbon-carbon double bonds.[97,98]

Typical rate constants are on the order of 10^3 $M^{-1}s^{-1}$.[98] The electrophillic ozone molecule essentially inserts itself across a double bond and forms a five-membered ring. The five-membered ring is unstable leading to rearrangement and eventually cleavage according to Figure 2.10.[97] Products of the cleavage are a carbonyl and peroxy biradical which are quenched in an aqueous or water vapor rich environment.[98] Electronegative species bonded to the unsaturated carbons tend to slow the reaction rate with ozone.

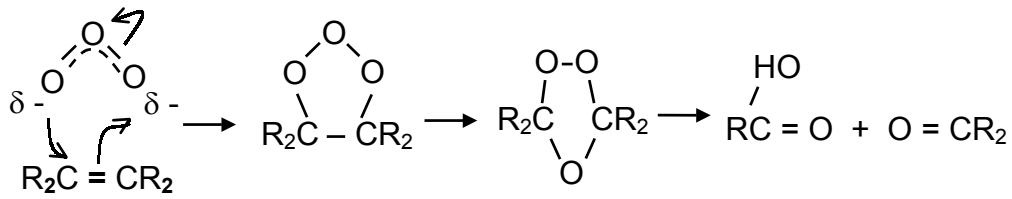

Figure 2.10. Ozonolysis reaction mechanism demonstrating cleaning of carbon-carbon double bonds.

While ozone can directly react with alkanes or halocarbons molecules, the rates are 5-6 orders of magnitude slower than the reaction with unsaturation sites.[98] While these rates may be important to atmospheric chemistry, it is acceptable to consider alkanes as unreactive. Oxygen or halogen-substituted alkanes react at rates comparable to their hydrocarbon analogues.[98] Certain substituted amines and hydrazines do react moderately with ozone. Alkynes react faster than alkanes, but reaction rates constants are still 2-3 orders of magnitude slower than alkenes.

Ozone dissolved in water or aqueous ozone is the most common and most applicable process for microelectronics processing. The solubility of ozone in water at room

temperature is nominally around 10 ppm, but it is strongly affected by pH, temperature, additives and impurites. Solubility is inversely proportional to both pH and temperature, which has important implications for application development.[95,99] Ozonated water has also become increasingly popular for water purification systems where much research has also been conducted.[100]

While molecular ozone does not readily react with many types of molecules, the byproducts of ozone decomposition can be aggressive towards organic materials. This is the basis of most cleaning processes utilizing ozone. The byproducts include radicals such as OH (hydroxyl radical), O_2^- (superoxide), O_3^- (ozone radical) and HO_2.[95,101,102,103] Formation of radicals is required to enhance the oxidative strength of aqueous ozone solutions; therefore, the study of decomposition of ozone has been a important focus of ozone research.

Similar to solubility, the rate and mechanism of decomposition in aqueous media depends strongly on pH and temperature. Addition of inhibitors and catalysts can also affect the rate of composition as well as the reaction byproducts available to oxidize the substrate. Because of the sensitivity on these factors and the short lifetimes of the radical intermediates, an accepted universal mechanism is currently unavailable. Numerous mechanisms for degradation have been proposed under conditions of low pH, carbonate ion inhibited and UV radiation. [95,101,103] The proposed mechanisms all differ and contain at least 8-10 steps. As an example, a proposed model of ozone decomposition is shown in Table 2.2 to demonstrate the complexity of decomposition.[101] The initiation step (step

1) is the rate limiting when compared to the rate constants of the propagation reactions. Estimation of the half-life of the radicals is on the order of nanoseconds.

Table 2.2. Model for mechanism for ozone decomposition. Radicals species are bolded.[101]

Step	Reaction	Rate constant
1	$O_3 + OH^- \rightarrow HO_2^- + O_2$	140 $M^{-1}s^{-1}$
2	$HO_2^- + O_3 \rightarrow \mathbf{O_3^-} + \mathbf{HO_2}$	5.5 x 10^6 $M^{-1}s^{-1}$
3	$\mathbf{O_2^-} + O_3 \rightarrow \mathbf{O_3^-} + O_2$	> 3.0 x 10^8 $M^{-1}s^{-1}$
4	$\mathbf{O_3^-} + \mathbf{OH} \rightarrow \mathbf{O_2^-} + \mathbf{HO_2}$	2.0 x 10^{10} $M^{-1}s^{-1}$
5	$\mathbf{O_3^-} + \mathbf{OH} \rightarrow O_3 + OH^-$	8.3 x 10^9 $M^{-1}s^{-1}$
6	$\mathbf{OH} + O_3 \rightarrow \mathbf{HO_2} + O_2$	2.5 x 10^7 $M^{-1}s^{-1}$
7	$\mathbf{O^-} + \mathbf{HO_2} \rightarrow \mathbf{O_2^-} + OH^-$	3.2 x 10^9 $M^{-1}s^{-1}$
8	$\mathbf{O^-} + \mathbf{O_2^-} (+H_2O) \rightarrow O_2 + 2OH^-$	1.8 x 10^8 $M^{-1}s^{-1}$
9*	$O_3^- \leftrightarrow O_2 + O^-$	5.0 x 10^3 $M^{-1}s^{-1}$
10*	$\mathbf{HO_2} + OH^- \leftrightarrow \mathbf{O_2^-} (+ H_2O)$	1.0 x 10^{10} $M^{-1}s^{-1}$
11*	$H_2O_2 + OH^- \leftrightarrow HO2^- (+ H_2O)$	1.0 x 10^{10} $M^{-1}s^{-1}$
12*	$\mathbf{OH} + OH^- \leftrightarrow \mathbf{O^-} (+ H_2O)$	4.0 x 10^{10} $M^{-1}s^{-1}$
13*	$H^+ + OH^- \leftrightarrow H_2O$	1.0 x 10^{11} $M^{-1}s^{-1}$

* Reactions are reversible with equilibrium constants depending on pH

An overall rate equation has been computed to fit ozone decomposition data from the range of pH 2-10 and is shown in equation 2.5.[99]

$$-d[O_3]/dt = 23.47[O_3]^{1.5}[OH^-]^{0.395} \qquad (2.5)$$

As demonstrated by the rate equation, the pH affects the rate of decomposition indicating the importance of the hydroxyl ion in the decomposition mechanism. The rate constants from a collection of researchers are shown in Figure 2.11.[99]

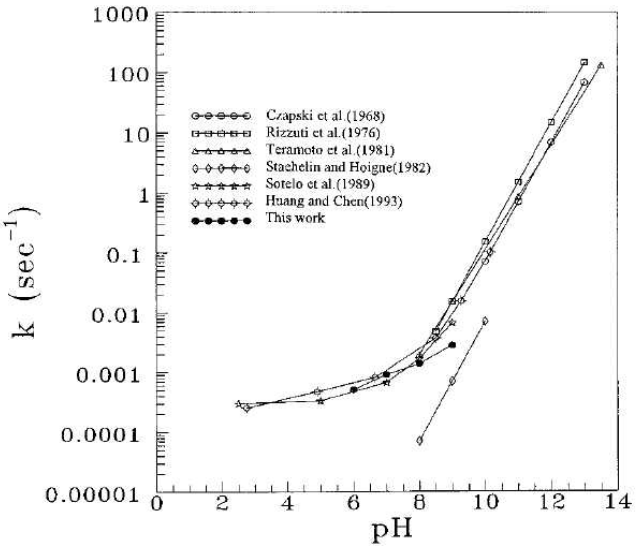

Figure 2.11. Comparison of the ozone decomposition rates fit to first order data.[99]

In addition to high pH, UV radiation has also been used to catalyze the decomposition of ozone.[103] UV radiation splits the ozone into molecular oxygen and dioxygen. It is believed that radiation promotes the formation of hydrogen peroxide from ozone in water. Hydrogen peroxide either splits due to the UV radiation or reacts with ozone to form hydroxyl radicals described in Equations 2.6-2.8.

$$O_3 + H_2O + h\nu \rightarrow H_2O_2 + O_2 \qquad (2.6)$$

$$H_2O_2 + h\nu \rightarrow 2OH \qquad (2.7)$$

$$O_3 + H_2O_2 \rightarrow OH + HO_2 \qquad (2.8)$$

Finally, inhibitors have been used to either slow the decomposition of ozone or scavenge free radicals.[95,100,101] Both interactions reduce steady state radical concentrations in aqueous ozone solutions. The two most common inhibitors are CO_3^{2-} and tertiary-butyl

alcohol (t-butanol). It was initially thought that CO_3^{2-} scavenges free radicals by oxidizing hydroxyl ions as shown in Equation 2.9.

$$CO_3^{2-} + OH \rightarrow CO_3^{-} + OH^{-} \qquad (2.9)$$

This reduction in hydroxyl concentration could not alone account for the decrease in observed rates; therefore it was concluded that carbonate ion also scavenges ozone radicals as shown in Equation 2.10.[101]

$$CO_3^{2-} + O_3^{-} \rightarrow CO_3^{-} + O_3 \qquad (2.10)$$

As indicated in Table 6.1, the ozone radical is important for several reaction steps. Another common inhibitor, t-butanol, interacts with hydroxyl radicals by a proton abstraction mechanism shown in Equation 2.11.[104]

$$OH + (CH_3)_3COH \rightarrow H_2O + \bullet CH_2C(CH_3)_2OH \qquad (2.11)$$

The alcohol radical reacts with oxygen to form peroxides, then proceeds through a series radical reactions eventually terminating in formaldehyde, dioxygen and various hydroxy alcohols.[104] This reaction is very fast with a rate constant of $6 \times 10^8\ M^{-1}s^{-1}$. [105]

2.5.2 IC processing using aqueous ozone

Because of its oxidative strength and reduction of chemical waste, ozone is attractive for IC processing. Early processing primarily involved ozone dissolved in DIW. The advantages of aqueous ozone, or ozonated water, are the moderate ozone solubility, the acceleration of decomposition, which produces radicals, and the removal of non-gaseous byproducts. In the early 1990s, investigation of ozone began as a replacement for sulfuric acid/hydrogen peroxide (SPM) treatments.[106,107,108] This step is typically the first of a series of wafer cleaning processes required prior to critical process steps such as diffusion and gate deposition. Replacement of hydrogen peroxide with ozone yielded comparable cleaning results for organic contaminants and reduced chemical usage. This process is now the first step of the IMEC clean; however, the sulfuric acid/ozone (SOM) step still requires temperature of 90 °C to be effective.

Because of its oxidizing capability, the SOM clean was extended to the removal of photoresist and post-plasma etch residues.[109] Using the SOM cleaning process, comparable photoresist stripping was observed, although the rates were slower than hydrogen peroxide containing mixtures. The SOM clean can also clean resist residue after a plasma based ashing process.[110,111] In an effort to further reduce the use of harsh chemicals, researchers continue to investigate ozone/DIW solutions.[112,113,114,115,116] Cleaning effectiveness with these treatments has been inconsistent as compared to SPM treatments. A balance of high ozone concentration, which in inversely proportional to temperature, and kinetic activation, which is proportional to temperature, must be met to ensure reasonable rates of oxidative attack. The aqueous ozone cleaning processes

require optimization of parameters to ensure reproducible removal. In addition, the target residue also affects the performance of the solution. This challenge still exists today requiring careful optimization of the ozone/DIW cleaning processes.

Several researchers have attempted to overcome the challenges of slow rates and inconsistent removal various techniques. Additives, such as NH_4HCO_3, have improved the rate of removal of photoresist with ozone chemistries.[117] The author surmised that the radical scavenging ability reduced the rate of decomposition and concluded that the ozone directly oxidized the photoresist. Studies in our lab have shown that interaction with alkyl ammonium bicarbonates promote photoresist removal by acting as a phase transfer catalyst and a base. Unless the photoresist contained a double bond, which was not mentioned, it is unlikely that it directly oxidized by ozone. Additives such as tetramethylammonium hydroxide, hydrochloric acid, nitric acid did not enhance removal rates, however, the spiking of ammonium hydroxide had the opposite effect.[114] The mass transfer rate of ozone to the wafer surface may also reduce the rate of photoresist attack. This problem has been addressed by modifying the application of the ozone. Spray tools demonstrated superior performance versus immersion.[115] Stripping using water vapor and gaseous ozone has also been successful.[116] Researchers have also investigated the use of super-saturated aqueous ozone and high pressure ozone to improve removal rates.[118,119]

2.6 Opportunities

The relationship between plasma etching conditions, fluorocarbon deposition properties and their effect on cleaning has not been well documented. With additional challenge of chemical compatibility with low-k material, many opportunities exists to make contributions. New cleaning chemistries are needed that are reactive to unwanted organic residues, but inert to organic components of low-k materials. Additionally, fundamental study of interactions between residue surfaces and the removal chemistry can lead to improved strategies for removal. With this knowledge, cleaning chemistries could be designed to react, swell or interfacially wet targeted residues enabling more selective removal of the material. The use of liquid-based reductive chemistry is markedly different than conventional use of solvents or oxidative strippers. It is the goal of this research to demonstrate compatibility with low-k materials, evaluate cleaning with industrial residues and understand the interactions that are important for effective removal.

CHAPTER 3

MATERIALS AND EXPERIMENTAL METHODS

3.1 Chemicals and Purification

All chemicals used in this research were purchased from Sigma-Aldrich and were reagent grade or higher. Solvents used for electrochemistry or radical anion chemistry were dried and stored over A4 molecular sieves for at least three days prior to use. These solvents include N, N-dimethylformamide (DMF), tetrahydrofuran (THF), N-methyl-2-pyrrolidone (NMP), dimethoxyethane, diglyme, dimethylsulfoxide (DMSO) and acetonitrile. Reagent grade isopropyl alcohol (IPA) and acetone were used to rinse samples and were used as received. Deionized water (DIW) was obtained from the house DIW system in the Microelectronics Research Center at Georgia Tech. Scintillation grade naphthalene and anthracene were 99.9% pure and used as received. Freshly cut sodium metal was stored in mineral oil and rinsed with hexane prior to use. Tetrabutylammonium iodide (TBAI) and tetrabutylammonium tetrafluoroborate were dried in a vacuum oven at 120 °C for at least 24 hours. Chemicals were stored in a drybox.

3.2 Equipment and Experimental Techniques

3.2.1 X-ray photoelectron spectroscopy

Because x-ray photoelectron spectroscopy (XPS) was used extensively in this research, appropriate background theory will be discussed.[120] XPS enables investigation of the

chemical composition and bonding structure of sample surfaces. In an ultra high vacuum chamber (<5 x 10^{-9} torr), monochromatic x-rays of a known energy level are generated and focused on a film sample. Atoms on the surface of the film absorb x-rays, resulting in the emission of photoelectrons by the photoelectric effect. To be detected, the photoelectrons must pass through the material without being re-absorbed or scattered by other atoms. The distance traveled is termed the inelastic mean free path (IMFP) or escape depth, and is dependent on the material being analyzed. This value is typically 5-10 nanometers resulting in only the surface of the sample being probed.

The difference between the original x-ray energy and the sum of detected kinetic energy and work function of the material is termed the binding energy, which is the amount of energy required to remove an electron from an atom. The electron detector scans through a specified range of binding energies and counts the number of photoelectrons detected at specific energy levels. A binding energy is specific to each element and each electron shell level, although some energy ranges overlap. The polarity of the atoms bonded to the specific atom can cause a shift in the binding energy. For example, the binding energy of a carbon atom bonded to a polar molecule, such as fluorine, is higher than that of a carbon-carbon bond. This allows differentiation of the CC, CF, CF_2 and CF_3 moieties in a fluorocarbon residue. The atom hybridization and oxidation state also affect the binding energy along with the electric potential of the sample. Conductive samples are typically grounded; non-conductive samples can become depleted of electrons and become positively charged. This effect can be alleviated by using an electron gun to

flood the sample with electrons or by manually shifting the spectrum by aligning a known peak to its reference binding energy.

To obtain binding energy spectra, the detector scans between a range of specific energy levels and counts the number of photoelectrons for a specified time. The maximum resolution of the scan (number of measurements over a certain range) is determined by the analyzer; higher resolution improves the accuracy of the measurement. Elemental peaks are differentiated by comparing observed peaks with known binding energy levels. For example, carbon atoms with nonpolar bonds appears at 284.8 eV. Fast low-resolution scans over the entire energy range indicate the presence of specific elements, although hydrogen and helium cannot be detected. High resolution scans over the binding energy of detected elements gives qualitative and quantitative information. The total number of electrons detected for each element versus the total number of electrons detected for all elements gives relative surface concentrations of those elements. For each element, peaks at different binding energies (which indicate different bonding configurations), can be fit using Gaussian-Lorentzian curves. The area under each curve enables quantification of the relative percentage of each atom in specific bonding configurations.

For this dissertation, XPS analyses were performed on a Physical Electronics (PHI) 1600 XPS system equipped with a monchromatic aluminum K_α source with an 0.8 mm spot size. The hemispherical analyzer operates at 187.85 eV pass energy. Chamber pressure during analysis was less than 5×10^{-9} torr. High resolution scans with resolutions of

either 0.025 or 0.050 eV/step and measurement times of 150 – 200 ms/step were typical. Analysis was completed using Multipak data analysis software (PHI). Fluoropolymer samples that shifted due to charging were aligned by setting the fluorine 1s peak to 689.67 eV.[120] Quantitative analysis of the data was performed using the Multipak software. Sensitivity factors were provided by PHI and are as follows: Carbon 1s: 0.314, Fluorine 1s 1.0, Oxygen 1s 0.733. Typical probing depth of the XPS is 5-10 nanometers depending on the material.

3.2.2 Spectroscopic ellipsometry

A Woollam M2000 variable-angle spectroscopic ellipsometer was used for thin film thickness measurements. Ellipsometry allows determination of both film thickness and refractive index by measuring the change in phase and polarization of polarized light after it reflects from the sample surface.[121] Typical analysis is performed using angles of 65°, 70° and 75° (with respect to the sample normal) and wavelengths between 600 nm to 1200 nm. The shape of reflected light is measured at each angle over the wavelength range. This data can be modeled using a three parameter Cauchy model which is effective at fitting data from polymeric and dielectric materials.[122] The model is shown is Equation 3.1 where the refractive index, n, is a function of three empirical parameters.

$$n(\lambda) = A + B / \lambda^2 + C / \lambda^4 \qquad (3.1)$$

Parameters are calculated based on minimization of the mean standard error between the model and the data. A standard error of the less than 30 is considered an acceptable fit

for this piece of equipment. Both refractive index and thickness are calculated from the model.

3.2.3 Atomic absorption spectrometry

A Varian SpectraAA atomic absorption spectrometer model AA10 was used to determine sodium concentrations in solutions.[123] The spectrometer was run in flame emission mode with a wavelength filter of 589.0 nm. An acetylene/compressed air feed fueled the flame. Calibration was completed using five aqueous sodium chloride solutions with concentrations between 0.2 to 1.0 mg/l or 1.0 to 20 mg/l based on the range of the unknown sample. Potassium chloride (100 mg/l) was added as an ionization buffer. Samples with concentration higher than 20 mg/l were diluted and each sample was measured at least three times.

3.2.4 Fourier transform infrared spectroscopy

FTIR spectroscopy measures the absorption of infrared radiation as it passes through a sample. Absorption at specific wavelengths indicates the presence of specific chemical bonds. Typically films with thicknesses of at least 500 nm are required to obtain FTIR spectra. A Mattson FTIR spectrometer model IR-10100 was used for bulk chemical analysis of thin films. The detector is a liquid nitrogen cooled mercury-cadmium-telluride unit with a range of 4000 to 600 wavenumbers (cm^{-1}). Samples were analyzed in transmission mode and the sample chamber was purged continuously with nitrogen.

3.2.5 Thin film spinning

Thin polymer films were spun on a Specialty Coating System Inc model P6204A spinner. Controls include spin speed (500-9,000 RPM), acceleration and deceleration rate.

3.2.6 Potentiostat

An ADInstruments Powerlab model 820 potentiostat was used in conjunction for electrochemical experiments. The potentiostat was controlled using a PC with ADInstruments EChem software (v. 1.5.2). Cyclic voltammetry could be performed with sweeps rates between 10 and 1000 mV/s and voltages between -5 and 5 volts. The potentiostat was operated in both galvanostatic (current controlled) and potentiostatic (voltage controlled) modes. An ammeter was connected between the working electrode and the potentiostat to measure the current.

3.2.7 ^{1}H nuclear magnetic resonance spectroscopy

^{1}H NMR analysis was performed on a Varian Mercury Vx 300. The original sample solvent of the sample was evaporated and replaced with a deuterated analogue. NMR peak identification was completed using known references.[124]

3.2.8 Dry Box/Purge Box

A Terra Universal acrylic dry box was used to prevent oxygen and water vapor contamination of solutions and samples. The dry box was purged continuously with dry house nitrogen at the rate of 7 scfh. The nitrogen line contained an in-line water vapor/oil filter. A feedthrough was used to transfer items into and out of the drybox.

Preparation and treatments of all radical anions and electrochemistry experiments were performed in the drybox.

3.2.9 Contact angle measurement system

Contact angles were measured using an AST Products model VCA 2500XE video contact angle system. To measure the contact angle, a 50 microliter drop of the liquid was placed on the sample using a computer controlled micro-syringe. A video capture device recorded the picture of the drop on the surface. Using the outline of the drop, the software automatically calculates the contact angle based on the captured image. The average of at least three measurements is reported with measurement variability typically +/- 3° or better.

3.3 Samples

3.3.1 APCI Samples

Air Products and Chemicals, Inc. generated a number of samples for the purpose of simulating post-plasma etch fluorocarbon residues. Samples were produced by exposing bare silicon wafers to fluorocarbon plasma etch environments. In total, three sets of samples were received. In the first set, which included nine samples, the fluorocarbon etch gas, oxygen feedgas flowrate and sample orientation were varied. These four-inch wafers were processed in a RF (radio frequency) parallel plate etcher for either one or two minute process times. Three of the samples were vertically aligned in an attempt to simulate sidewall etch residues. Specific details of the process conditions and characterization of the resulting films is the subject of Chapter 4.

A second sample set was supplied to evaluate proposed cleaning processes. The six-inch wafer sample was generated in a high density plasma reactor using a process based on C_4F_8. The etching recipe resulted in a fluorocarbon film with a thickness range of 200-240 nm. Plasma operating conditions were 200 W total power, 20 °C chuck temperature and 35 mTorr chamber pressure. The total feedgas flow was maintained at 200 sccm consisting of 26 sccm of C_4F_6, 28 sccm of oxygen and 146 sccm of argon. The thickness varied between 200 and 240 nm across the wafer due to nonuniformity of the film deposition. This second sample set was resistant to delamination by acetone and IPA, unlike previous thick film samples. Small samples (1-2 cm^2) were cleaved from the wafer for analysis. The third sample set is a replicate of the second film sample to provide additional samples. These last two samples sets were used to evaluate radical anion cleaning processes and have been designated AP2-1 and AP3-1.

3.3.2 Dielectric material samples

To evaluate low-k process compatibility, samples of Coral™ and methylsilsesquioxane (MSQ) were provided by Novellus Systems, Inc.(San Jose, CA). Coral™, a commercial low-k material from Novellus, is a plasma-deposited carbon-doped silicon dioxide with a dielectric constant of 2.6-2.7. Methylsilsesquioxane (MSQ) is a porous spin-on silsesquioxane-based material with a dielectric constant of approximately 2.6.

3.3.3 Patterned Etch Residue Samples

Novellus Systems, Inc. supplied patterned samples that were etched in a fluorocarbon-based plasma. Such samples enabled evaluation of experimental cleaning processes with

actual post-etch residue samples that would be encountered industrially. The patterns consisted of arrays of vias ranging in size between 130 and 1000 nm. The dual-damascene low-k etch stack consisted of two 500 nm layers of Coral™, separated by a silicon-carbide (50 nm) etch stop layer. Patterning was accomplished using a combination of a silicon dioxide hard mask (50 nm), a barrier anti-relflective coating (BARC, 50 nm) and a poly-hydroxystyrene/t-BOC-based photoresist mask. After the C_4F_8-based etching process, approximately 400 nm of fluorocarbon residue and photoresist remained on the silicon dioxide hard mask. Removal was evaluated by both optical microscopy, XPS and SEM (scanning electron microscope) analysis. Further characterization is completed in Chapter 6.

3.3.4 Polytetrafluoroethylene (PTFE)

PTFE samples were cut from a one-sixteenth inch sheet of virgin electrical grade PTFE purchased from McMaster-Carr (Atlanta, GA). These samples were used to evaluate defluorination processes visually as indicated by the darkening of the surface. Samples were prepared by rinsing with DIW, IPA, and dried prior to use.

3.3.5 Teflon AF

Thin films of Teflon AF 1600 were deposited on substrates using spin casting. The Teflon AF polymer is supplied by Dupont dissolved in a perfluorinated solvent (FC75 from 3M Company). Because of the extreme hydrophobicity, films do not adhere well on silicon substrates. As recommended by Dupont, silicon substrates coated with 1000 angstroms of copper provided adequate adhesion for Teflon AF films. These films were used to demonstrate patterning using surface modified radical anion films.

3.4 Chemical Treatments of Samples

3.4.1 Generation of naphthalene radical anion using sodium

All chemical procedures were performed in the dry box described previously. Radical anions were generated by mixing dried THF and naphthalene in oven-dried 4 dram vials. Solutions were agitated until the naphthalene completely dissolved. The nominal concentration of naphthalene is 100 mM unless otherwise specified. Next, pieces of freshly cut sodium were rinsed with hexane and prepared by scraping the surface and exposing fresh sodium metal. At least 2.5 times the stoichiometric (1:1) amount of sodium was added to the naphthalene/THF solutions. The appearance of the dark green naphthalene radical anion was immediately observed on the surface of the sodium. Vials were sealed and agitated for at least one hour prior to use. The vials became opaque within two minutes. Determination of radical anion concentration was accomplished using sodium atomic absorption spectroscopy and titration using DIW. Details of these procedures are given in Chapter 4.

3.4.2 Thin film exposure to sodium radical anions

Reduction treatments were performed using solutions of 100 mM naphthalene in THF with a 2.5x excess of sodium metal in 4 dram vials. All experiments were completed in the dry box. Thin film fluorocarbon samples (~ 1 square cm) were held using stainless steel tweezers and completely submerged into the sample vial for the specified time. The tweezers pierced a septum which provided sealing during treatments. Samples were removed, immediately rinsed with IPA and then dried with nitrogen. After removal from the drybox, samples were rinsed with DIW and IPA, then dried with nitrogen. The

combination of IPA and DIW is necessary to remove residual solvent and sodium from the film surface.

3.4.3 Ozone treatments

A PCI Ozone Control Systems, Inc. ozone generator (model G-2) produced a 3 vol% ozone stream from a pure oxygen source at the rate of 2 scfh.[125] This stream was bubbled through a diffuser in a 100 mL amber beaker of de-ionized water. The solution was bubbled for 10 minutes prior to sample exposure. Samples were suspended in the solution using tweezers for a specified time.

3.4.4 Thin film exposure by 'drop' treament

Edge effects or edge delamination can be a problem on small thin film samples cleaved from a wafer. By completely submerging samples in solutions, the edge of the samples, and thus the film/substrate interface, are exposed. Some solutions can wet the interface, resulting in rapid delamination of the film. The interface between an etch residue and substrate is typically not exposed while cleaning wafers; therefore, the residue cleaning results using small samples may not give analogous cleaning results compared to those with entire wafers.

In order to investigate the significance of edge effects, samples were routinely treated using the 'drop' method. Either single or multiple drops were placed on the center of a larger sample. Care was taken to not contact the sample edge with the cleaning solution. This process limited the cleaning solution to penetration through the surface of the film only and more realistically simulated cleaning of production-generated films and

residues. To remove the drop, the cleaning solutions were typically rinsed with a benign solvent (IPA) or removed using a glass capillary, then rinsed in IPA.

3.5 Electochemical Cells and Procedures

Two electrochemical cells were fabricated for the generation of radical anions. Both cells were made of glass with high-density polyethylene lids. Polyethylene is chemically resistant to the radical anions and electrochemical solvents. Bulk radical anion generation requires separate anode and cathode compartments to ensure accumulation. Without compartment separation, cathode byproducts or the cathode electrode oxidize, and thus degrade, radical anions. Both cells use a medium porosity (10-15 um pore size) glass frit to separate the working and counter electrode compartments. Generation of radical anions was performed inside the drybox. Electrical and gas connections were made using feedthroughs through the drybox walls with shielded coaxial cables (shield grounded to minimize electrical interference). The smaller cell was designed for rapid generation of radical anions with an integrated sample compartment to avoid solution transfer issues. The larger cell incorporates a UV-visible fiber optic dip probe that enables in-situ radical anion concentration measurement. This cell was modified to allow sample exposure when solution agitation and constant radical anion concentration was required.

3.5.1 Reference electrode

A double-junction reference electrode was constructed based on standard chemicals for non-aqueous environments.[123] To create each chamber and junction, an asbestos fiber

was sealed in the tip of a glass Pasteur pipette. The reference chamber was filled with 0.1 M silver nitrate in acetonitrile. The second chamber was filled with the solvent and electrolyte that were used in the experiment. This chamber provided a buffer against silver ion or acetonitrile contamination. A silver wire was placed in the reference solution which served as the electrode. The two chambers were connected using a piece of Tyvec tubing. A diagram of the reference electrode is shown in Figure 3.1. The reference potential routinely measured 360-400 mV vs SCE as determined by the ferrocene/ferrocenium redox couple. Reported potentials were corrected to SCE using the measured ferrocene/ferrocenium redox potential. The silver ion solution was changed regularly.

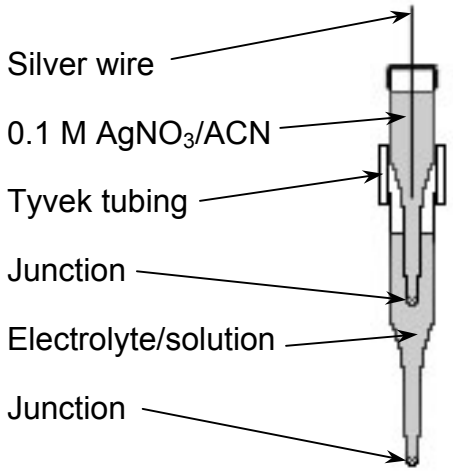

Figure 3.1. Double junction silver/silver ion reference electrode fabricated from two pipettes.

3.5.2 Thin film cell

This electrochemical cell was fabricated in order to facilitate generation of radical anions and subsequent sample exposure to the radical anion solution; this cell is shown in Figure

3.2. A relatively high concentration of radical anions (> 20 mM) is required to rapidly defluorinate surfaces; therefore, a smaller volume cell is ideal. Additionally, radical anions generated in this work are also unstable; therefore, rapid generation is required to maintain high concentrations. This cell is capable of operating with only 0.75 mL of solution in the working compartment and contains a separate compartment allowing treatment of a thin film (~1 square cm) without disassembly of the cell or transfer of solution.

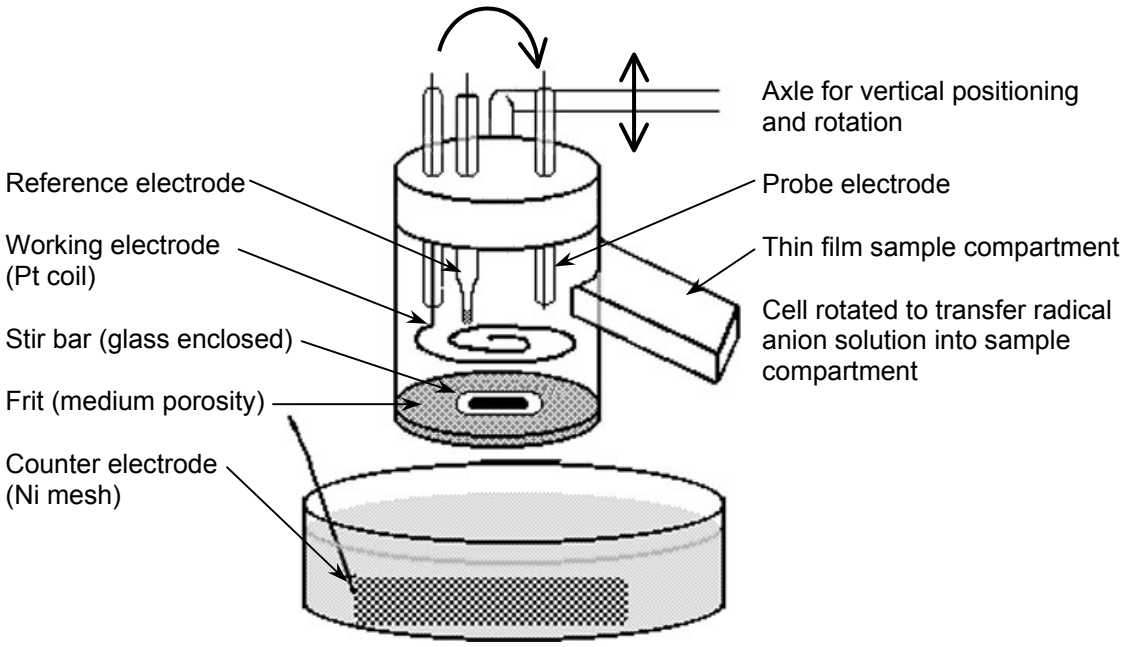

Figure 3.2. Pictorial representation of thin film sample cell.

After radical solution is generated, the cell is tilted to transfer solution. Only one of the two glass enclosed platinum electrodes were connected to the potentiostat at any time. A platinum coil electrode (1.72 cm^2 area) was used to generate radical anions while a second probe electrode, with much smaller area (0.20 mm^2), was used for cyclic voltammetry. A nickel mesh with surface area greater than 25 cm^2 was used for the counter electrode. The working compartment was supported by an axle that pierced the

cover, allowing both rotation and vertical positioning. Area of the medium frit was 1.25 cm^2.

For experiments, nominal concentrations of the background electrolyte (tetrabutylammonium iodide) and naphthalene were 0.1 M. Separate working electrode and counter-electrode compartment solutions were mixed in 4 dram vials. Naphthalene was added only to the working cell solution. Prior to being transferred to the respective compartments, solutions were purged with filtered house nitrogen for at least 15 minutes to remove dissolved oxygen. The volume of the solution that was added to the counter electrode compartment was typically 8-10 mL. The working cell could operate with as little as 0.75 mL and up to 2.0 mL before the sample compartment flooded. A thin film sample was loaded into the sample compartment of the cell. Solutions were added to each compartment and the working electrode compartment was lowered to contact the counter electrode bath. For electrolysis experiments, the magnetic stir bar was activated to provide agitation and preventing species diffusion from limiting the generation rate. For thin film treatments, radical anions were generated galvanostatically. After reaching the desired concentration, the working compartment was raised from the counter electrode solution bath and tilted to transfer the reactive radical anion solution into the thin film compartment. After a specified exposure time, the cell was disassembled and the thin film sample retrieved and rinsed. Disassembly and sample removal typically required less than 3 seconds.

3.5.3 Dip probe cell

The dip probe cell is larger than the thin film cell to accommodate the dip probe. The cell configuration is pictured in Figure 3.3. The cell could accommodate up to 10 mL of solution in the working electrode compartment; however, 2-5 mL was used nominally. A platinum mesh electrode (15 cm^2) was used to generate radical anions. The fiber optic dip probe with a reflective tip provided absorption measurements. Details of this device are given in the next section. A nickel mesh electrode was used as the counter electrode and a glass-coated magnetic stir bar provided agitation of the solution in the cell. Area of the medium frit is 2.85 cm^2. This cell was used for both dip probe measurement and sample exposure when agitation was necessary.

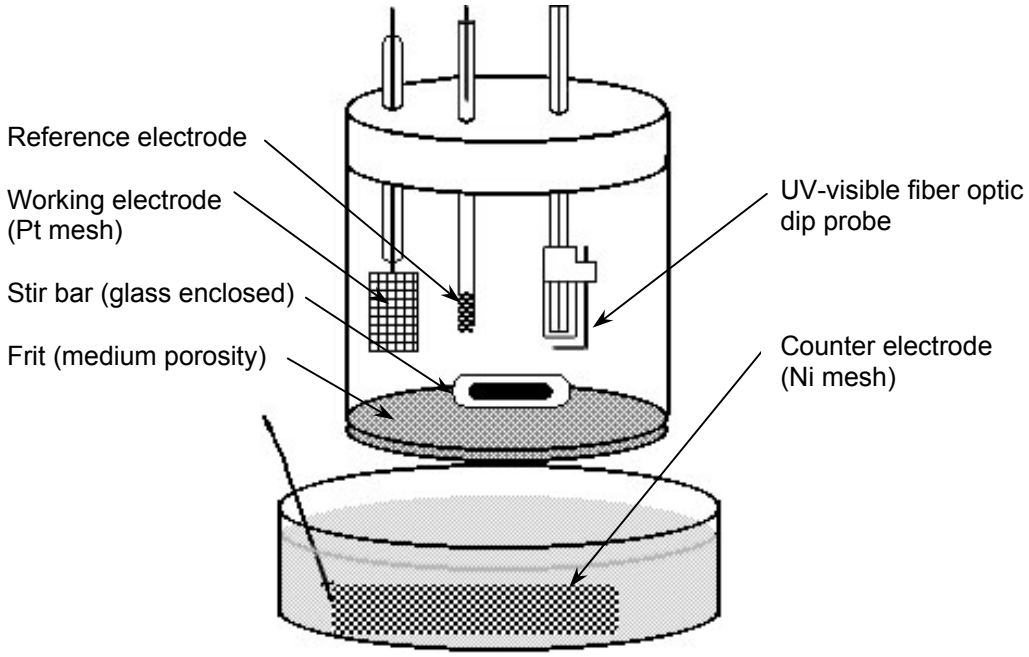

Figure 3.3. Pictorial representation of dip probe cell.

For dip probe/absorption experiments, solutions for each compartment were mixed in a manner similar to that for the previous thin film cell procedure. Solutions were purged with nitrogen for 10 minutes, then added to the respective cell compartments. The volume of working cell solution, which is important for molar absorptivity calculations, was measured using a volumetric flask. A sufficient volume of solution was added to the counter electrode compartment to match the solution level to that in the working electrode compartment. This configuration prevented significant volume changes during experiments by ensuring no hydrostatic pressure difference between the compartments. Dip probe absorption measurements were then conducted.

There are two drawbacks to the thin film cell for sample exposure. There is no way to provide agitation to the solution when the samples are being exposed. Secondly, the larger area frit and subsequent larger electrolysis current enabled generation of higher concentration of radical anions. Agitation and higher radical anion concentration proved to be necessary for effective residue removal. For sample treatments, the dip probe was replaced with a rod connected to a clip that suspended samples above the solution. To expose samples, the sample was lowered into the solution. After a specified exposure time, the cell was disassembled and the sample removed and rinsed.

3.5.4 UV-visible spectroscopy with dip probe

An Ocean Optics model USB2000 spectrometer was used to collect UV-visible spectra. The dip probe consisted of a bifurcated fiber optic probe with a custom-made adjustable reflection tip. One fiber optic cable provided the light source from a tungsten bulb and the other fiber collected reflected light for analysis. A custom tip, shown in Figure 3.4, was fabricated to accommodate the relatively small size of the electrochemical cell.

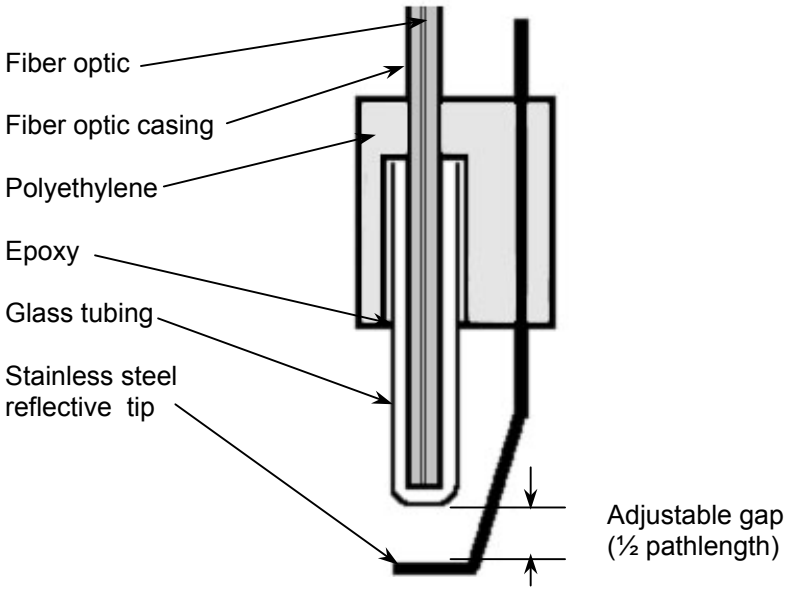

Figure 3.4. Custom made probe tip for in-situ UV-visible measurements.

The steel fiber optic casing acted as an electrode when submerged during electrochemical generation. The tip generated unwanted byproducts and interfered with galvanostatic control of the electrolysis current. The custom made tip enclosed the probe in glass, thus, preventing electrical contact with the solution. A polished stainless steel tip provided reflection. The distance between the glass tip and the reflective tip could be adjusted

from 0.5 mm to 10 mm. The pathlength for absorption calculations is twice the distance between the glass casing and reflective tip. The protective glass tubing was affixed to the polyethylene using epoxy that did not contact the solution. The fiber optic cable is transparent between 250 and 900 nm; however, the glass tip limits the usable range to 400 to 900 nm, primarily in the visible range.

3.5.5 Dip probe measurements

For dip probe measurements, the probe was submerged in the solution. The integral time, which is manually selected in the dip probe software (Ocean Optics OOIBase32), is the amount of time used to sample the light intensity over the entire wavelength range. This value controls the collected signal intensity (gain) and must be optimized to maximize intensity, but must be maintained below the detector saturation level. (4000 counts). Typically, the scan time was set to 30 ms and each spectrum was an average of 5-10 samples resulting in a sampling every 0.15 to 0.30 seconds. A reference spectrum was taken after the probe was submerged in the solution, but before radicals were generated. The absorption spectrum was monitored and specific wavelengths were recorded over time. Absorption is defined as the base ten logarithm of the inverse of the percent transmission (of the reflected light) where the percent transmission is determined by comparison to the reference spectrum. The spectrometer enabled measurement of a maximum absorption value of ~1.0 equating to detection of 10% of the reflected light compared to the reference level.

For each experiment, the software was configured to record absorption values at specified wavelengths, typically several of the maxima in absorption spectrum. Next, the

potentiostat was configured to supply current in the galvanostatic mode at a specific value. An increase in absorption was observed over time. The supplied current was measured by an ammeter in line between the potentiostat and the cell and was typically 0.10-0.15 mA less than the specified current. After 10-20 seconds of application, the potentiostat was turned off. This process was repeated for different currents ranging from 0.25 mA to 20 mA. The ratio between the absorption rate and the current was used to calculate the molar absorptivity. This value was used to determine the concentration of the radical anions; details of the analysis are covered in Chapter 6.

CHAPTER 4

FLUOROCARBON MODEL RESIDUES CHARACTERIZATION

4.1 Overview

In this chapter, plasma deposited etch residue samples received from Air Products and Chemicals, Inc. are characterized. These samples are used to evaluate the effects of different plasma etching parameters on the residue formed during the process. Modified etching variables include different fluorocarbon etch gases, inclusion of oxygen in the feedgas and sample orientation in the plasma chamber. Based on residue characterization, an approach to cleaning is formulated and preliminary cleaning treatments are conducted using sodium naphthalene radical-anion chemistry. The effects of concentration, rinsing and exposure time on the residue samples are evaluated. The penetration rate of the radical anion reaction is determined and modeled.

4.2 Characterization of Fluorocarbon Residues

In order to develop effective cleaning processes for post-etch fluorocarbon residues, it is important to determine the chemical composition and bonding structure of the target residue. The plasma etching environment can have a significant effect on the residue composition, chemistry and adhesion to the substrate. These factors are important in the development of approaches for cleaning processes and in establishing an understanding of removal mechanisms. First, the effect of fluorocarbon plasma etch parameters on residue chemistry is determined.

4.2.1 Deposition parameters

'Model' etch residue samples were provided by Air Products and Chemicals Incorporated (APCI) and used to understand the effect of plasma process conditions on the residue formed during fluorocarbon etching processes. This first set of consisted of 9 different runs and was used specifically to investigate the effect of the fluorocarbon species, the addition of oxygen in the feedgas and the orientation of the sample with respect to the electrodes on the deposited fluorocarbon film.

Bare silicon wafers (4 inch) were exposed to plasma etching environments in a commercial RF (radio frequency) parallel plate RIE (reactive ion etch) etcher. Chamber pressure was maintained at 50 mTorr with 200 W of power (1.1 W/cm^2) and 200 sccm total feedgas flow. Fluorocarbon etch feedgases consisted of varying amounts of the fluorocarbon etch gas, oxygen and argon, typical for standard etch recipes. No surface cleaning or pre-treatment was performed on the wafers prior to processing. The process conditions for each run is described in Table 4.1.

Table 4.1. Process parameters for residue samples as specified by APCI

Run ID	Etch Gas	Etch Gas Flow (sccm)	Oxygen Flow (sccm)	Argon (sccm)	Process Time (min)	Orientation
1	C_4F_6	12	24	64	2	Horiz.
2	C_4F_6	12	0	88	1	Horiz.
3	c-C_4F_8	12	6	82	2	Horiz.
4	c-C_4F_8	12	0	88	1	Horiz.
5(V)	c-C_4F_8	12	6	82	2	Vertical
6(V)	C_4F_6	12	24	64	2	Vertical
7(V)	c-C_5F_8	12	15.6	72.4	2	Vertical
8	c-C_5F_8	12	15.6	72.4	2	Horiz.
9	c-C_5F_8	12	0	88	1	Horiz.

The three fluorocarbon etch gases utilized for plasma residue generation were linear-C_4F_6, cyclic-C_4F_8 and cyclic-C_5F_8. The chemical structures are shown in Figure 4.1.

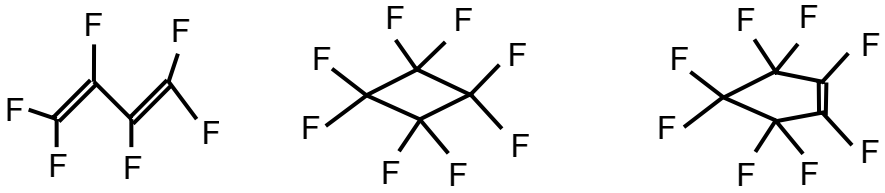

Figure 4.1. Chemical structures of the etch feedgases.

Samples were either oriented horizontally (conventional orientation with wafer on lower electrode/chuck) or vertically using a specially designed quartz holder that positioned two samples 1 mm apart oriented normal to the plasma. The latter orientation attempts to simulate plasma deposition on via sidewalls where ion bombardment is minimal, and deposition occurs to prevent lateral etching. The ratio of etch gas to oxygen was chosen by APCI based on experience with silicon dioxide etching recipes. The argon flow rate was adjusted to maintain a constant overall flowrate and residence time in the chamber. For runs that included oxygen in the feedgas, the process time was one minute whereas runs without oxygen addition were two minutes. Under the specified conditions, some combinations likely do not etch silicon dioxide anisotropically (runs with high deposition rate); however, the runs were included for comparison.

4.2.2 Thickness measurement

The thickness of each residue sample was measured by spectroscopic ellipsometry. The Cauchy model, which is the standard model for evaluation of polymer films, was used as the material model for the fluorocarbon residue.[121] Complete details about fitting

ellipsometry data to Cauchy models is described in Chapter 3. The complete model stack consisted of a 0.5 mm silicon substrate, a 20 angstrom layer of native silicon dioxide and the fluorocarbon residue. A 20 angstrom native oxide is typical of untreated silicon wafers exposed to air.

For all but samples 2 and 9, determination of both the refractive index and thickness of the fluorocarbon using a Cauchy model was unsuccessful. Using the conventional method of minimization of the error between the data and model, unrealistic values were obtained which is likely due to the small sample thickness. For the thicker samples (2 and 9), the resulting model parameters were reasonable and the refractive index was similar to literature values of 1.46-1.48.[23,126] In order to measure the remaining samples, Cauchy model parameters from sample 2 were utilized in the model which essentially set the refractive index for each film to that of sample 2. This procedure allowed determination of the film thickness for the remaining samples. Ellipsometry results are shown in Table 4.2.

Table 4.2. Spectroscopic ellipsometry measurements of the fluorocarbon residues

Sample	Sample Description *	Thickness (nm)	Color (Visual)
1	C_4F_6 - 24 O_2	4.54	None
2	C_4F_6 - 0 O_2	220	Yellow
3	C_4F_8 - 6 O_2	2.27	None
4	C_4F_8 - 0 O_2	4.91	None
5(V)	C_4F_8 - 6 O_2	0.38	None
6(V)	C_4F_6 - 24 O_2	2.80	None
7(V)	C_5F_8 – 15.6 O_2	3.25	None
8	C_5F_8 – 15.6 O_2	1.74	None
9	C_5F_8 - 0 O_2	125	Blue

* Sample description includes fluorocarbon gas and oxygen flowrate in sccm

Visual observation agreed with the film thickness measurements. The two thicker samples appeared yellow and blue while the thinner samples displayed no apparent color. In the absence of oxygen in the feedgas, the two etch gases that contain double bonds (C_4F_6 and c-C_5F_8) deposited rapidly on the substrate surface. The mechanism is likely similar to free radical polymerization wherein a free radical reacts with a double bond forming another radical. This chain reaction process likely occurs on the wafer surface causing rapid film formation.

For the remaining samples, it is unclear if the deposition was extremely slow or if a steady state film thickness existed. Steady state or constant thickness residues have been observed with thicknesses ranging from 2.0 to 20 nanometers depending on the surface, etch gas, power and reactor configuration; film deposition typically requires less than one minute to reach steady state.[18,20,23] Unfortunately, depositions with similar feedgas, but differing process times were requested from APCI, but never received. Based on the process time and the relative thinness of the samples, the film was likely a slowly depositing film. Research has shown that, in the absence of oxygen in the substrate, silicon dioxide etching atmospheres result in a steady film deposition. This would be the case for silicon surface exposure to a silicon dioxide etching atmosphere. This is the basis for selectivity while etching silicon dioxide over silicon, which is strongly dependent on the plasma power and oxygen to fluorocarbon ratio.

In all cases, oxygen addition to the etch feedgas reduced the thickness of the observed fluorocarbon deposition. This is a result of film etching by the formation of volatile and

stable byproducts such as CO, CO_2 and COF_2. Cleavage of carbon-fluorine bonds is aided by ion bombardment. Etching of the fluorocarbon film by oxygen species is necessary to prevent deposition of thick fluorocarbon films that inhibit reactive species from reaching the silicon dioxide interface. High deposition rates, demonstrated by samples 2 and 9, illustrate the result when oxygen is not included in the etch gas formulation. Although the ratio of the oxygen to fluorocarbon in the feedgas was varied, the molecular differences in the fluorocarbon feedgases confound any effects.

Fluorocarbon deposition was detected on samples aligned vertically in the etch chamber. If the vertical samples properly simulate sidewalls, the samples should not experience significant ion bombardment. Again, comparison of the effect of the fluorocarbon gas is confounded by the varied ratio of oxygen to fluorocarbon in the feedgas; however, comparisons can be made between the horizontally and vertically oriented samples etched using similar recipes. For etch residues formed using C_4F_8 and C_4F_6, deposition on the vertically aligned samples is less than that on the horizontal sample; however, the opposite phenomenon is observed with the C_5F_8 samples. If physical sputtering dominates during etching, the deposition rate will be higher on the sidewalls (or vertical surfaces) than on the horizontal surfaces; if adsorption is rate controlling, sidewall deposition rates will be lower. Since examples of both scenarios exist in these data, no definitive conclusion can be drawn, except that fluorocarbon films form on vertically oriented samples and the thicknesses are comparable to those on horizontal surfaces.

4.2.3 Contact angle measurement

Measurement of water contact angle on surfaces is an extremely surface sensitive technique and can be used to detect changes in the surface chemistry. Additionally, the ability of an aqueous solution to 'wet' a residue is important for cleaning small features, dissolving a film and/or attacking an interface. The water contact angle of each sample was measured and the results are shown in Table 4.3. For comparison, the contact angle of polytetrafluoroethylene (PTFE), is 114°. Contact angles of plasma deposited fluorocarbon films typically range between 60° and 100° depending on the extent of fluorination.[126] As expected, the contact angle correlates well with the fluorine to carbon ratio (measured by XPS) with an r-squared correlation coefficient of 0.90. Because of the thickness of the thinner films and the possibility of non-continuous layers, the underlying hydrophilic silicon dioxide layer may influence the contact angle measurement.

Table 4.3. Contact angle measurements of fluorocarbon residues

Sample	Sample Description	Contact Angle (Static)
1	C_4F_6 - 24 O_2	83
2	C_4F_6 - 0 O_2	94
3	C_4F_8 - 6 O_2	81
4	C_4F_8 - 0 O_2	91
5(V)	C_4F_8 - 6 O_2	64
6(V)	C_4F_6 - 24 O_2	53
7(V)	C_5F_8 – 15.6 O_2	59
8	C_5F_8 – 15.6 O_2	79
9	C_5F_8 - 0 O_2	102

4.2.4 X-ray photoelectron spectroscopic characterization

To determinate chemical composition and bonding structure, high resolution XPS analysis was performed on each sample. The atomic compositions calculated from the XPS spectra are reported in Table 4.4. Carbon, fluorine and oxygen were detected in all

films. Deconvolution of high resolution XPS spectra is detailed in Chapter 3 and the deconvoluted spectra of all detected spectral peaks for each sample is located in Appendix A. The underlying silicon and silicon dioxide from the substrate was observed in all but the thick samples (2 and 9) because the XPS probing depth is greater than the thickness of the films. Oxygen is detected in all films, even those where oxygen is not a feedgas in the etch process. Oxygen contamination is common with plasma deposited fluorocarbon films by reaction of trapped free radicals with oxygen or water vapor upon exposure to air after deposition.[30] The underlying silicon dioxide also contributes to the measured oxygen concentration.

Table 4.4. XPS elemental analysis of fluorocarbon residues.

Sample	Sample Description	F:C Etch Gas	Atomic Composition (at%) C	O	F	Si	F:C*
1	C_4F_6 - 24 O_2	1.5	48	10	36	6	0.74
2	C_4F_6 - 0 O_2	1.5	54	4	42	0	0.78
3	C_4F_8 - 6 O_2	2	37	20	23	20	0.61
4	C_4F_8 - 0 O_2	2	44	5	46	5	1.05
5(V)	C_4F_8 - 6 O_2	2	28	31	11	30	0.39
6(V)	C_4F_6 - 24 O_2	1.5	30	27	14	29	0.49
7(V)	C_5F_8 – 15.6 O_2	1.6	32	27	16	25	0.49
8	C_5F_8 – 15.6 O_2	1.6	44	19	20	17	0.47
9	C_5F_8 - 0 O_2	1.6	53	4	43	0	0.83

* Calculated based on total carbon and total fluorine content

The fluorine to carbon ratio is a common method for comparison of plasma deposited fluorocarbon films. Adhesion, hydrophobicity, and dielectric constant are dependent on this ratio.[67] For the samples deposited without oxygen in the feedgas, the fluorine to carbon ratio correlates with the fluorine to carbon ratio in the etch feedgas. Oxygen addition to the feedgas reduces the fluorine to carbon ratio observed in the residues due to enhanced etching of the film, resulting in a more crosslinked, less fluorinated residue.

The incorporation of oxygen in the feedgas affected the cyclic etch gases (C_4F_8 and C_5F_8) much more significantly than the linear feedgas. This phenomenon is discussed later in this section.

More detailed information can be gained by high resolution analysis of the XPS spectra for each element. Using known binding energy values for various bonding configurations, the elemental peaks can be deconvoluted. The location and shape of the sub-peaks are fairly obvious in the overall high resolution spectrum as shown in Figure 4.2. The carbon peak can be divided into the following bonding configurations: CF_3 (294.0 eV), CF_2 (292.1 eV), CF (289.5 eV), $\underline{C}$-CF_x (287.3 eV) , C-C/C-Si/C-H (285 eV).[126] Because the film is plasma deposited, it is expected that no unsaturation exists and all carbon atoms contain four single bonds. For example, CF implies a carbon center bonded to three other carbons and one fluorine atom. From the oxygen and silicon spectra, various amounts of C-O, Si-O, Si-Si, C-F and Si-F bonds are also detected in each of the samples. The Si-Si and Si-O bonding arise from the silicon substrate. Si-F and Si-C bonding are typical at the interface of fluorocarbon residues.[26] Finally, F-C and C-C bonds result from the fluorocarbon residue and C-O bonds result from either surface contamination or are incorporated into the bulk of the film during deposition.

The carbon 1s XPS spectrum for each film deposited without and with oxygen is shown in Figures 4.2, 4.3 and 4.4. Interestingly, only the C_4F_6-based residue did not change significantly with the addition of oxygen. With the addition of oxygen in the feedgas, the residues generated using the cyclic gases (C_4F_8 and C_5F_8) became much more carbon rich

and the percentage of carbon-carbon bonding increased considerably. The obvious major difference between the etch gases relates to the cyclic nature of the structure. The strain of the four-member ring and the five-membered ring containing a double bond counteract any stability enhanced by their cyclic nature. In addition, no resonance structures are possible that would have improved stability. Additionally, the larger molecular size and thus collision cross section of the cyclic molecules increases the probability of collisions resulting in increased fragmentation, but this resulted in little structural differences in the films produced without oxygen. If the cyclic molecules are predominately deposited on the growing surface, their lack of stability may enhance etching by oxygen radicals. In typical fluorocarbon plasmas, however, deposition occurs primarily by small CF_x radicals.[16] Based on information available, no definitive explanation can be offered for this phenomenon at this time.

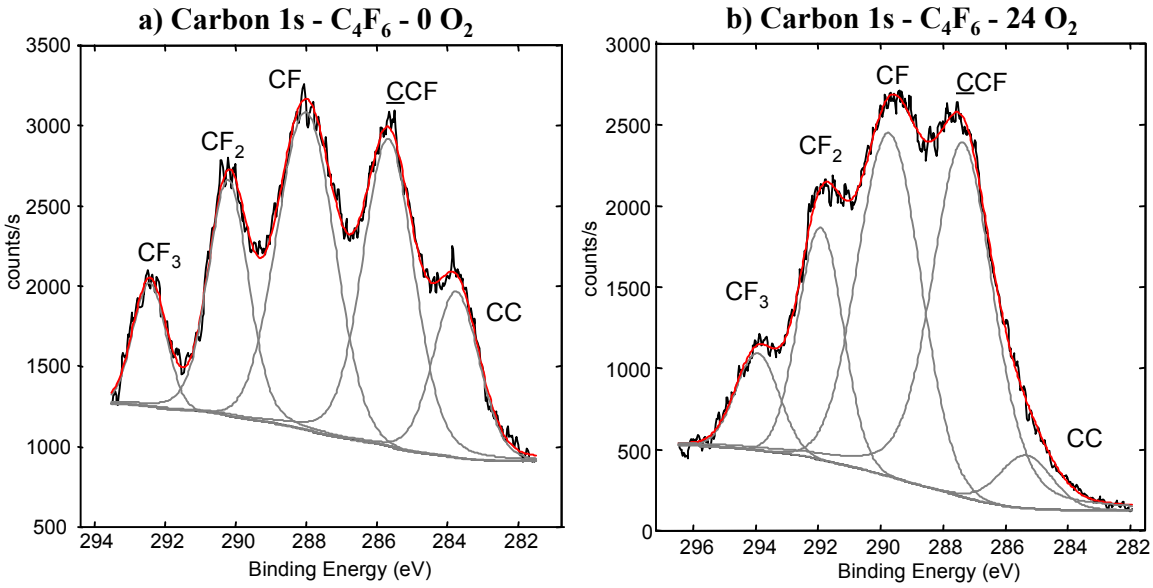

Figure 4.2. Carbon 1s XPS analysis of sample 2 (a) and sample 1 (b) to demonstrate the effect of oxygen in the feedgas with C_4F_6 residues

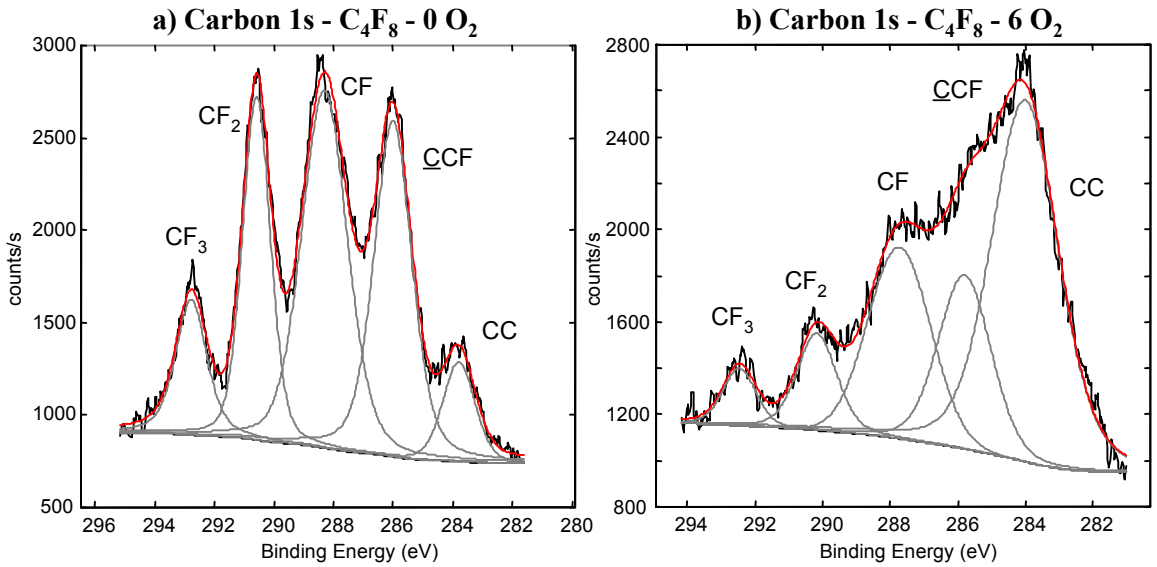

Figure 4.3. Carbon 1s XPS analysis of sample 4 (a) and sample 3 (b) to demonstrate the effect of oxygen in the feedgas with C_4F_8 residues

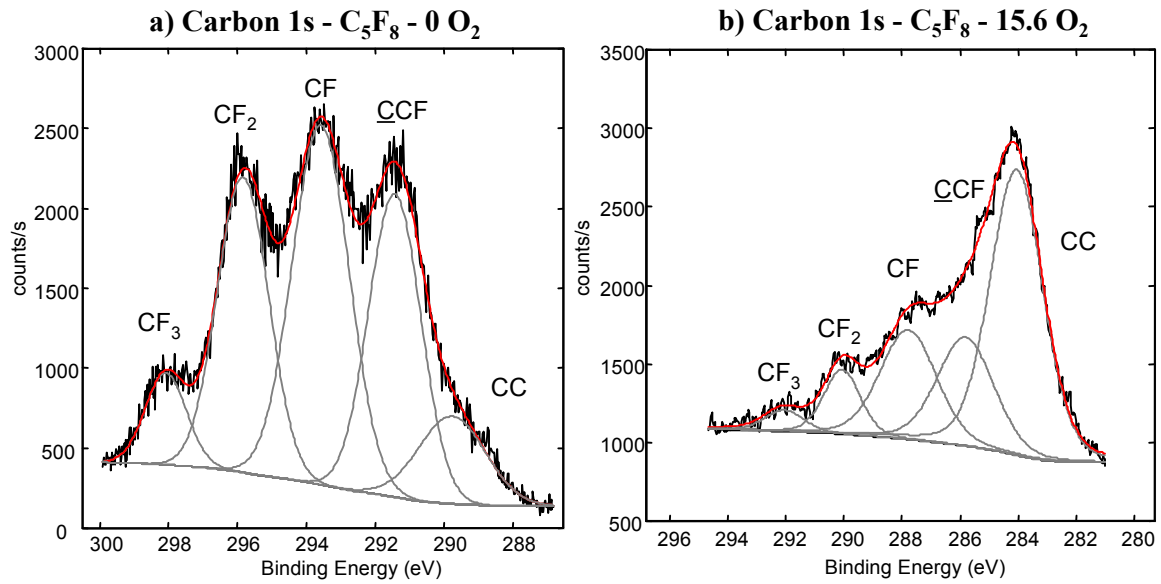

Figure 4.4. Carbon 1s XPS analysis of sample 9 (a) and sample 8 (b) to demonstrate the effect of oxygen in the feedgas with C_5F_8 residues

4.2.5 Crosslink density estimation

Based on the curve fitting of high resolution XPS analysis, the percentage of each type of carbon bonding structure present is quantified and shown in Table 4.5.

Table 4.5. Comparison of CF bonding structure in each sample.

Sample	Sample Description	Percent of each bond in carbon peak				
		C-C	C-CF_x	-CF	-CF_2	-CF_3
1	C4F6 - 24 O_2	14.0	29.5	31.6	17.8	7.0
2	C4F6 - 0 O_2	4.5	38.9	33.8	16.2	6.6
3	C4F8 - 6 O_2	49.0	17.8	21.5	7.8	3.9
4	C4F8 - 0 O_2	6.7	28.7	34.9	20.2	9.6
5 (V)	C_4F_8 - 6 O_2	60.7	18.7	12.8	3.2	4.6
6 (V)	C_4F_6 - 24 O_2	51.3	17.5	17.1	8.6	5.4
7 (V)	C_5F_8 – 15.6 O_2	43.2	26.8	18.6	7.4	4.0
8	C5F8 - 15.6 O_2	49.4	20.1	20.1	7.8	2.8
9	C5F8 - 0 O_2	10.9	21.2	38.5	23.2	6.2

Using this information, the percentage of crosslinking in each film can be estimated. A previous method proposed an estimation by the summation of the carbon moieties that participate in crosslinking (carbons bonded to 3 or 4 other carbons - CC, CCF, CC moieties) divided by the total number of carbons atoms.[26] This results in the percentage of carbons that crosslink, but may not be indicative of the true crosslink density. For example, only a single crosslink can originate from a CF carbon; however, two crosslinks can originate from a CC center. The carbon moieties are treated equally in the method mentioned above. In addition, any branching or chain termination by a CF_3 carbon is not taken into account. Thus, a weighted estimation is proposed to provide a more accurate assessment of crosslink density. This approach is described in Equation 4.1.

$$Crosslink\% = \%(CC) + \%(CCF) + \frac{\%(CF)}{2} - \frac{\%(CF_3)}{2} - \frac{\%(CO)}{2} \qquad (4.1)$$

Each CF center accounts for half of a crosslink while a CC or a CCF atom account for 2 halves (or one) of a crosslink. A CF_3 group or a CO bond terminate a location where half of a crosslink could occur; therefore, they are subtracted. The amount of carbon-oxygen bonds that are present is determined from the oxygen XPS spectra and are typically less than 4 at%. Since the numbers are already percentages, there is no need to divide by the total number of carbons. This is designated as method 1.

Another estimation (method 2) of crosslinking density can be determined by normalizing the fluorine to carbon ratio between the maximum and minimum crosslinking possible in fluorocarbon materials. Diamond or graphite can be considered the maximum crosslinked material with a fluorine to carbon ratio of 0. The minimum crosslinked fluorocarbon is polytetrafluoroethylene with a fluorine to carbon ratio of 2.0 (excluding ends of chain). By normalizing the fluorine to carbon ratio between 0 and 2.0, a percentage can be obtained. For APCI samples, this generally yields higher crosslinking estimates relative to method 1, but the results correlate well for these two approaches. Method 2, however, neglects carbon-oxygen bonds and assumes that only carbon and fluorine are present. The presence of oxygen would further reduce the crosslinking percentage estimation. While these methods only provide estimates, relative comparisons are valid. Table 4.6 shows the results of crosslink density calculations using the two different methods. In addition, an alternative, more accurate determination of the fluorine concentration is listed. In this determination, the amount of silicon-fluorine is

subtracted from the total amount of fluorine resulting in a more accurate determination of the fluorine to carbon ratio (F:C*).

Table 4.6. Calculation of fluorine to carbon ratio and crosslinking percentage estimates

Sample	Sample Description	F-C in F 1s Spectrum (%)	F:C*	% Crosslinked Method 1 **	% Crosslinked Method 2 ***
1	C4F6 - 24 O_2	35	0.72	53	64
2	C4F6 - 0 O_2	39	0.73	55	64
3	C4F8 - 6 O_2	20	0.53	75	74
4	C4F8 - 0 O_2	46	1.05	47	48
5 (V)	C_4F_8 - 6 O_2	8	0.28	82	86
6 (V)	C_4F_6 - 24 O_2	12	0.39	73	81
7 (V)	C_5F_8 – 15.6 O_2	14	0.43	77	78
8	C5F8 - 15.6 O_2	15	0.35	76	83
9	C5F8 - 0 O_2	40	0.75	47	63

* Fluorine to carbon that neglects fluorine bonded to silicon
** Method 1 is based on weighted amounts of CF_x moieties
*** Method 2 is based on the fluorine to carbon ratio

The carbon 1s XPS spectra samples aligned vertically (samples 5-7) are similar to those of the horizontal samples with similar etch recipes. If the vertically aligned samples truly represented films formed on via sidewalls, they should have experienced little ion bombardment; however a significant amount of crosslinking is observed. The high crosslink density implies that the vertically oriented samples do not effectively mimick sidewall depositions. The 1 mm separation may also be too large to assume only vertical ion bombardment. Additionally, the quartz holder and vertical samples may have interfered with the sheath which controls the direction of ion bombardment.

4.2.6 Other characterization techniques

For the thick film samples (2 and 9), attempts were made to determine if the oxygen contamination was present in the bulk of the film or if it was only present at the surface.

Both angle resolved XPS and depth profiling by argon sputtering techniques were attempted. Angle resolved XPS analysis is used to determine compositional changes in a film with depth and determine if the surface is compositionally different from the bulk film. Measurements at different detector angles relative to the sample, probe the film to varying depths. If composition does not change as a function of detector angle, the surface reflects the bulk; otherwise, the surface is different from the bulk. On sample 2, the carbon to oxygen ratio changed from 7.2 to 8.6 with detector angles from 25° to 75° (with respect to normal) indicating a higher oxygen concentration at the surface. This analysis, however, does not prove the absence of oxygen in the bulk of the film; rather it simply demonstrates an oxygen gradient and higher concentrations at the surface.

Depth profiling by argon sputtering during XPS analysis is also common. Argon sputtering of samples 2 and 9 resulted in selective removal of both oxygen and fluorine as well as increasing carbon crosslinking. The resulting sputtered surface appeared drastically different from the original surface and likely did not reflect the bulk film; therefore, these results are inconclusive. Argon sputtering is often ineffective for polymer depth profiling because polymers are not uniformly removed by sputtering.

FTIR analysis should give conclusive evidence of oxygen incorporation into the film if the presence of C-O bonds are detected. Both transmission and reflectance techniques were attempted with as many as 4048 scans; however, meaningful spectra were not obtained. The thinness of the film and scattering from the single sided polished silicon wafer were likely responsible for the failure to produce a reliable FTIR spectrum. Typical

films on silicon substrates for FTIR analysis are normally at least 0.5 microns thick with a double sided polished wafer to reduce scattering.

4.3 Conventional Cleaning of Fluorocarbon Etch Residues

Etch residue samples were exposed to conventional cleaning chemistries to establish a baseline for comparison to experimental approaches. Table 4.7 shows surface composition, based on XPS results, for films generated with C_4F_6/O_2 gas (sample 1) after various cleaning treatments. Sample 1 was treated with common semiconductor cleaning chemistries. It is convenient to evaluate film thickness and cleaning ability by monitoring the underlying silicon in surface XPS composition analysis; higher silicon content indicates at least partial removal of the fluorocarbon film.

Table 4.7. Chemical treatments and XPS analysis of sample 1

Chemical	Exposure Time (min)	Temperature (°C)	Carbon (at%)	Oyxgen (at%)	Fluorine (at%)	Silicon (at%)
Control (None)	-	-	50.5	12.6	31.9	5.1
Deionized water	4	55	49.0	13.8	31.1	6.1
Hydrogen Peroxide	4	55	48.8	14.3	31.1	5.8
TMAH	20	20	46.3	20.1	22.0	11.7
TMAH	4	54	41.9	20.8	21.9	15.4
Hydrofluoric Acid	0.5	20	42.5	10.7	42.9	3.9
TPM	4	50	18.3	35.7	8.0	38.0
APM	4	60	13.8	39.8	4.9	41.5

Key: TPM – Tetramethyl ammonium hydroxide, hydrogen peroxide, water (1:1:5 vol)
APM – Ammonium hydroxide, hydrogen peroxide, water (1:1:5 vol)

No chemical changes were observed from exposure to deionized water (DIW) or hydrogen peroxide at room or elevated temperatures. Tetramethylammonium hydroxide is commonly used as a photolithographic developer in the IC industry; however, experiments in our lab demonstrate a limited cleaning capacity on some residues with a

concentrated version (25 wt% TMAH in water). Exposure to TMAH in water attacks and modifies the surface, but removal is incomplete. XPS results indicate removal of some CF_2 and CF groups; however, CF_3 and C-C moieties remain unchanged. Hydrofluoric acid treatments were unable to undercut the residue and little modification was observed, likely due to an inability to wet and penetrate the fluorocarbon residue. The SC-1 step of the RCA clean (ammonium hydroxide/hydrogen peroxide/DIW) is typically used for removal of organic contamination. This treatment cleaned the surface most effectively. Complete removal of fluorinated carbon is observed; however, some residual Si-F bonds remain on the surface. Replacement of ammonium hydroxide with TMAH in the SC-1 clean was equally effective at removal.

Exposure of sample 2 or 9 (thicker residues) to any wet chemical treatment except DIW caused rapid lift off of the film. Apparently, the lack of oxygen in the feedgas resulted in a poor interface between the film and the substrate.

4.4 Significance of Structure on Cleaning

The high degree of crosslinking observed in all residues will prevent residue removal by simple dissolution with a solvent. Several viable options remain for effective cleaning of this residue. If an underlying film is present, such as photoresist, solvent molecules could penetrate through the residue and dissolve the photoresist, thus lifting off the residue. Finding a solvent to wet or penetration a fluorocarbon film can be difficult. Another concern with this removal mechanism is that soluble underlying photoresist films can become crosslinked by the radiation in the plasma atmoshphere or intentionally to

improve etch resistance. In addition, an insoluble underlying film is not present with residues located on the sidewalls and bottoms of via structures. To undercut these residues, silicon dioxide, copper or barrier layers must be etched, which is undesirable, but is currently the most effective and common removal technique.

Similar to removal by undercutting an underlying material, a residue can be removed by wetting of the interface between the residue and the substrate similar to the role of surfactants. To remove an organic from a hydrophillic surface such as silicon dioxide, the ideal molecule would posses a hydrophillic end and an organic end. The same issues are important with wetting the residue and allowing penetration of solvent through the film. The low surface energy of fluorocarbon materials generally prohibits wetting. The presence of interface bonding, such as silicon-carbon bonds, could also inhibit this removal mechanism. These bonding structures were detected by XPS on the thin film samples.

Wetting of small features is also an issue for cleaning of residues. Low surface energy fluorocarbon materials can inhibit wetting of small features. The capillary force, which drives wetting of small features, is proportional to the cosine of the solid-liquid contact angle. As the angle approaches 90 or higher, the forces approaches zero or becomes negative (>90). Aqueous-based liquid cleaning solutions would not effective at wetting features coated in fluorocarbons that have a water contact angle approaching 90 or higher.

The conventional cleaning method using aggressive chemical oxidizers, primarily OH radicals, to unselectively cleave carbon-carbon bonds. That lack of selectivity is problematic with organic containing low-k materials. The possibility of selective cleavage of carbon-carbon exists, but, based on the chemical composition of the fluorocarbon residue, poses challenges. Cleavage on nonpolar single carbon-carbon bonds should be avoided to prevent cleavage of silicon-carbon or hydrocarbon bonds typically found in low-k materials. The possibility of cleaving carbon centers bonded to a CF_3 or CF_2 group is unlikely due to fluorine shielding and sterric hindrance. Selective oxidation of moderately polarized bonds such as CF-C-C may be possible, but the author is unaware of any chemistry capable of such selective cleavage that could be practically implemented.

Overall, the type of fluorocarbon etch gas did have an effect on the residue structure. The fluorocarbons that contained a double bond deposited significantly, however; the presence of oxygen in the feedgas negated the high deposition rate. In general, a greater amount of oxygen may be necessary for fluorocarbon etch gas recipes where the etch gas contains double bonds compared to those that do not. The fluorine to carbon ratio of the resulting residue, which predicts the wetting behavior, correlated with the fluorine to carbon ratio of the feedgas. The depositions without oxygen contained roughly the same proportion of carbon moieties. The addition of oxygen resulted in a decrease in the fluorine to carbon ratio (and increase in crosslinking) with the cyclic feedgases, but had little effect on the linear feedgas.

With respect to cleaning, more heavily crosslinked films are more difficult to remove if dissolution is the mechanism. If simple liftoff is the mechanism, then crosslinking is not as important, however, penetration of the film and wetting become the significant factors. The cyclic etch gases with oxygen produced the lowest fluorine to carbon, and thus most wetting films. Because of the heavy crosslinking and the desire to avoid unselective oxidative chemistry, a cleaning mechanism based on liftoff would be the most favorable for these residues.

The small degree of oxygen incorporation (< 4 at%) into the residue is not significant for formulating cleaning strategies. The differences in etch gases does have an effect on the chemical composition of the residue. In two of the three cases, the incorporation of oxygen decreases the fluorine to carbon ratio significantly and crosslinks the film. Both methods of crosslink estimates infer at least a 48% crosslink density, which is extremely high by polymeric standards. The addition of oxygen may also cause greater adhesion between the residue and the substrate.

For formulation of etch gas recipes based on minimizing the cleaning required, saturated etch gases are preferred versus unsaturated. Oxygen incorporation into the feedgas may be dictated to control the deposition rate. With the saturated etch gas (linear-C_4F_6), oxygen is not required and can be used to control other etch parameters. Further oxygen should be minimized to minimize the degree of cross-linking in the residue. The carbon to fluorine ratio in the feed gas also correlate with the ratio in the deposited residue. A larger F:C ratio prohibits wetting, while a lower ratio likely infers higher crosslink

density. Neither of these effects are desired for residue removal. While plasma etch parameters such as the feedgas species and relative amounts will be optimized primarily based on the performance of the etch process, removal of the post-etch residue should also be a considered.

4.5 Cleaning Approach Using Radical Anions

Conventional cleaning of post etch fluorocarbon residues typically involve several process steps with at least one being based on oxidative chemistry. Examples include oxygen ashing, oxygen RIE or solutions of sulfuric acid and hydrogen peroxide. With the incorporation of low-k materials containing organic components, these strongly oxidative approaches are no longer selective to the residue.

An alternative chemical approach is using a reductive chemistry. Alkane or siloxane components in low-k materials are generally inert to reducing chemistries. As discussed in Chapter 2, radical anions are commonly used in organic chemistry as reducing agents and can produced easily using conventional components and ambient temperatures. The crosslinked nature of the residues prevent simple dissolution unless carbon-carbon bonds are broken; however, radical anions can be used to modify the fluorocarbon residue making it more susceptible to removal by other means. In addition, wetting of the residue is also important for cleaning of small features and enabling penetration through the residue to cause undercutting. Although sodium is incompatible with IC processing, sodium naphthalene radical anions are stable and can be generated easily. Radicals based

on this chemistry will be used to modify model etch residues and to demonstrate feasibility of the approach residues.

4.6 Etch Residue Treatment Using Sodium Naphthalene Radical Anions

4.6.1 APCI residue for cleaning evaluation

The first set of APCI model etch residues were inadequate for evaluation of cleaning treatments. The thick samples delaminated with exposure to organic solvents. The thin samples were difficult to characterize. The index of refraction could not be measured and the underlying silicon dioxide confounded XPS of the residue measurements and estimations of penetration depth of the reaction.

APCI supplied us with a new etch residue sample that was generated in a high density plasma reactor using a C_4F_6/O_2 recipe and an exposure time of 175 seconds. This new residue was thicker and more chemically resistant. Complete process details are given in Chapter 3. The six-inch wafer on which the sample was deposited was relatively non-uniform with a thickness of 230 nm at the center and 200 nm near the edge. The carbon 1s XPS spectrum of the sample is shown in Figure 4.5. The atomic concentration measured 49.6 at% carbon, 45.7 at% fluorine and 4.7 at% oxygen. The resulting F:C ratio is 0.92 and crosslink density estimates are 46% and 54% using method 1 and method 2, respectively. This sample is designated sample AP2-1 and will be used to evaluate residue cleaning throughout the remainder of this chapter. Due to the non-uniformity over the six-inch wafer, the XPS composition and carbon 1s XPS spectra may vary somewhat. Experiments were typically conducted on 1 cm square samples cleaved

from the original wafer. To make comparisons for each experiment, samples were cleaved in close proximity. One sample from the group was always re-analyzed as a control.

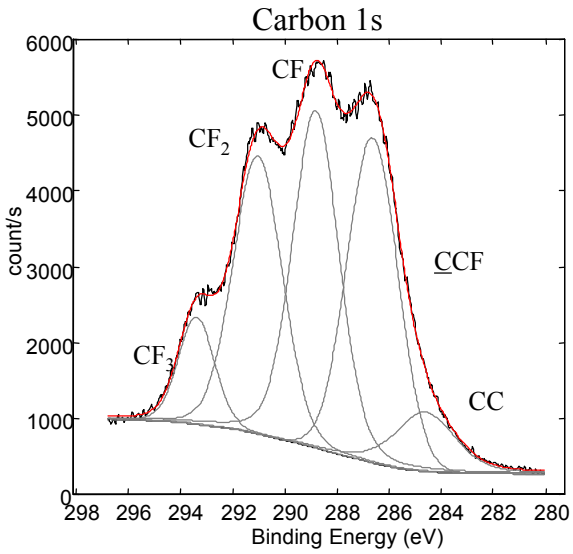

Bond	Percentage
CC	7.29
CCF	29.42
CF	30.59
CF_2	25.49
CF_3	7.21

Figure 4.5. Carbon 1s XPS spectrum of APCI sample AP2-1. To the right, the relative percent of each carbon moiety is shown.

4.6.2 Defluorination of flurocarbon films using sodium-naphthalene solutions

As a basis for comparison and to demonstrate feasibility, solutions of sodium naphthalenide in tetrahydrofuran (THF) were used for initial defluorination treatments on sample AP2-1. Solutions of sodium naphthalene radical anion were prepared as described in Chapter 3. Radical naphthalene-based solutions were selected because of the high rate of defluorination of PTFE as compared to other polycyclic aromatic hydrocarbons.[79] Naphthalene radicals react 50-times faster than anthracene. In addition, solutions of sodium naphthalene are stable over time and the concentration of radicals can be determined relatively accurately.

Unless otherwise specified, 100 mM solutions of naphthalene were used for defluorination treatments. Radical concentrations were measured using two techniques. Recall that naphthalene radical anions react rapidly with water, forming equimolar amounts of dihydronaphthalene and naphthalene. The loss of opacity of the radical anion solution can be observed allowing destructive titration of the radical using water. Titration was completed using a syringe with 0.1 μl precision. The second technique is atomic absorption measurements of sodium ions in solution. The concentration of sodium ions in the solution equates to the concentration of sodium naphthalene ion pairs. Atomic absorption measurements and calibration are described in Chapter 3. The solubility of sodium metal (with no PAH) in the THF was found to be negligible. Measurements of the radical using the two techniques yielded radical concentrations of 85-90 mM using a 100 mM solution of naphthalene. These values agree with literature where the equilibrium concentration is listed as 0.85.[76] Throughout this work, the solution described as 100 mM sodium-naphthalenide implies that the solution contains 85-90 mM concentration of radical anions.

X-ray photoelectron spectroscopy (XPS) was the primary tool used for surface characterization of plasma residues following sodium naphthalene defluorination treatments. Upon exposure to the radical anion solution for more than five seconds, the AP2-1 sample color changed from light to dark yellow. This observation is comparable to the darkening of PTFE surfaces following comparable defluorination treatments and is attributed to increased surface roughening causing significant light scattering. Longer

treatments of 20-30 minutes cause the sample to visible roughen and eventually delaminate form the substrate.

The pre and post defluorination treatment carbon 1s XPS spectra for sample AP2-1 are shown in Figure 4.6. After a 30 second treatment in 100 mM sodium-naphthalene solution, the surface is nearly defluorinated. As is typical of deflurination treatments, nearly all of the carbon-fluorine bonds are converted into carbon-carbon and carbon-oxygen bonds.

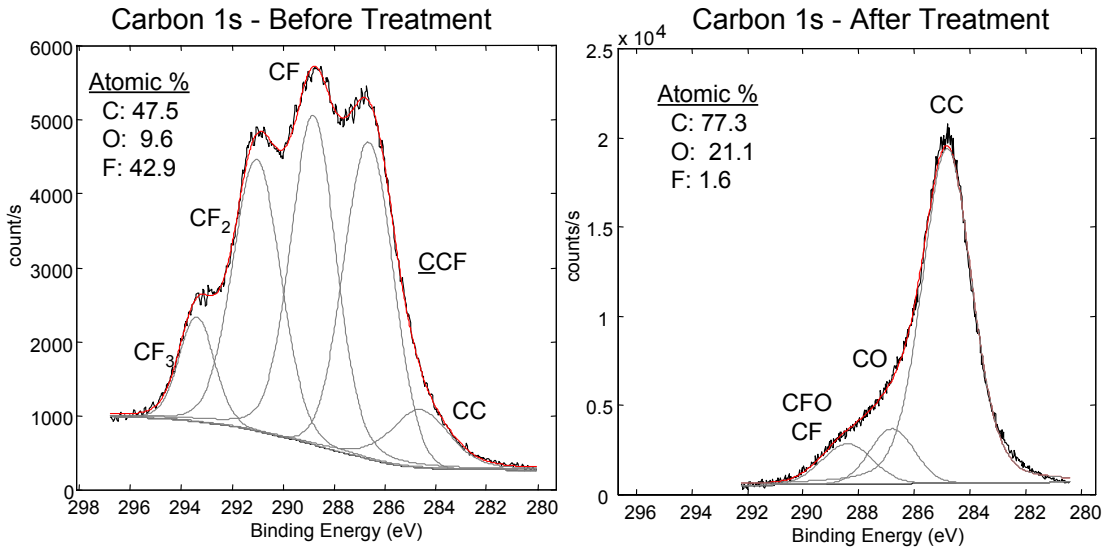

Figure 4.6. Carbon 1s spectra before (left) and after (right) sodium-naphthalene defluorination treatment (100 mM, 30 sec) on sample AP2-1

Although differentiation between carbon-hydrogen bonds from carbon-carbon bonds using XPS is impossible, some may exist. Because only 1.6 at% of fluorine is detected, only a very small fraction of carbon-fluorine bonds remain on the surface. The overall amount of oxygen detected increases; however, the ratio of carbon to oxygen decreases

slightly indicating a little oxygen incorporation into the film. This result varied between no incorporation to up to 50% increase in the carbon-oxygen ratio caused by reactions with unpassivated radical or ions with atmospheric or chemical contamination. This variability is a common observation, as oxygen incorporation depends on atmospheric contamination or exposure, solvent and water rinsing and time between defluorination, rinsing and analysis.[67] The contact angle with water changed from 90° to 25° after treatment.

The defluorinated sample was also analyzed using bulk thin film techniques such as transmission FTIR, attenuated total reflectance (ATR) FTIR and FT-Raman. Because the defluorinated layer thickness was so thin, no meaningful spectra were obtained. Attempts to treat samples for an extended period (>20 minutes) to generate thicker defluorinated layers resulted in delamination of the film from the substrate. As discussed in Chapter 2, PTFE samples measured with FTIR were exposed to the radical anion for 8 days.[67]

4.6.3 Identification of unsaturation in defluorinated residues

Literature reports indicated the presence of unsaturation in PTFE surfaces after radical anion treatments using FT-Raman analysis.[67,129] Unfortunately, FT-Raman and FTIR analysis yielded no meaningful results in this study due to the low thickness of the defluorinated layer. An alternative method to identify surface functional groups is chemical tagging in combination with XPS analysis. Carbon-carbon double bonds undergo an addition reaction with bromine which can easily be detected by XPS as shown in Equation 4.2.

$$– C = C – + Br_2 \rightarrow – CBr – CBr – \qquad (4.2)$$

Similar treatments have been used for the identification of unsaturation in polybutadiene-based polymers.[127] Model etch residue samples defluorinated for one-minute with 0.1 M sodium naphthalene were exposed to bromine vapor at 40 °C for ten minutes. After DIW and IPA rinses, bromine-exposed samples were analyzed by XPS. Surface composition was 61.6 at% carbon, 21.9 at% oxygen, 10.6 at% fluorine and 5.9 at% bromine. The carbon to fluorine and carbon to oxygen ratio did not change significantly (<3%) after the bromine treatment. No bromine was detected on the surface of an untreated model etch residue sample after a similar bromine vapor treatment. The carbon to bromine ratio of 10:1 suggests that approximately 5% of the carbon-carbon bonds were unsaturated. The unsaturation generated in the reduced residue will be exploited to permit complete residue removal.

4.6.4 Effect of radical anion concentration and treatment time

The effect radical anion concentration on the defluorination process was determined. AP2-1 samples were exposed to concentrations of 25, 50 and 100 mM for 15 seconds. Carbon, fluorine and oxygen XPS spectra at each time are shown in Figure 4.7. As expected, the samples exposed to higher concentrations of radical anions were defluorinated at a faster rate. The CF moieties are defluorinated prior to the CF_3 and CF_2 moieties at the 25 mM concentration. With higher concentrations, the CF_3 and CF_2 moieties are also become effectively defluorinated during the treatment time. The two

different peaks observed in the oxygen spectra correlate to CF_xO bonding (536 eV) and C-O bonding (532 eV). Because the carbon to oxygen ratio changed little, the defluorination process results in an increase in the C-O peak and a reduction in the CF_xO peak. The fluorine peak decreases, as the surface becomes defluorinated.

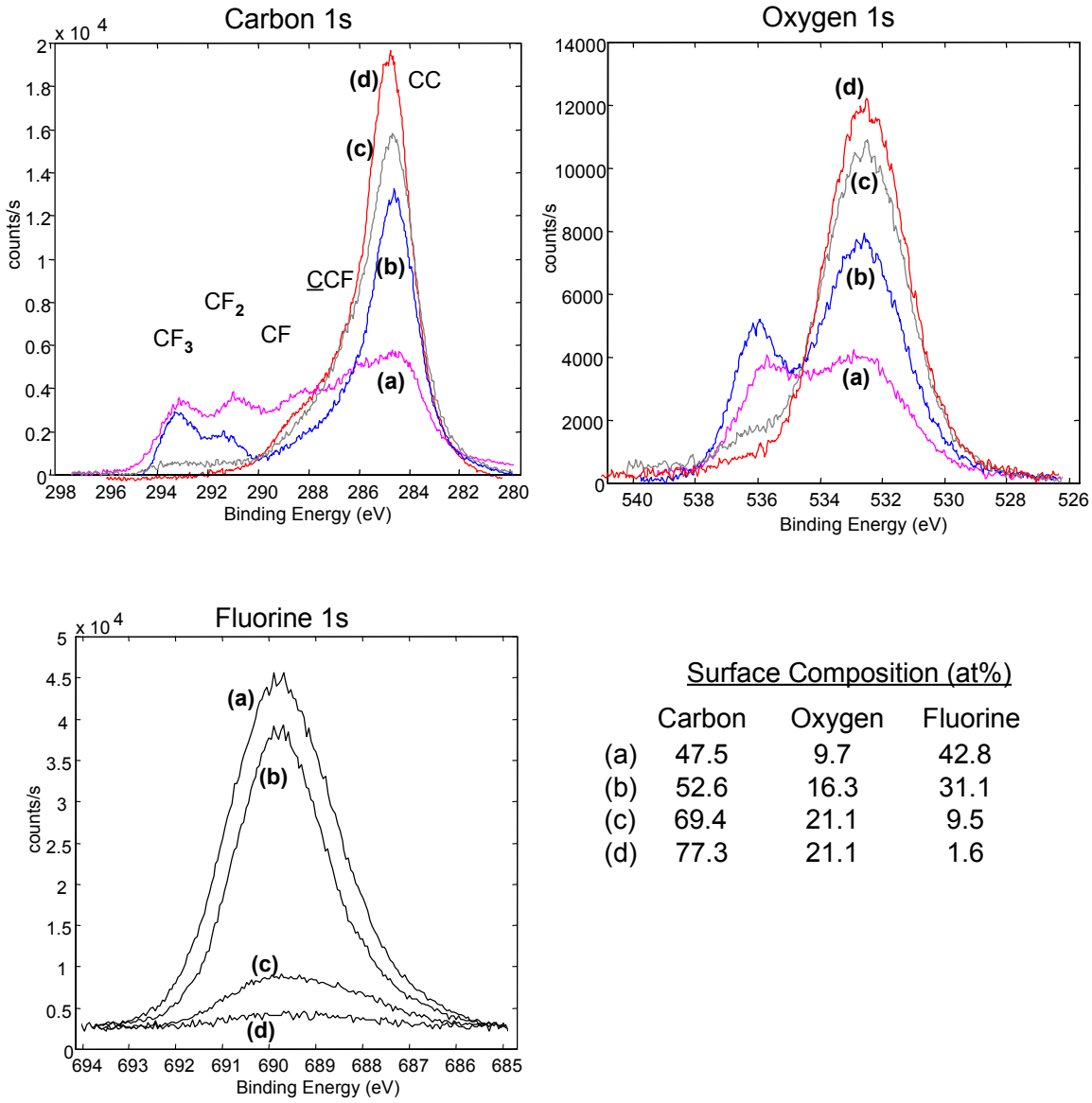

Surface Composition (at%)

	Carbon	Oxygen	Fluorine
(a)	47.5	9.7	42.8
(b)	52.6	16.3	31.1
(c)	69.4	21.1	9.5
(d)	77.3	21.1	1.6

Figure 4.7. Carbon 1s XPS spectra after 30 second treatments using various sodium naphthalene radical anion concentrations. (a) - no treatment, (b) - 25 mM, (c) - 50 mM, (d) 100 mM.

XPS analysis was also completed after various treatment times using the same concentration. After treatments of 100 mM naphthelene radical anion, the surface was completely defluorinated after only a 10 second treatment; treatments shorter than 10 seconds were difficult to perform reproducibly. When the concentration was reduced to 25 mM of naphthalene radical anion, the defluorination process could be monitored. The progression of the carbon XPS spectra is comparable to those in Figure 4.8. The concentration of carbon-carbon bonding moieties increased while the CF_x moieties decreased with CF being reduced before CF_3 and CF_2 bonds. Table 4.8 shows the surface composition as a function of treatment time using 25 mM naphthalene radical anion.

Table 4.8. Surface composition of AP2-1 as a function of treatment time by 25 mM radical anion

Treatment time (s)	Carbon (at%)	Oxygen (at%)	Fluorine (at%)
0	54.6	10.0	35.4
10	63.4	14.0	22.6
20	66.4	18.8	14.8
30	76.8	14.0	9.2

4.6.5 Probing of reaction depth of defluorination

The reaction penetration depth of the radical anion defluorination was determined using a step-wise removal scheme. The scheme is illustrated in Figure 4.8. After the defluorination treatment, a selective oxidation process using aqueous ozone is used to remove the defluorinated layer. Samples were exposed to a solution of DIW with ozone bubbled through a diffuser. While bubbling, the pH reached a steady state value of 8.0 and the concentration of dissolved ozone in equilibrium with the vapor stream (3 vol% ozone) was estimated to be 13 mg/l or 0.27 mM.[128] After removal of the defluorinated

residue, ellipsometry is used to measure the remaining thickness of the fluorocarbon residue. By subtraction, the thickness of material removed (and defluorinated can be determined).

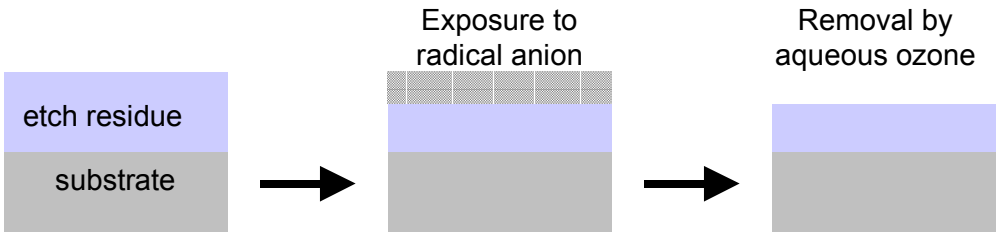

Figure 4.8. Scheme to determine defluorination reaction penetration.

The selective oxidation is effective because of the presence of unsaturation in the defluorinated residue. The amount of unsaturation in radical-anion defluorinated PTFE samples has been measured as high as 25%.[129] As discussed in Chapter 2, ozone acts as a selective oxidant that can cleave carbon-carbon double bonds, while being relatively inert to carbon-carbon single bonds and fluorocarbon surfaces. After ozone treatments, removal of the defluorinated layer is confirmed using XPS surface analysis and ellipsometry. Carbon XPS spectra after each process step are shown in Figure 4.9.

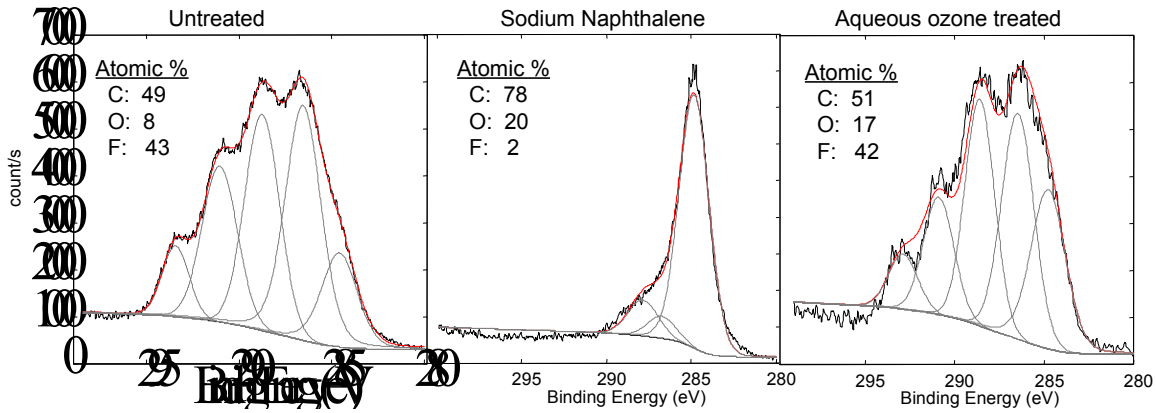

Figure 4.9. Verification of removal of defluorinated layer by carbon 1s XPS spectra.

After the treatment, the resulting surface composition is similar to that of the original fluorocarbon surface as verified by the carbon XPS spectrum; atomic concentrations were 44% carbon, 42% fluorine and 14% oxygen. The thickness of the remaining fluorocarbon was measured after the defluorinated layer was removed, which allowed determination of the reaction penetration depth; results are shown in Table 4.9 and are plotted in Figure 4.10 as a function of sodium naphthalenide exposure time.

Table 4.9. Raw data for calculation of the radical anion penetration depth

Radical anion exposure time	Thickness before treatment (nm)	Thickness after ozone (nm)	Difference (nm)
10	222.5	195.6	26.9
40	223.2	180.1	45.1
60	221.8	143.6	43.1
90	221.5	160.5	61.0
120	213.2	168.1	78.2

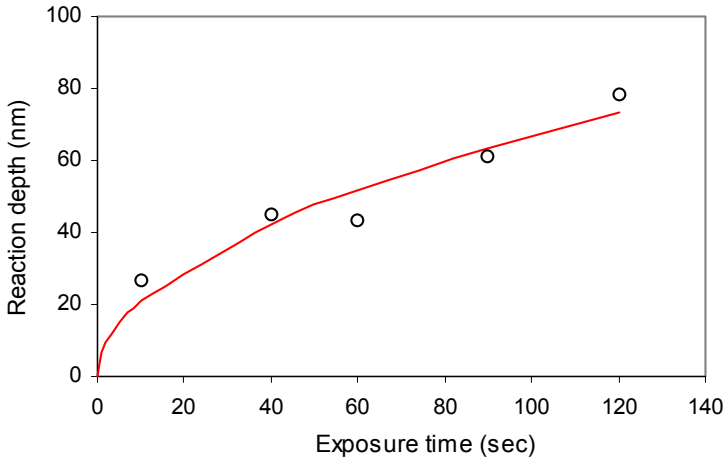

Figure 4.10. Plot of radical anion penetration depth as function of exposure time.

Over the exposure times investigated (10-120 sec), the average rate of penetration was 27 nm/min. A linear trend line does not intersect the origin indicating that the reaction rate changes over time, likely becoming diffusion-limited as it penetrates the film. The shape of the data matches similar data by McCarthy where the mass loss over time for PTFE defluorination was measured.[67] The data are fit to a model described in the following section. A ten second radical anion treatment is capable of completely defluorinating and penetrating through a typical 20 nm fluorocarbon etch residue present on industrial samples. An etch residue sample exposed to ozone without the defluorination treatment showed no thickness or chemical change.

With regards to semiconductor cleaning processing, the aqueous ozone process may or may not be necessary for effective removal of residues. This oxidative process is necessary for removal of 'model' etch residues because the radical anion treatment alone does not chemically attack the crosslinked carbon-carbon bonds in the fluorocarbon

residue. This treatment can actually increase the crosslink density; as a result, simple dissolution or removal of the defluorinated layer cannot occur. No significant chemical modification or removal was observed when the defluorinated surface was exposed to organic solvents or bases. Therefore, the ozone treatment is necessary to break carbon-carbon bonds and form short soluble oligomers, thus, removing the defluorinated layer. Although an aggressive oxidation chemistry would be effective in breaking all carbon-carbon bonds, such chemistries would be less compatible with other organic or organic-containing low-k materials present during IC fabrication.

For actual fluorocarbon residues, the thickness of the fluorocarbon layer is typically less than 20 nm and can be less fluorinated than the 'model' residues. The fluorine to carbon to ratio of actual residues has been measured as low as 0.25. This would lead to a decrease in the formation of double bonds and a reduction in effectiveness of the selective ozone process. The removal of 'model' planar residues neglects the effects of an underlying photoresist layer and the effects of wetting of small features.

4.6.6 Modeling of penetration depth

In order to extract physical parameters from the fluorocarbon removal data, a surface reaction with diffusion model is constructed. The starting point for this model will be the quasi-steady state model for penetration and diffusion of a reaction interface into a surface.[130] Reaction rate dependence on the surface depth has been observed previously and was attributed to diffusion limitations. However, a question exists regarding the exact cause of the diffusion limited reaction. Consideration of the processes occurring suggests that diffusion of naphthalene radical anions through the defluorinated layer to

the interface limit the reaction rate. It has been determined, however, that the defluorinated layer is electrically conductive which may provide electron transport from the solution to the interface.[67] In this case, the defluorination could appear to be diffusion limited due to increased surface area (due to porosity) or by a buildup of reaction products that must diffuse out of the through the layer. The porous defluorinated layer, however, may not be conductive under actual process conditions (when saturated with solvent). McCarthy concluded that it was likely a combination of radical penetration and electron conduction, but found no evidence that favored either mechanism.[67]

With no conclusive evidence that electrical conduction plays a role, it will be assumed that naphthalene transports the electron through the defluorinated layer and that this mechanism is responsible for the observed diffusion limited reaction. Using the coordinate system in Figure 4.11, the interface between the defluorinated layer and the fluorinated layer is designated at z = l.

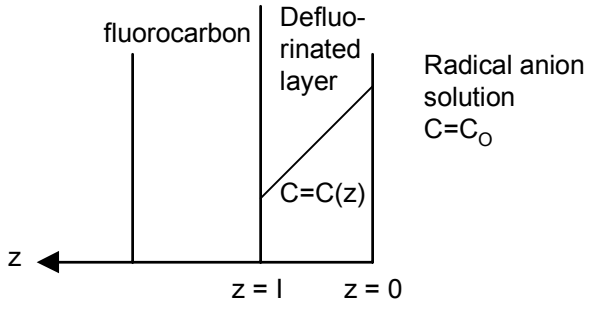

Figure 4.11. Coordinate system for the diffusion limited-reaction model for radical anion penetration into the model residue surface.

At the interface, the surface reaction rate of defluorination must equal the rate of diffusion of reactants to the interface. This is shown mathematically in Equation 4.3

where k is the reaction constant, C(I) is the radical anion concentration at the interface, D is the naphthalene radical anion diffusion coefficient and k is the second-order surface reaction constant. Because diffusion in the film is much slower, diffusion in the solution to the surface is assumed to be sufficiently fast to avoid depletion.

$$kC(I)^2 = -D\frac{dC}{dt}\Big|_{z=I} \tag{4.3}$$

The reaction of radical anions with PTFE has been determined previously to be second order with respect to naphthalene.[79] This reaction will assumed to be second order as well because of the mechanistic similarities. Assuming steady state diffusion Equation 4.4 results where C(0) is the concentration in the solution and b is the partition coefficient between the radical anion concentration absorbed in the film and the concentration in the bulk solution. This assumption will be evaluated later.

$$kC(I)^2 = -D\frac{(C(I) - bC(0))}{I} \tag{4.4}$$

Using the quadratic formula and selecting only the positive root, the value of the naphthalene radical anion concentration at the interface, C(I), can be determined.

$$C(I) = \frac{\sqrt{D^2 + 4kIbC(0)D} - D}{2kI} \tag{4.5}$$

The rate the interface penetrates into the fluorocarbon film is equal to the reaction rate divided by the molar density of fluorine, ν, in the fluorocarbon film as shown in Equation 4.6.

$$\frac{dI}{dt} = \frac{kC(I)^2}{v} \qquad (4.6)$$

The fluorine molar density, in units of mol F/cm^3 film can be calculated using molar film composition determined by XPS and an estimated model film density. The density of a similarly plasma deposited fluorocarbon film, measured using a quartz crystal microbalance, is 1.87 g/cm^3.[131] The molecular weight for the film can be estimated by weighting the molecular weight of each element by the atomic composition detected by XPS analysis. Very little should be present in the plasma deposited film. To calculate the fluorine molar density, the film density is divided by the film molecular weight and multiplied by the atomic percentage of fluorine detected in the film. An average molecular weight for the film was 15.33 g/mol, resulting in a fluorine molar density of 0.0524 mol F/cm^3 film. The concentration at the interface, C(I), found in Equation 4.5, can be substituted into Equation 4.6 resulting in Equation 4.7.

$$\frac{dI}{dt} = \frac{k}{v}\left(\frac{\sqrt{D^2 + 4kIbC(0)D} - D}{2kI}\right)^2 \qquad (4.7)$$

This differential equation cannot be solved implicitly, but the equation can integrated be numerically. The solution can then be compared to the depth of the interface as a function of time that was measured in Section 4.6.5.

The variables, k, D and b are currently unknown; however, researchers have determined rate information for the reaction of sodium naphthalene with a PTFE surface.[79] Due to the similarities between the PTFE and the model residue and the lack of more applicable information, the rates will be assumed to be comparable. In the previous experiments,

the surface area of PTFE substrate was much greater than the concentration of radical anions, thereby eliminating the effect of diffusion into the PTFE surface. Unfortunately, the reaction constant obtained from that work (3.1 $M^{-1}s^{-1}$) cannot be directly equated to the surface reaction rate constant used in the current model with units of $M^{-1}s^{-1}cm$. The initial reaction rate, when the PTFE surface is first exposed to the radical anions, however, should be similar. At 0.1 M concentration of sodium-naphthalene, the initial rate of surface defluorination was found to be 0.26 mmol/sec. This information can be used to calculate a surface rate constant.

To determine the surface reaction coefficient, the initial rate of defluorination found above will be matched to initial the rate in the model. The initial molar rate must be transformed into a penetration rate using the fluorine molar density, ν, (52.4 $mmol/cm^3$) and the exposed sample area, a (1 cm^2). The relationship is shown is Equation 4.8.

$$Rate(cm/s) = \frac{Rate(mol/s)}{v} a \qquad (4.8)$$

The initial rate of penetration, assuming no diffusion limitations, is 4.69 x 10^{-3} cm/s or 49600 nm/s. For initial conditions, the value of b = 1 is used (bulk solution contacting surface) and the diffusion coefficient is set to 1 cm^2/s to ensure that diffusion does not limit the rate. To achieve an initial rate as specified above, the surface reaction constant must equal 3.21 x 10^4 $M^{-1}s^{-1}cm$. With the information currently available, this will serve as an estimate for the surface reaction rate constant.

The Thiele modulus is a ratio between the diffusion rate and reaction rate. As discussed previously, the reaction becomes diffusion limited as evidenced by the curvature in the data shown in Figure 4.11. For diffusion-limited reactions, the Thiele modulus is significantly larger than 1. For this system, the Thiele modulus is defined in Equation 4.9.

$$\Theta = \frac{kbC(0)I}{D} \qquad >> 1 \qquad (4.9)$$

Using a characteristic length of the system, I, as the maximum interface depth (120 nm), a bulk concentration of 90 mM and the previously estimated value for the surface reaction constant, we find that the b/D must be greater than 29 for the reaction to be diffusion-limited. With liquid/polymer diffusion coefficients ranging between 10^{-7} and 10^{-12} cm^2/s, this condition will be easy to satisfy. This value is large because the reaction rate constant is large; any diffusion will limit the rate satisfying the Thiele modulus requirement. To achieve a good fit to the observed data, as shown in Figure 4.13, the product of the partition coefficient and the diffusion coefficient should equal 1.4×10^{-10} cm^2/s.

Little information exists regarding liquid partition coefficients with polymer systems, especially for systems as specific as this one. The diffusion coefficient of liquid benzene in high density polyethylene polymer has been reported as 5×10^{-9} cm^2/s[132]. High density polyethylene is likely more dense than the defluorinated layer where diffusion occurs; however, the hydrocarbon-based composition is similar. The diffusion coefficient for benzene can be used to estimate the diffusion coefficient for naphthalene using a

correlation of molar volumes. [133] In this work, a linear relationship is demonstrated between the log of the molar volume and the liquid phase diffusion coefficient of polycyclic aromatic hydrocarbons. The correlation estimates a naphthalene diffusion coefficient of 5.2 x 10^{-10} cm^2/s. Using this value, a partition coefficient of 0.26 best fits the measured data as shown in Figure 4.12. Although it is difficult to assess the accuracy of these calculated values, the diffusion coefficient is within the range for solvent/polymer systems.[130] The porosity of the defluorinated layer may be responsible for the large partition coefficient of 0.26. Techniques to obtain more precise measurements of the data are discussed in the future work section of Chapter 8.

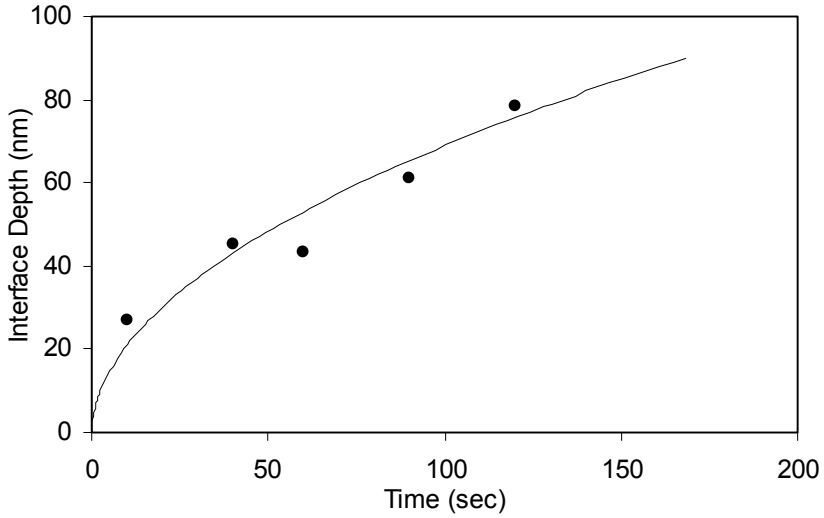

Figure 4.12. Best fit of data for base case model. Parameters set to C(0) = 0.9 M, k = 32100 $M^{-1}s^{-1}cm$, b=0.26 and D = 5.2 x 10^{-10} cm^2s^{-1}.

Using the above information, the use of the steady state diffusion assumption can be evaluated. If Dt/l^2 is much greater than 1, the steady state assumption is valid, where t is time and l is a characteristic length. For a worst case scenario, where l=100 nm and t=100 seconds, the value is 5.2×10^6, satisfying the steady state assumption. The effect of different bulk concentrations can also be predicted using the model shown in Figure 4.13. Unfortunately, availability of samples prevented verification of the model using different bulk concentrations.

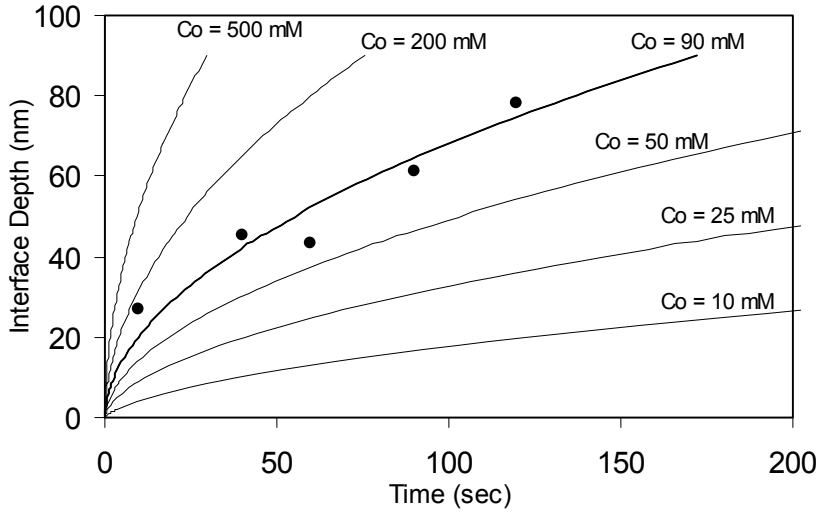

Figure 4.13. Predicted effect of bulk concentration on the penetration rate using model parameters: $k = 32100\ M^{-1}s^{-1}cm$, b=0.26 and $D = 5.2 \times 10^{-10}\ cm^2s^{-1}$.

4.7 Conclusions

Samples provided by Air Products and Chemicals, Incorporated, have been characterized by ellipsometry, high resolution XPS and contact angle measurements. The molecular structure of the fluorocarbon etch gas and the addition of oxygen in the etch feedgas have

significant effects on the specific etch residue formed. A significant amount of crosslinking exists in all of these residues prohibiting simple dissolution as a means for residue removal. Reductive chemistries that react with the fluorocarbon provide an alternative to strong oxidative chemistries, although ozone is necessary to completely remove the residue. It is expected that aqueous ozone, lacking activation by UV or hydrogen peroxide, will be compatible with low-k materials. Sodium naphthalene radical anion treatments could effectively defluorinate the model residue at an average rate of 27 nm/min. The defluorinating treatment could completely penetrate industrial residues, with a typical thickness of less than 20 nm, in less than one minute. Aqueous ozone processing removed the defluorinated layer effectively, permitting measurement of the penetration depth. Without activation through UV radiation or hydrogen peroxide, aqueous ozone processing may be mild enough for low-k cleaning because of the extremely low concentration of hydroxy radicals. Unsaturation, however, must be present in the residue for this process to be useful. Modeling of the residue penetration rate indicated that penetration became diffusion limited. Extraction of physical parameters from the data was completed; however, the accuracy of the diffusion coefficient estimation is unknown.

CHAPTER 5

GENERATION OF IC-COMPATIBLE RADICAL ANIONS

5.1 Overview

Alkali metals, such as sodium, are major contaminants in IC processing. Two methods of producing sodium-free naphthalene radical anions are investigated. The use of an ion-exchange reaction proved unsuccessful due to the nature of the ion pair and a lack of ionization of species in the solvents. The second approach, which uses electrochemical means of generation, was successful; however, the lifetime of the anions is finite. The concentration over time and degradation rates are determined using a UV-visible dip probe that monitors the absorbance of radical anions.

5.2 Sodium in IC processing

Modification and removal of fluorocarbon plasma etch residues was demonstrated using a solution of sodium naphthalene radical anions and aqueous ozone processing. Unfortunately, the use of sodium metal and sodium ions would be problematic for IC manufacturers. Sodium, like other alkali metals, is a contaminant in IC processing. Sodium can rapidly diffuse through materials to electrically sensitive areas of devices such as the source, drain and channel of transistors causing problems with transistor operation, reproducibility and reliability. IC manufacturers have spent an enormous effort to remove alkali metal contamination from sources such as chemicals, gases, and quartz and ceramic components of equipment. Even if sodium could be effectively rinsed from surfaces after processing, the use of sodium in any chemical process would be

unacceptable to IC manufacturers. Therefore, two methods have been explored to produce naphthalene radical anions without the use of sodium or other alkali metal.

5.3 Removal Of Sodium Using Ion Exchange Reaction

Because of the long term stability and ease of generation, the first attempts to remove sodium were initially based on solutions of sodium naphthalene-generated radical anions. Using an ion exchange reaction, sodium ions could be replaced with an alternative stabilizing cation. The only organic-soluble cations commonly used in IC processing are tetraalkylammonium ions. More specifically, tetramethylammonium hydroxide is commonly used as a basic developer in photolithographic processing. An ion exchange reaction could be used to replace the sodium counter-ion with a compatible ion such as the tetrabutylammonium ion. The proposed reaction is shown in Equation 5.1 with tetrabutylammonium chloride (TBACl). The reaction byproduct, sodium chloride, is insoluble in organic solvents resulting in precipitation and allowing eventual separation from the radical anion solution.

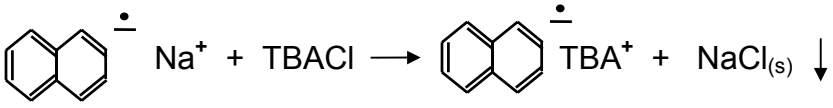

(5.1)

The tetrabutylammonium ion was chosen to replace sodium because of its solubility in most organic solvents. Tetramethylammonium halides, on the other hand, are not soluble in organic solvents. Additionally, generation using electrochemical methods with tetrabutylammonium-based electrolytes provide partial stabilization to the radicals.[86,134] The electron exchange rates between anthracene radical anions have been measured in

the presence of tetrabutylammonium ions, although sodium was not removed from the solution.[86] Other research has been conducted on the pairing of stilbene radical anions with tetrabutylammonium ions generated by pulse radiolysis techniques; however, the radical lifetime was on the order of micro-seconds.[134] Based on these literature reports, radical anions may be stabilized in the presence of tetrabutylammonium cations.

The solubility of several tetraalkylammonium salts in THF was evaluated by visual inspection of solutions with salt concentrations of 0.25 mg/ml after one hour of agitation. Tetramethylammonium chloride, tetrabutylammonium chloride, tetrabutylammonium bromide and tetrabutylammonium iodide are insoluble in THF; tetrabutylammonium tetrafluoroborate ($TBABF_4$) and tetrabutylammonium nitrate are soluble in THF. The soluble salts, $TBANO_3$ and $TBABF_4$, should cause the ion exchange reaction to occur more rapidly in solution compared to the addition of insoluble salts where the reaction must occur at the solid-liquid interface. In this case, agitation is necessary to adequately contact the insoluble salt and radical anions in the solution.

5.3.1 Reaction observations

Sodium naphthalene solutions were prepared as specified in Chapter 3. The radical naphthalene solution was separated from the excess sodium prior to use in ion exchange reactions. The reaction between the salt and the sodium naphthalene was monitored visually because no equipment was available to quantitatively monitor the visible spectrum with radical anion concentrations as high as 0.1 M. Sodium naphthalene solutions appear green when very dilute; however, at higher concentrations, the solutions become opaque. A change in the counter ion does cause a significant shift in the visible

spectrum of the radical anion; therefore, visual monitoring is capable of detecting the presence or degradation of the radical anions in the solution.[134] Based on the molar absorptivity of the naphthalene radical anion, which is measured in the Chapter 5, a radical anion concentration of 0.05 mM absorbs 25% of transmitted light (through a 1 cm vial). This amount of absorption can be detected visually.

In the absence of protic contamination sources, sodium naphthalene solutions are stable indefinitely. The tetraalkylammonium salts must be as dry as possible to prevent protonation of radical anions by water; drying procedures are covered in Chapter 3. The water content of the salts, measured using Karl Fischer titration, was less than 0.5 wt%. Additional purification techniques such as liquid extraction with acetone and diethyl ether were unable to reduce the water content further.

Addition of a stoichiometric amount of $TBANO_3$ or $TBABF_4$ to 0.1 M sodium naphthalene in THF solutions quickly resulted in a change in color of the solutions from green to red. Solution samples taken at various times showed no decrease in sodium content as measured by atomic absorption spectroscopy (AAS). Similar results were observed when the reactants were cooled to 0 °C. Over 20 minutes, the opacity of the solution began to fade and final solution color was between orange and red. A precipitate was observed, but significantly less than a stoichiometric amount of sodium nitrate or sodium tetrafluoroborate that should be formed had the reaction proceeded. Clearly, the NO_3^- and BF_4^- ions failed to drive the ion exchange reaction and precipitate the sodium ion out of the solution.

Addition of a stoichiometric amount of TBACl to a 0.1 M sodium naphthalene solution resulted in a similar decay of the opacity of the solution, although the decay occurred at a much slower rate. Solutions were agitated to improve contact between the solution and the insoluble TBACl salt. Over the course of the reaction, the solution color changed from green to red then to reddish-orange, similar to the above observations. When cooled to 0 °C or -72 °C (using acetone-dry ice bath), a similar color transition, albeit slower, was observed. Over the course of the reaction, the solution was sampled for sodium concentration analysis by AAS; however, inconsistent results were observed. The sodium concentration remained fairly constant near the initial value of 900-950 mg/l and then suddenly dropped to 300 ppm or lower. This change in sodium concentration correlated with the of loss opacity of the solution which occurred after 30 minutes of agitation. The reaction byproducts are analyzed in the next section to determine the mechanism of degradation.

As a control in the process, a stoichiometric amount of DIW was intentionally added to a solution of sodium naphthalene to cause complete degradation of the radical anions. The solute and precipitate were collected and analyzed. As discussed in chapter 2, two moles of sodium naphthalene react readily with two moles of water to form one mole of naphthalene, one mole of dihydronaphthalene and two moles of sodium hydroxide according to the generic reaction scheme shown in Equation 5.2. In the case of water, R-H represents H_2O. Analysis of the reaction solute and precipitate are described in the following section.

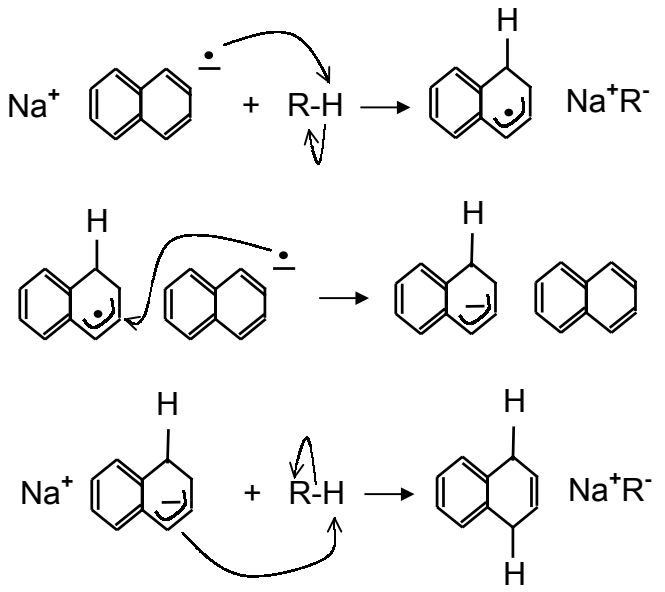

(5.2)

5.3.2 Chemical analysis of reaction products

In order to determine why the radical anion degradation occurred, analysis of the reaction byproducts was performed. The following products were produced by the reaction of 0.1 M sodium naphthalene and a stoichiometric amount of TBACl performed at 0 °C. Comparable analysis on the water-qeunched radical was also performed. Solute and precipitate were separated using a centrifuge. Analysis of the solute by gas chromatography/mass spectroscopy (GC/MS) was inclusive. Both naphthalene and dihydronaphthalene were detected by GC/MS; however, sufficient peak separation in the gas chromatogram to quantify the amounts of each species was not achieved. The mass spectroscopy ion fragmentation fingerprint of naphthalene and dihydronaphthalene was also too similar to quantify relative amounts. For similar reasons, discrimination of tetraalkylammonium salts from trialkylamines was not possible using MS techniques.

The solute was also analyzed by H^1 NMR spectroscopy. The solute was prepared by vacuum evaporation of the THF solvent and replacement with deuterated-THF. Complete ^1H NMR analysis of the TBACl/sodium naphthalene and the water quenched reactions are presented in Appendix B. Both 1,4-dihydrogen naphthalene (DHN) and naphthalene (Naph) were detected in the water quenched reaction at a ratio of 1:1.7 (Naph:DHN). Based on the stoichiometry of protonation, 75% of the naphthalene was converted into the radical, comparable to the previously measured range of 85 to 90%.

Dihydronaphthalene, tetrabutylammonium ion and tributylamine were identified in the NMR analysis of solute from the TBACl/sodium naphthalene reaction. The ratio of naphthalene to 1,4-DHN is 1.5:1 indicating approximately 80% conversion of naphthalene to radical anions during the initial generation with sodium. The ratio of DHN to tributylamine was 1:1.9 and the ratio of DHN to TBA ion was 1:0.9.

The collected precipitate from both the TBACl and the water quenched sample were analyzed for sodium and hydroxide ion content. After centrifuging, the precipitate was vacuum dried to remove residue solvent. To remove the TBACl from the precipitate, extraction with acetone was performed. For sodium concentration analysis, a measured amount of DIW was added to the precipitate and the concentration of sodium was measured with AAS. Percent recovery of sodium in the precipitate ranged between 90% and near 100% for both the water-quenched sample and the TBACl reaction sample. It is assumed that the sodium was indeed in the form of sodium chloride or sodium hydroxide based on its selective solubility in acetone and water.

The concentration of hydroxide ions in the precipitate was also measured. The precipitate was washed with acetone to remove TBACl, followed by addition of a specific volume of DIW. The pH of the solution was measured indicating the concentrationt of hydroxide ions present. For the water-quenched sample, where sodium hydroxide is expected, a pH of 11.0 was recorded with addition of 100 mL of DIW corresponding to a hydroxide ion concentration of 1×10^{-3} M or 1×10^{-4} total moles of OH^- in the precipitate. Assuming 90% conversion of the original 1.5 mL of 0.1 M sodium naphthalene solution, 1.35×10^{-4} moles of OH- were expected in the precipitate. This result is within the experimental error and confirms the products in the water quenching experiments.

The precipitate from the TBACl/sodium naphthalene radical was analyzed similarly. Initially, 1.5 mL of a 0.1 M solution and 50 mg of TBACl were combined. The precipitate was washed with acetone and dissolved in 100 mL of DIW. The pH measured only 0.1 units higher than the DIW, indicating only a very small amount of hydroxide ions in the precipitate.

5.3.3 Mechanism of radical anion degradation

Three possible reactions could occur in the degradation of the naphthalene radical anion when combined with TBACl. These possibilities are shown in Reactions 5.4, 5.5 and 5.6.

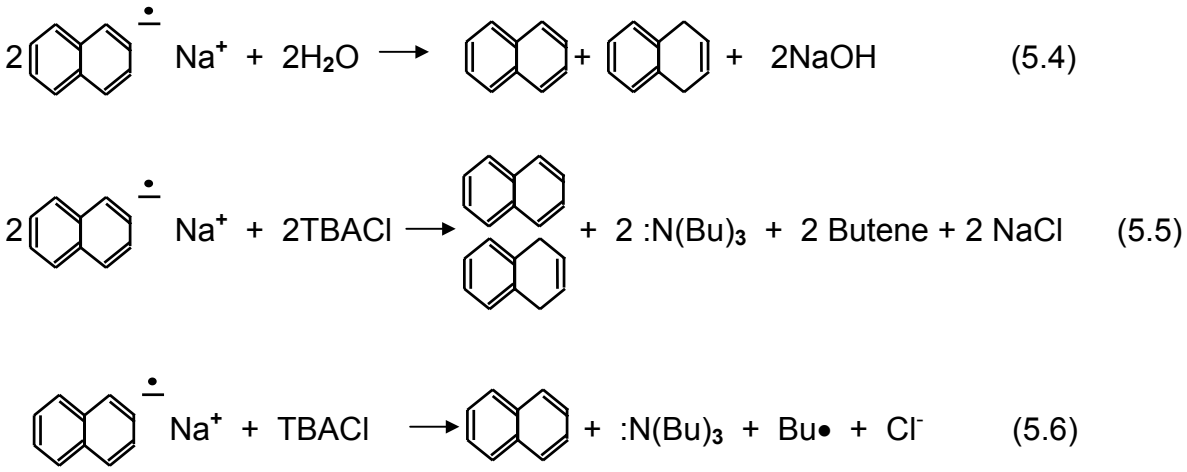

As shown in Equation 5.4, the radical anion can become protonated by water contamination resulting in the formation of naphthalene, dihydronaphthalene and sodium hydroxide. In Equation 5.5, the radical anion deprotonates TBACl causing a Hoffman elimination reaction resulting in the formation of tributylamine, 1-butene and sodium chloride. Hoffman elimination by a strong base is shown in Equation 5.7. Finally, the radical anion could transfer its electron to TBACl resulting in the formation of tributylamine and a butyl radical as shown in Reaction 5.6. The butyl radical would likely disproportionate or gain another electron from a radical anion, form a carbanion and deprotonate the nearest organic species.

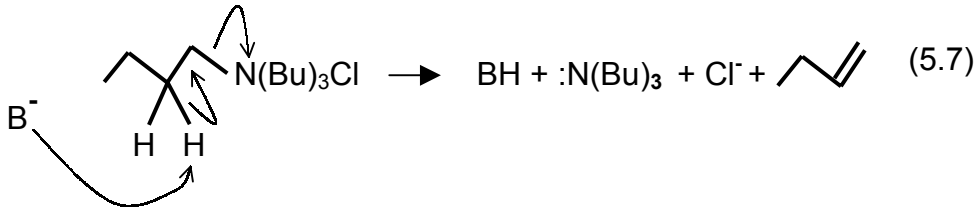

(5.7)

From analysis of the solute, a substantial amount of dihydronaphthalene is detected; therefore, the electron transfer reaction (Equation 5.6) does not occur to a significant extent. In addition, the presence of tributylamine is also detected. Analysis of the precipitate indicates the presence of sodium, likely in the form of sodium chloride, but very little hydroxide ion is detected. By process of elimination, the Hoffman elimination reaction mechanism must be primarily responsible for the degradation of the radical anions when exposed to TBACl. As further evidence, the ratio of DHN to tributylamine was nearly 1:2 as predicted by the Hoffman elimination mechanism.

5.3.4 Alternative chemicals

Several other combinations of solvents and salts were invoked in an attempt to perform the ion exchange reaction. Since water contamination of TBACl was not the primary cause of degradation of the radical anion, new solvents and reactants were evaluated by visual observation. The presence of hydroxyl radicals in the precipitate was also used to ensure that water contamination was not causing degradation. Replacement of TBACl with tetramethylammonium chloride produced little reaction. Although the opacity of the radical anion did not significantly decrease, little sodium was detected in the precipitate and the sodium concentration in the solution decreased only slightly after 1 hr. This is likely due to the poor solubility of tetramethylammonium ion in THF. Sodium

naphthalene radical anions can also be generated in dimethoxyethane (DME) and hexamethylphosphoramide (HMPA). Replacement of THF with DME produced similar results to those using THF. Generation of radical anions in HMPA is difficult because solvated electrons are also stable. Experiments showed that excess sodium metal versus naphthalene resulted in the generation of solvated electrons. When sodium was measured, the concentration in the solution was double that of the initial naphthalene concentration indicating the presence solvated electrons. Addition of TBACl caused the loss of the radical. In addition, use of HMPA in production processes is impractical because this material is a powerful carcinogen. Attempts to generate radical anions in dimethylformamide, which is the most common solvent for electrochemical generation, were unsuccessful.

5.3.5 Conclusions from ion exchange reactions

As will be discussed in the next chapter, naphthalene radical anions can be generated in the presence of tetrabutylammonium cations. There exists, however, a finite degradation rate of the radical. Sodium naphthalene-radical ion pairs exist as close or tight pairs in THF and loose ion pairs in DME.[134] It is possible that TBA-radical anion ion pairs were formed during the reaction; however, the rate of degradation was comparable to the rate of formation. Another possibility is that tetraalkylammonium salts do not adequately ionize in THF or DME. The dielectric constants of THF and DME are 7.5 and 5.5, respectively. If the salts do not sufficiently ionize, the loss of the sodium counter-ion by reaction with chlorine may cause the naphthalene radical anion to become unstable or more reactive resulting in the Hoffman elimination reaction. Naphthalene radical anions

have a reduction potential of –2.6 V (vs SCE) and tetrabutylammonium salts should be resistant to reduction by potentials of less than –3.3 V (vs SCE).[135]

From a practical standpoint, removal of sodium from the sodium naphthalene radical anions would not likely be adopted industrially. Chemical purity specifications typically require metallic contaminant concentrations less than 1 ppb. With the finite lifetime of TBA paired radical anions, generation and subsequent purification would have to be performed on demand, which is not practical. While the alternative option of electrochemical generation requires more equipment, sodium contamination issues are avoided.

5.4 Electrochemical Generation of Radical Anions

Electrochemical generation is an alternative means of radical anion production that enables generation without sodium contamination in the solution. The electrochemical solution, containing only organic electrolytes and naphthalene in an organic solvent, meets IC chemical compatibility requirements. Generation of radical anions using electrochemical means has been demonstrated previously; however, typically only low concentrations of the radical anion have been produced. Solutions of up to 15 mM of radical anthracene were capable of defluorinating PTFE surfaces although rates and penetration depths were not investigated.[72] No reports of surface modification or cleaning using electrochemically generated naphthalene radical have been reported. As mentioned previously, the faster reaction rate of naphthalene radical anions with

fluorocarbon surfaces relative to that of anthracene radicals is ideal for cleaning applications.

During electrochemical generation, molecules are reduced at an inert electrode instead of using sodium as the reducing agent. Electrical potential is generated at the electrode, thereby raising the energy level of the electrons. At a certain potential, electrons have sufficient energy to transfer from the electrode to the naphthalene molecule in solution forming a radical anion. Because of the high negative potentials required for naphthalene, only platinum or mercury electrodes are capable of reducing naphthalene in solution. To maintain electrical neutrality in the solution, an oxidation reaction occurs at the counter electrode. When tetrabutylammonium iodide is used as a background electrolyte, the reaction that occurs is the oxidation of I^- to I_2. To prevent oxidation of the naphthalene radical by I_2 or the counter electrode, the working and counter electrode must be separated using a porous glass frit. Neutrality is maintained in both working electrode and counter electrode compartments by diffusion of ions through the frit. The generation process is shown schematically in Figure 5.1. The diffusion of TBA+ ions is slower than I- ions resulting in a junction potential across the frit.

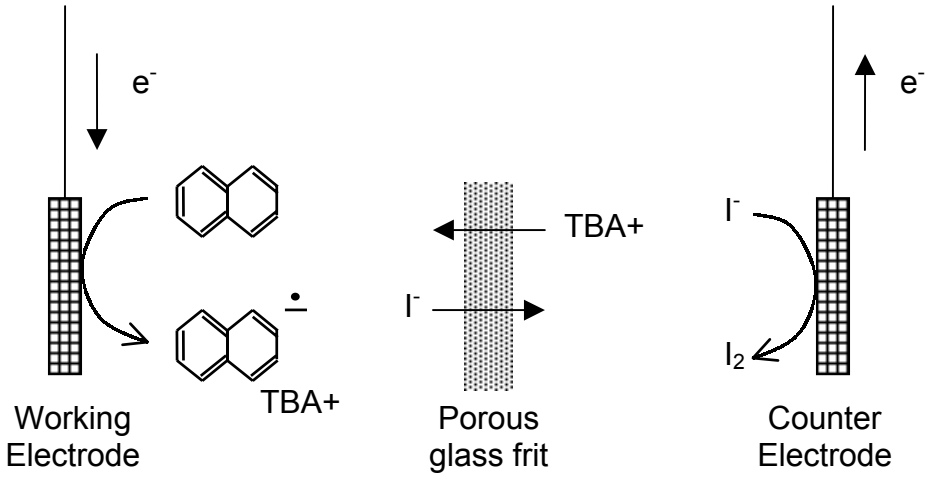

Figure 5.1. Pictorial representation of electrochemical generation of naphthalene radical anions.

Electric potential can only be measured relative to a reference or known potential. To precisely measure and maintain the reduction potential during generation, a home-made silver/silver ion reference electrode is used. The reference electrode consists of a silver wire submerged in a solution of 0.1 M silver nitrate. This is a standard reference electrode for nonaqueous applications. Fabrication and assembly of the electrode is described in Chapter 3.

Potentials are typically reported against a common standard reference such as the standard calomel electrode (SCE). This particular aqueous electrode is incompatible with our system because water reacts with radical anions. To standardize potential values, an internal standard with a known and stable redox potential is added to the electrochemical solution after experiments. The most common internal standard is the ferrocene/ferrocenium redox couple which measures +0.46 V vs SCE in DMF.[136] Using this information, the reported potentials can be corrected to the SCE potential. Unless

otherwise noted, the reported potentials have been corrected and referenced to the SCE potential using the ferrocene/ferrocenium couple.

5.4.1 Cyclic voltammetry

For cleaning applications, it is important to determine the concentration of the radical anions in the cleaning solution. For bulk generation of electro-active species or electrolysis, the efficiency of generation and the degradation of the reactants must be evaluated to determine the concentration over time. During electrochemical generation of naphthalene radical anions, each electron results in the production of one radical species; however, unwanted side reactions could also occur reducing the efficiency to less than 100%. Additionally, it has been observed that the radicals are not stable and degrade at a finite rate. The rate at which degradation occurs must be determined to estimate the radical anion concentration.

Cyclic voltammetry (CV) is a technique used for characterization of electrochemical reactions.[137] Using a potentiostat, the potential of the working electrode (versus the reference) is swept between a specified initial and final potential value and then reversed. The current is measured while the potential is being swept. A voltammogram is produced by plotting the measured current versus the negative of the voltage. The negative of the potential is used by convention. Various qualitative and quantitative pieces of information associated with the reaction and electrode processes can be determined from this graph. All cyclic voltammetry experiments were performed using the thin film cell and the probe electrode (area of 0.20 mm^2) described in Chapter 3.

The minimum and maximum potential or the potential window for performing electrochemical reactions depends on the solvent, electrode materials and the electrolyte. For electrolysis by reduction, the negative limit is important, and this limit is typically defined by the voltage where reduction of the background electrolyte begins to occur. The lower potential limit for tetrabutylammonium-based electrolytes in DMF is between -3.0 and -3.1 V vs Ag/Ag+.[138] Different tetraalkylammonium electrolytes, such as tetraphenyl or tetramethyl, do not provide significantly lower potential limits. The mechanism of degradation has been determined to be electron transfer from the electrode to the tetrabutylammonium ion described in Equation 5.6.[138] Other resources typically predict the lower limit for tetraalkylammonium salts in DMF as ~ -3 V vs SCE.[139] This range was confirmed by performing CV analysis on solutions containing only the background electrolyte, 0.1 M TBAI (tetrabutylammonium iodide), in DMF. The resulting voltammogram is shown in Figure 5.2.

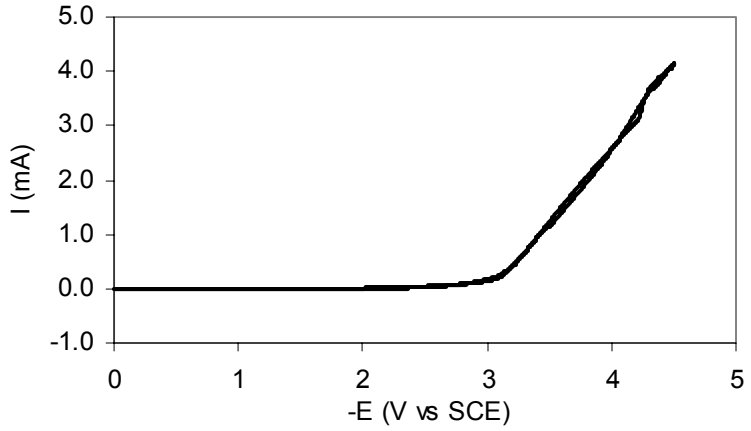

Figure 5.2. CV of 0.1 M TBAI/DMF with a sweep rate of 100 mV/s. Electrolyte degradation begins at -3 V vs SCE.

For the DMF/TBAI system, when the potential falls below -3.0 volts (vs SCE), reduction of the electrolyte occurs. To ensure that 100% of the current reduces naphthalene, the voltage must be kept above -3 volts. The voltammogram also indicates that the reduction of the electrolyte is not a reversible reaction because of the absence of an oxidation current (I<0) during the reverse sweep. Unless otherwise noted, electrochemical experiments were performed with a background electrolyte concentration of 0.1 M TBAI.

CV sweeps were completed on a solution containing 0.1 M naphthalene in TBAI/DMF. The voltammogram showing the reduction and oxidation of naphthalene is shown in Figure 5.3.

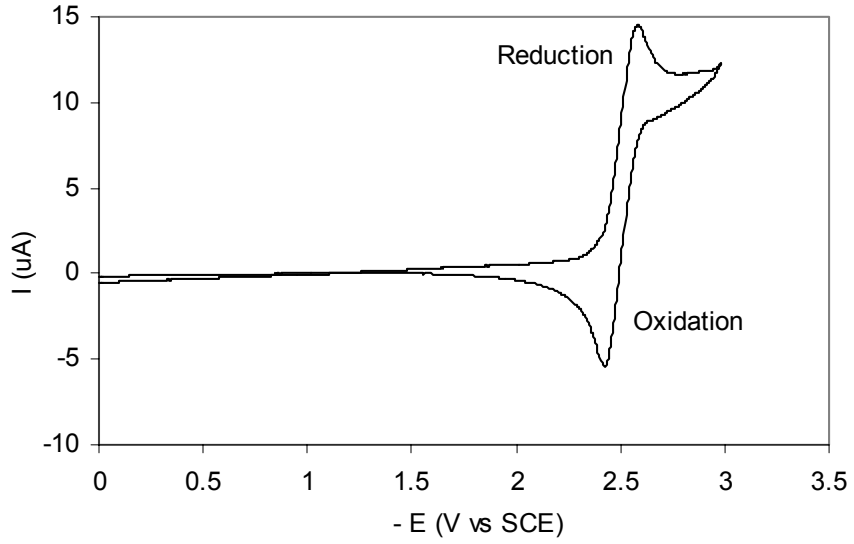

Figure 5.3. Cyclic voltammogram of naphthalene in DMF. The scan rate is 25 mV/s.

In the voltammogram, naphthalene reduction begins at 2.4 V. As the potential increases, the rate of radical generation also increases as indicated by the increasing current. In the solution near the electrode, the naphthalene is depleted. When the concentration at the

electrode surface reaches zero, the naphthalene reduction is limited by mass transfer of naphthalene from the bulk. This causes a subsequent decrease in the current and results in a peak in the voltammogram. After the first peak, the current begins to rise slightly again due to reduction of the electrolyte. The voltage sweep is then reversed. At -2.5 V, the radical anion begins to oxidize (I<0). An oxidation peak occurs because of similar depletion effects and mass transfer limitations of the radical anion.

The potential halfway between the reduction and oxidation peaks is termed the half wave potential and is typically used to describe the potential of the redox reaction. The half wave potential for naphthalene measured -2.50 V vs SCE, slightly lower than the typical reported value of -2.6 V. The separation between the reduction and oxidation peaks is 160 mV. For a reversible single electron transfer process, the oxidation and reduction peaks should be separated by 58 mV.[137] The peak separation increases linearly with the square root of the voltammogram sweep rate indicating uncompensated resistance in the cell.[140] Unfortunately, this particular potentiostat cannot measure or automatically compensate for solution resistance. Extrapolation to zero sweep rate still indicates a separation 120 mV. Possible causes for this phenomenon include quasi-reversibility due to electron transfer between radical anions and naphthalene or protic contamination reacting with the radical. For bulk electrolysis of naphthalene, the potential should remain above -3 V (vs SCE) to maintain 100% efficiency.

5.4.2 Bulk electrolysis and demonstration of defluorination

Experiments were performed to evaluate the defluorinating ability of electrochemically generated naphthalene radical anions. Radical anions were generated using the thin film

cell and the associated procedures described in Chapter 3. The working compartment was charged with approximately 1.5 mL of a solution containing 0.1 M naphthalene and 0.1 M TBAI in DMF. The counter electrode compartment was filled with 10 mL of 0.1 TBAI in DMF and a PTFE sample was loaded into the thin film compartment. Bulk electrolysis was performed using galvanostatic or current controlled generation with the platinum coil electrode. The maximum current was 5 mA (3.6 mA/cm^2) without exceeding -3 V. The voltage was typically -2.8 to -2.9 V (vs SCE). For 1.5 mL of solution, 5 mA of current for 5 minutes should produce a concentration of 10 mM of naphthalene radicals assuming 100% generation efficiency and no radical decay.

After generation, the compartment was rotated to transfer the solution to the thin film compartment and thereby expose the PTFE sample. With only 20 seconds of exposure, the PTFE sample surface (initially white) darkened considerably comparable to that observed upon exposure to sodium naphthalene solutions. XPS analysis confirms surface defluorination; the fluorine content was reduced from 33 at% to less than 2 at%. Clearly, electrochemically generated radical anions are able to defluorinate the fluorinated surface.

5.4.3 Concentration and degradation rate measurements

In order to study the effects of radical anion concentration on cleaning performance, a method to determine concentration is needed. Coloumometry can be used to monitor the generation rate; however, radicals have finite lifetimes because of their high reactivity. Degradation of the radicals occurs during generation, thereby requiring complete characterization of both processes. Because naphthalene radical anions absorb radiation

in the UV and visible range, the concentration can be monitored in-situ according to the Beer-Lambert law shown in Equation 5.8, where absorbance (A) is proportional to molar absorptivity (ε), concentration (c) and the light pathlength (l). Absorbance can be reliably measured between 0 and 1.0. The molar absorptivity parameter is characteristic of both the radical and the solvent and is also a function of the wavelength at which the measurement is made.

$$A = \varepsilon l C \qquad (5.8)$$

Measurement of the molar absorptivity is performed using a UV-visible dip probe immersed in an electrochemical cell as described in Chapter 3. As indicated by Equation 5.8, the absorbance is proportional to the concentration of the radical anion; however, determination of absolute concentrations is difficult without knowing the molar absorptivity. By differentiating Equation 5.8 with respect to time, the relationship between the change in absorption and change in concentration remains proportional to the molar absorptivity as indicated in Equation 5.9 where α is the derivative of the absorption with respect to time.

$$dA/dt = \alpha = \varepsilon l \, dC/dt \qquad (5.9)$$

Generation rate can be controlled by the electrolysis current. By measuring the increase in absorption at various currents, the molar absorptivity can be determined. The relationship between measured current and radical anion concentration is given by

differentiation of Faraday's law with respect to time. This is shown in Equation 5.10, where i is current, V is the working cell volume and F is Faraday's constant (96500 C/mol). This relationship assumes 100% current efficiency and negligible degradation of reactive species.

$$dC/dt = i / (F\ V) \qquad (5.10)$$

By combining equations 5.9 and 5.10, the relationship between the change in absorption and the measured current is given by Equation 5.11.

$$\alpha = \varepsilon\ l\ i / (F\ V) \qquad (5.11)$$

With a known solution volume and pathlength, the molar absorptivity can be determined from the slope of a plot of α versus electrolysis current. For the greatest sensitivity, absorption is measured at the wavelength where maximum absorption occurs.

5.4.4 Determination of molar absorptivity of anthracene radical anion

To validate the above procedure to establish equipment sensitivity, the molar absorptivity of anthracene was measured and compared to reported values. The absorption spectrum of anthracene is shown in Figure 5.5. The spectrum shape and maxima are in agreement with those in previous reports.[141] For this analysis, the absorption is monitored at 732 nm.

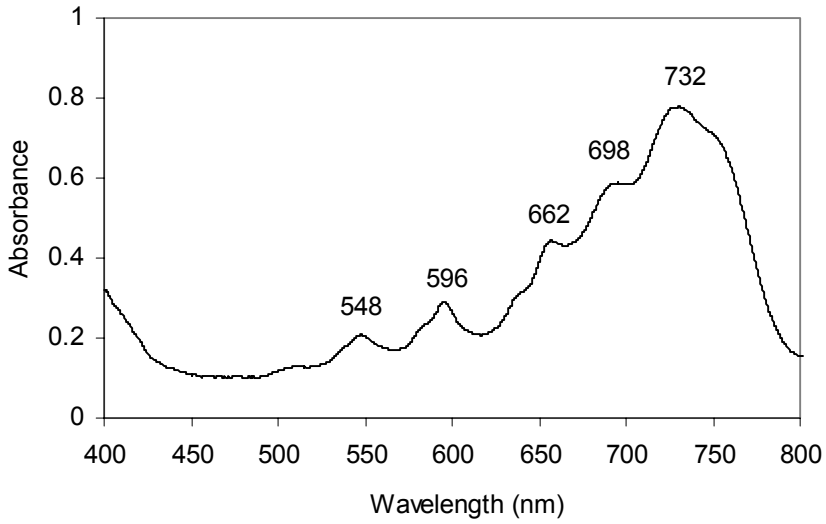

Figure 5.5. Visible absorption spectrum of the anthracene radical anion.

Using procedures described in Chapter 3, the absorption at 732 nm is recorded as the electrolysis current is cycled on and off. The applied current ranged between 0.5 to 10 mA. A typical plot of absorption versus time is shown in Figure 5.6.

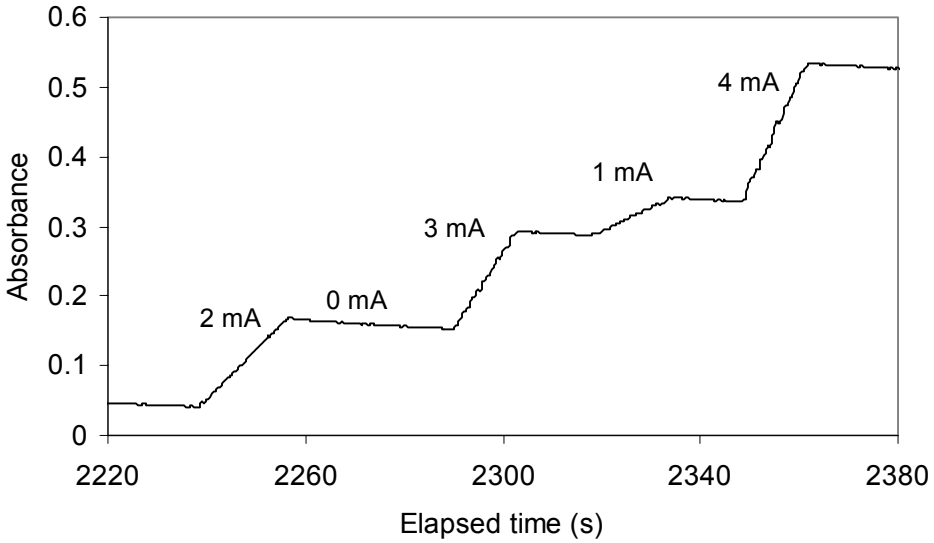

Figure 5.6. Absorption monitored at 732 nm during cycling of the electrolysis current.

The degradation rate of anthracene when no current is applied, while finite, is significantly slower than even the lowest generation rate as demonstrated in Figure 5.6; therefore, degradation can be neglected in the analysis for determination of the molar absorptivity. The change in absorption is evaluated for each electrolysis current; the rate, α, is plotted versus the electrolysis current in Figure 5.7. The slope of a linear regression line is proportional to the molar absorptivity according to Equation 5.11. The slope must be multiplied by FV/(il) to calculate the molar absorptivity. The value determined in this analysis is 9220 $cm^{-1}M^{-1}$, which agrees with the previously reported range of 9200-9400 $cm^{-1}M^{-1}$.[141] The x-intercept of the regression line intersects the origin indicating no significant absorption change with zero current. This validates the assumption that degradation of the anthracene is much slower than generation and can be neglected in this analysis.

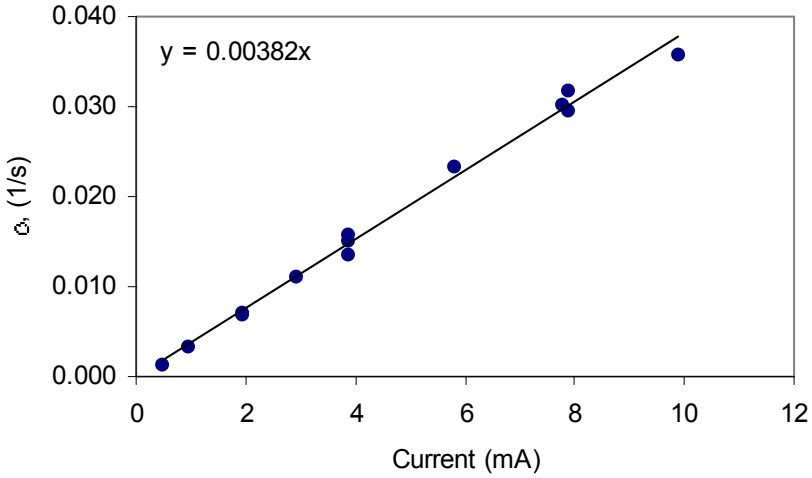

Figure 5.7. Absorption increase, α, versus applied electrolysis current for anthracene radical anion generation. The slope of the regression line is proportional to the molar absorptivity.

5.4.5 Determination of molar absorptivity of naphthalene radical anion

The visible absorption spectrum for naphthalene is shown in Figure 5.8. Over the visible range, the wavelength with maximum absorption occurs at 859 nm; however, monitoring the absorption at 805 nm reduced the noise in the measurements. This occurred because the amount of reflected light from the probe tip significantly decreases at higher wavelengths.

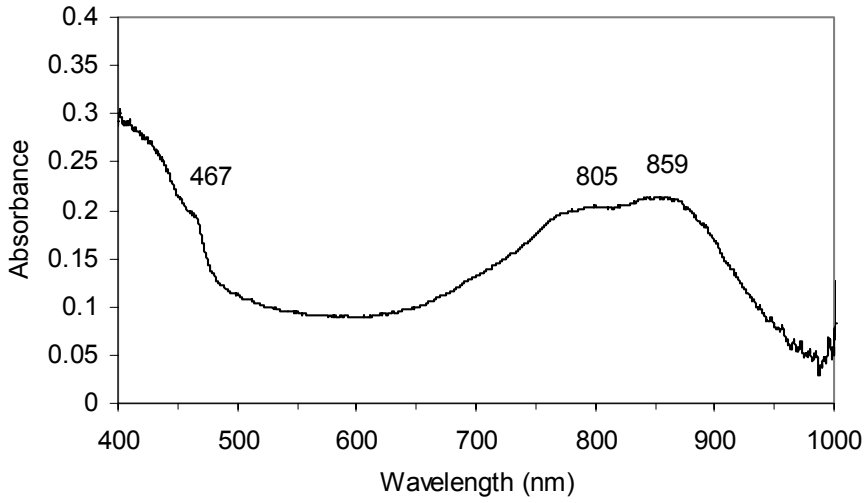

Figure 5.8. Visible absorption spectrum of naphthalene radical anions.

During electrochemical generation of naphthalene, the degradation rate is significant; therefore, the degradation must be incorporated into the model for determination of the molar absorptivity. The reaction that consumes radical anions is assumed to obey concentration dependent decay. Since the reaction order is unknown, both the reaction order and rate constant are determined using two different methods: initial rate analysis and differential analysis. Initial rate analysis is based on Equation 5.11 which demonstrates the relationship between the initial degradation rate, α_o, the reaction constant, k', the initial absorption, A_o, and the reaction order, n, of concentration dependent decay.

$$\alpha_o = - k' A_o^n \qquad (5.11)$$

For initial rate analysis, radical anions are generated electrochemically, then, at specific concentration (absorbance) levels, the electrolysis current is discontinued and the degradation rate of the radical anion is recorded. This procedure is repeated at a variety of different absorbance values. The order and rate constant are determined by plotting the log of the negative of the initial degradation rate, $-\alpha_o$, against the log of the initial absorbance value, A_o, as shown in Equation 5.12. The intercept of a linear regression line is equal to the log of the rate constant and the slope is equal to the reaction order.

$$\log(-\alpha_o) = \log(k') + n \log(A_o) \qquad (5.12)$$

This plot is shown in Figure 5.9 where an order of 0.7 and a reaction constant of 0.0035 s^{-1} is calculated. The rate constant, k', is valid only with respect to the absorbance rate and must be converted to concentration units.

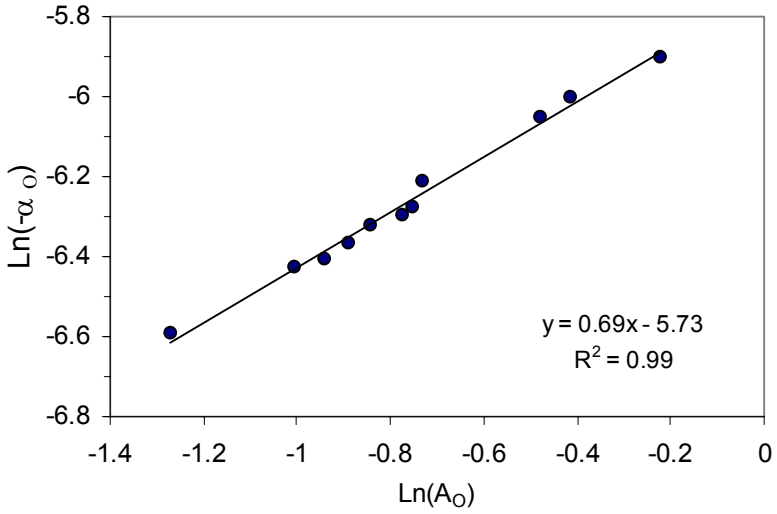

Figure 5.9. Initial rate analysis of naphthalene radical anion degradation.

In order to convert the reaction rate constant to concentration units, the rate law for degradation of absorbance, shown in Equation 5.13, must be written in terms of concentration.

$$\alpha = - 0.0035\ A^{0.7} \qquad (5.13)$$

To convert the equation to concentration, both sides are divided by εl; therefore, the rate constant, in terms of concentration, k, is equal to $k'/(\varepsilon l)^{0.3}$. This parameter will be evaluated after the molar absorptivity is determined in the next section.

In addition to an initial rate analysis, a differential analysis is performed to verify that the order and rate constant do not change as a function of time. Similar to the previous analysis, radical anions are generated until the absorbance approaches 0.9. The electrolysis current is terminated and the complete degradation to zero absorbance is

recorded. The instantaneous rate at each concentration is obtained by measuring the slope of the graph of absorption versus time. Using Equation 5.13, a plot of the log of instantaneous rate versus the log of the concentration allows determination of the reaction order and rate constant. This plot is shown in Figure 5.10.

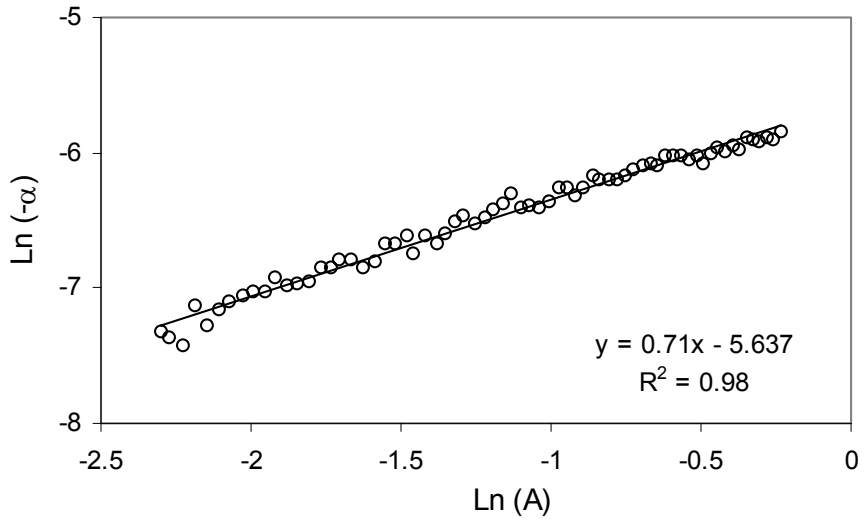

Figure 5.10. Differential analysis of naphthalene radical anion degradation. The linear regression indicates an order of 0.71 and a rate constant of 0.00356 s^{-1}.

A time dependent order is measured to be 0.71 with a rate constant of 0.00356 s^{-1}. These results are very close to the order and rate constant obtained with the initial rate analysis indicating that the kinetics do not change appreciably over concentration or time. This also indicates that reaction byproducts do not affect the reaction rate (product inhibition). Using the values determined above the rate law for decay of radical naphthalene anions is compared to observed data. The fit is good as demonstrated by Figure 5.11.

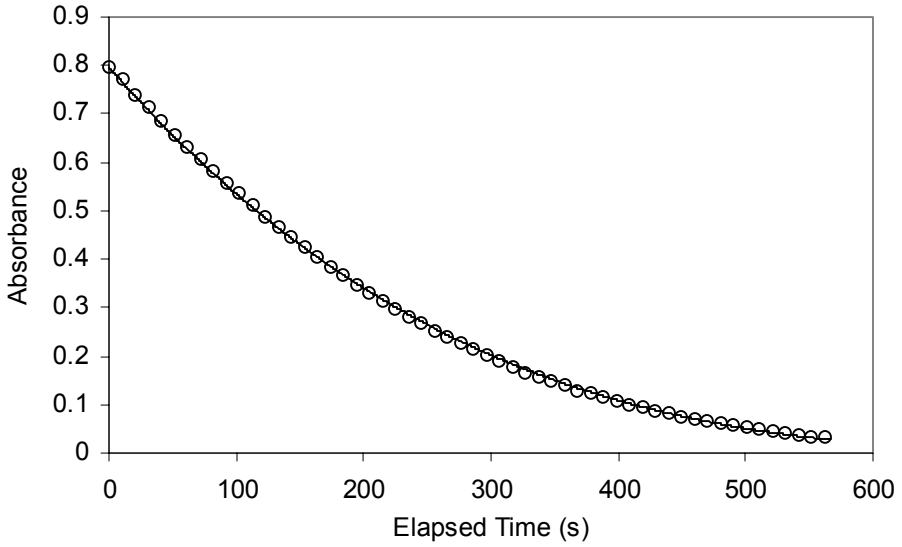

Figure 5.11. Fit of naphthalene radical anion degradation using kinetic parameters, n = 0.70 and k' = 0.0035 s^{-1}.

With the degradation rate fully characterized, the previous approach is repeated for naphthalene radical anions to determine the molar absorptivity. Currents ranging from 0.5 to 15 mA are applied to the electrochemical cell and the corresponding increase in absorption is measured. Because the degradation rate is comparable to the generation rate, degradation must be taken into account in the determination of the molar absorptivity. Equation 5.10 is modified to include a degradation term, $-kC^n$, to account for the simultaneous decay of the radical anions during generation. This new equation is combined with Equation 5.11, to produce Equation 5.14 which demonstrates the relationship between absorption rate, electrolysis current and degradation rate.

$$\alpha = \varepsilon l(i / FV - k\, C^{0.7}) \qquad (5.14)$$

Simplifying using $k = k'/(\varepsilon l)^{0.3}$ and $A = \varepsilon lC$.

$$\alpha = \varepsilon li / FV - k' A^{0.7} \qquad (5.15)$$

This differential equation cannot be solved explicitly; however, over short times, the degradation rate can be assumed constant and dependent only on the initial absorption. This allows substitution of A_o for A, and, after rearranging, results in Equation 5.16 for short times.

$$\alpha + k' A_o^{0.7} = \varepsilon li / FV \qquad (5.15)$$

The left side of the equation is plotted versus current in Figure 5.12. To determine the molar absorptivity, the slope is multiplied by FV/l. Using this analysis, the molar absorptivity of naphthalene was determined to be 2580 $M^{-1}cm^{-1}$. With this value, the rate constant with respect to concentration, k, is calculated to be 5.37×10^{-4} $M^{0.3}s^{-0.3}$.

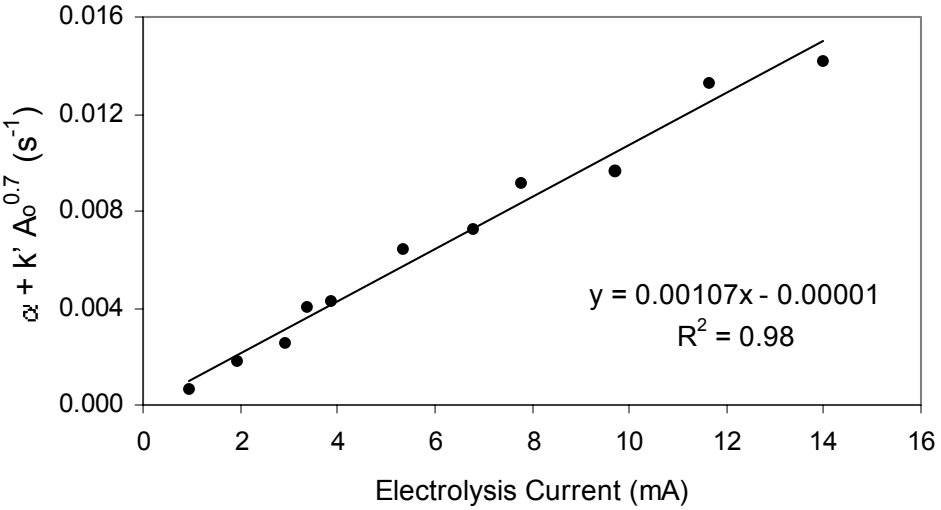

Figure 5.12. Determination of naphthalene radical anion molar absorptivity by plotting left and right side of Equation 5.15. Based on the slope, the molar absorptivity was determined to be 2580 $M^{-1}cm^{-1}$

With the degradation characterized and molar absorptivity estimated, the concentration of naphthalene radical anions can be estimated at any time for a specific electrolysis current. Using numerical integration of Equation 5.16, Figure 5.13 can be constructed to estimate the concentration as a function of electrolysis current.

$$dC/dt = i / FV - k\,C^{0.7} \qquad (5.16)$$

For the remaining chapters, naphthalene radical anions are predicted using the above model.

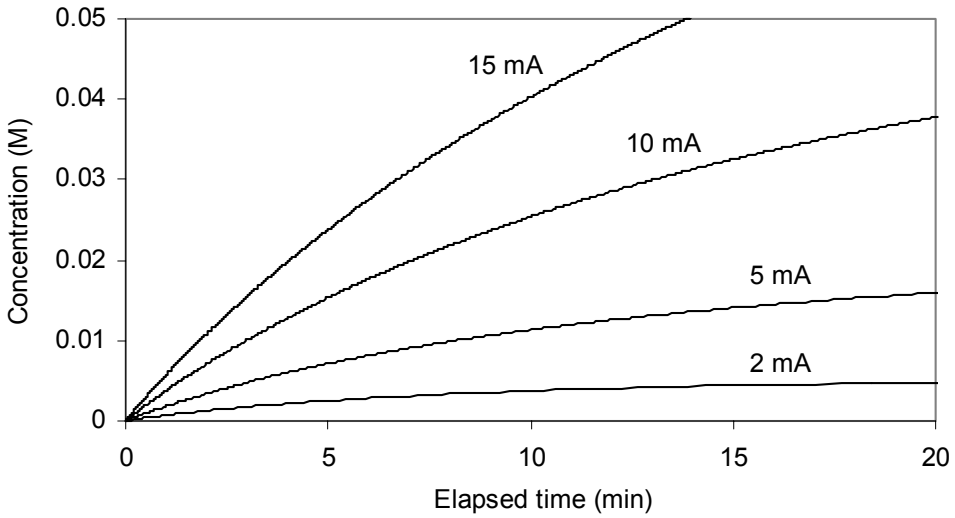

Figure 5.13. Estimation of radical anion concentration as a function of electrolysis current with a solution volume of 1.5 mL.

5.4.6 Degradation mechanism

A variety of possibilities exist that could cause the degradation of radical anions; however, the most likely cause is protonation by air or solvent contamination. The radical anion degradation rate was unaffected when all sources of visible or UV radiation were absent, eliminating interaction with radiation as a possibility. Dianon formation or radical anion reactions with the electrolyte are also unlikely because they are not driven thermodynamically.

Kinetic information for the protonation of radical anions by water is available for both naphthalene and anthracene radicals anions generated using sodium. The rate laws are

first order in both water and the radical anion. In the solvent dimethoxyethane, the nature of the ion pair, which affects reactivity, is similar to radicals electrochemically generated in DMF. Protonation reaction constants for naphthalene and anthracene radicals are 234 and 17 $M^{-1}s^{-1}$ respectively.[142,143] This surprisingly large difference in reactivity likely accounts for the significant difference between the degradation rates of anthracene and naphthalene radicals. With the rapid reaction rates, residual water in the solvent or electrolyte would be consumed quickly; therefore, water in the solution is likely not a significant cause of the degradation once the radicals are generated.

In order to determine if the degradation occurred in the bulk solution or at a surface in the solution, degradation was recorded with and without agitation from the magnetic stirrer. A reproducible change in degradation rate was observed and is shown in Figure 5.14. The new degradation rate followed a rate law with an 1.3 order and a reaction constant of 0.0077 s^{-1}. The difference in degradation rates indicates that the degradation was affected by species diffusion. This also indicates that the degradation was caused at least partially by surface reactions, although reactions in the solution could also be significant. No gradient of radical anions was observed visually.

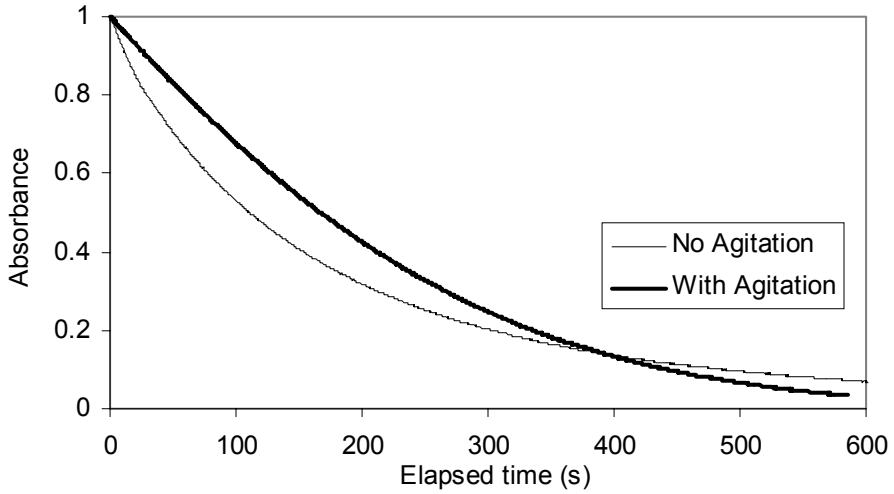

Figure 5.14. Comparison of degradation rates of naphthalene radical anion with and without agitation by a stir bar.

The radical degradation was allowed to proceed without agitation; however, if agitation was applied during the degradation, an immediate increase in the absorption was observed providing further evidence that a gradient is present. Two possible causes for a surface reaction are protic contaminants in the atmosphere above the solution or reduction of iodine (I_2) that diffuses through the frit that separates the working and counter electrode compartments. Degradation is still observed after being seperated from the cell to a separate vial; therefore, iodine diffusion is also not a significant cause for degradation. Although the nitrogen for the dry box is filtered for water vapor using in-line cartridge filters (Matheson Tri-Gas Item #451), it appears that the primary cause of degradation is water vapor or oxygen in the atmosphere above the solution. Degradation rates measured after replacing the filters did not affect the rate. In addition, a constant nitrogen purge above the anion radical solution resulted in a degradation reaction order of 1.9, close to the predicted value of 2.0 for a protonation reaction. While it is unfortunate

that the nitrogen atmosphere contains trace contaminants causing degradation of the radical anions, it is more important that the concentration can be predicted reliably.

5.4.7 Generation in alternative solvents

The generation and degradation rate of naphthalene radical anions was also evaluated in several other solvents. Cyclic voltammetry indicated reduction of naphthalene in NMP was possible; however, the radicals did not accumulate in the cell. Similarly, the typical absorption spectrum of radical naphthalene was not observed during electrolysis in the probe cell during generation with NMP. Cyclic voltammetry also indicated that generation did not occur in acetone, although the solvent meets the requirements for generation.

Radical anion generation and accumulation was achieved in both dimethylsulfoxide (DMSO) and acetonitrile solutions. Comparable generation and degradation analysis was performed using 0.1 M TBAI as a background electrolyte. Degradation rate and molar absorptivity is compared in Table 5.1.

Table 5.1 Comparison of radical anion rates and properties in different solvents

	DMF	DMSO	Acetonitrile
Degradation reaction			
Order, n	0.70	0.69	0.45
Rate constant, k' (s^{-1}) *	0.0035	0.00140	0.0205
Rate constant, k ($M^{(1-n)}s^{-1}$) **	0.000537	0.000206	0.00134
Molar absorptivity at 805 nm ($M^{-1}cm^{-1}$)	2580	2410	2040

* With respect to absorption

** With respect to concentration

The degradation rate is significantly different is each of the following solvents suggesting that the protic solvent contaminants may play a role in the degradation process. The degradation rate of radical anions in acetonitrile is too rapid to be used practically and is likely due to ineffective drying of the solvent. More effective drying techniques for acetonitrile are required.

Conclusion from generation and degradation analysis

Cyclic voltametry analysis suggests that naphthalene radical anions are being generated at 100% efficiency as long as the galvanostatic voltage is maintained above -3 volts vs SCE. If generation is not 100%, the efficiency changes little over the current range between 0.5 and 18 mA as indicated by the linear relationship between generation currents and absorption measurements. Based on this technique, the molar absorptivity of naphthalene radical anions were measured in DMF, DMSO and acetonitrile. With the degradation process characterized, radical anion concentration can be estimated during generation. Radical anion generation was not achieved in acetone and NMP, solvents that are commonly used in semiconductor cleaning processes.

CHAPTER 6

INTERACTIONS WITH FLUOROCARBON RESIDUES

6.1 Overview

Model etch residue films were initially characterized and modified using naphthalene radical anions generated using sodium metal. Model etch residue samples exposed to solvents used in electrochemical reactions rapidly delaminated from the substrate making these films unsuitable for evaluation of electrochemically generated radical anions. In order to understand the interaction between the solvent and residues, a surface energy model is used to investigate residue/solvent interactions. Additionally, industrial-supplied patterned etch residues were used to assess the cleaning capabilities of naphthalene radical anions generated electrochemically. Evaluation was completed by optical and electron microscopy and XPS surface analysis. The effects of radical anion concentration and exposure time were evaluated. From the observations and data obtained, a mechanism is proposed for residue removal using radical anions.

6.2 Model Etch Residue Cleaning Using Electrochemically-Generated Radicals

6.2.1 Solvent interactions with fluorocarbon residues

Initial experiments indicated that exposure of model etch residues to naphthalene radical anions electrochemically-generated in DMF and DMSO caused the residue to rapidly delaminate from the substrate. While this delamination demonstrates effective cleaning of the model residues, it is difficult to obtain mechanistic information with such a rapid

delamination. Further experimentation showed that comparable delamination occurred when etch residue samples were immersed in those two pure solvents. As a result, the role of the radical anions is unclear compared to the solvent/fluorocarbon interaction. Solvents such as THF and acetonitrile, however, did not cause delamination. Understanding and predicting interfacial wetting and solvent absorption into the residue are thus key for the design of effective residue removal chemistries. Prediction of this interaction can assist in fundamental understanding as well as aid in development of cleaning processes. Further experiments and solvent property analyses were performed in order to relate the wetting and absorption abilities to solvent properties.

Submerging etch residue samples in pure solutions of DMF, DMSO and NMP at room temperature resulted is delamination of the fluorocarbon film from the silicon substrate in less than 15 seconds. Exposure of the substrate/film interface at the sample edge could contribute to wetting of the interface and subsequent delamination. To evaluate this effect, samples were exposed using the 'drop' method where a single drop of the solution is placed in the center of a sample to avoid exposure of the residue/substrate interface at the sample edge. This method more accurately simulates cleaning of large substrates such as wafers where the interface is not exposed directly to the solution. Procedural details of this technique are given in Chapter 3.

Results of exposure using the 'drop' method, however, were comparable to immersion. The three solvents appeared to penetrate through the residue and wet the fluorocarbon/substrate interface causing delamination at the silicon/fluorocarbon

interface. In fact, large pieces of the fluorinated film were suspended in the solvent drop during exposure. If the solvent was removed by a capillary and dried in air, the film re-deposited onto the surface, although this film had undergone significant physical modification. Optical microscope images of film samples exposed to DMF are shown in Figure 6.1.

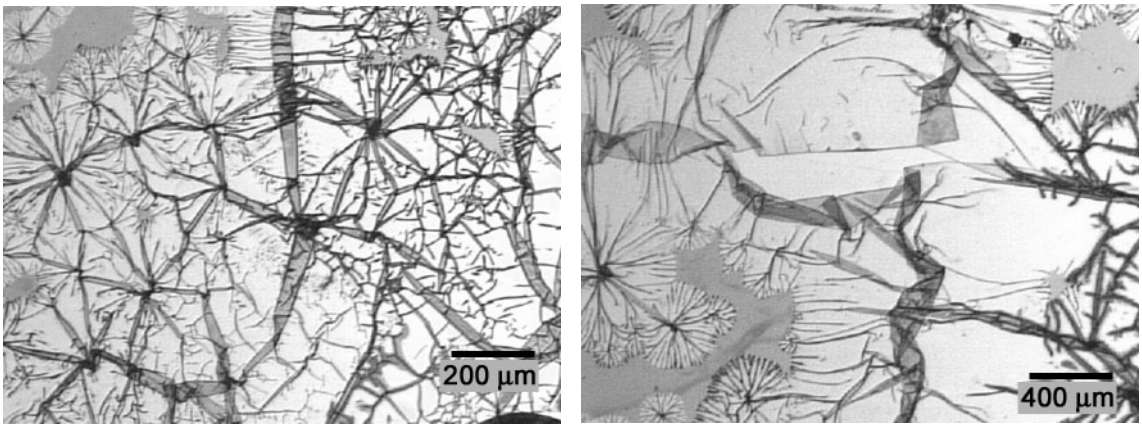

Figure 6.1. Optical micrographs of fluorocarbon exposure to DMF solvent.

Clearly, after the solvent was dried from the residue, considerable cracking and wrinkling was observed. This physical modification of the film resulted from the stress due to interfacial wetting between the residue and the substrate. From the optical micrographs, it appears that wetting may have originated at finite points, possibly pinhole defects in the residue rather than uniform absorption through the fluorocarbon residue. Prior to exposure, no defects were observed by optical microscopy or SEM analysis. Pinhole defects are also unlikely to occur in a blanket plasma deposited film of this thickness (230 nm). XPS analysis of the solvent-exposed residue indicated no chemical change of the model residue.

The mechanical force from rinsing an exposed sample using a stream of isopropyl alcohol from a squirt bottle resulted in removal of the wet portion of the film from the substrate. Comparable exposure from acetonitrile and THF did not penetrate or delaminate the fluorocarbon residue. Even with complete immersion of the sample and exposure of the interface at the sample edge, acetonitrile and THF did not wet the fluorocarbon substrate interface. Similarly, XPS analysis confirmed that these solvents caused no chemical change to the surface of the residues. Properties of the five solvents and water are listed in Table 6.1 and chemical structures are shown in Figure 6.2. NMP is included for comparison because it is a major component in several commercial post-plasma etch cleaning formulations.[144]

Table 6.1 Comparison of solvent properties [145,146]

	DMF	NMP	DMSO	ACN	THF	Water
Boiling point (°C)	153	202	189	81.6	66	100
Dielectric constant (25 °C)	36.7	36.7	46.7	37.5	7.6	80
Dipole moment (Debye)	3.86	4.09	4.1	3.44	1.75	1.87
Hildebrand parameter ($Cal^{1/2}cm^{-3/2}$)	12.1	11.2	12.9	11.9	11.0	23.5
Hansen - dispersive parameter ($Cal^{1/2}cm^{-3/2}$)	8.5	8.8	9.0	7.5	9.3	7.6
Hansen - polar parameter ($Cal^{1/2}cm^{-3/2}$)	6.7	6.0	8.0	8.8	5.0	7.8
Hansen - hydrogen bonding parameter ($Cal^{1/2}cm^{-3/2}$)	5.5	3.5	5.0	3.0	1.8	20.7
Fluorocarbon etch residue delamination	Yes	Yes	Yes	No	No	No

Fluorocarbon etch residue delamination caused by the solvents may be predicted by specific solvent properties. The dielectric constant of a material is a measure of the polarity and the polarizability (induced polarity). A larger dielectric constant indicates a

greater ability to transfer charge or stabilize polar or ionized species in solution. The dipole moment of a molecule is another measure of the polarity and indicates unequal electron sharing due to electronegativity differences. The Hildebrand solubility parameter is a measure of the cohesive energy density of the solvent. This parameter is commonly used to predict the solubility of polymers in solvents (by minimizing the difference between the solvent and polymer Hildebrand parameters).[145] Hildebrand solubility parameters for polymers are determined by trial and error using a variety of solvents. The solubility parameter is estimated from the solvent that causes maximum swelling of the polymer. Hansen further refined the solubility parameter by separating the contributions from dispersive interactions, polar interactions and hydrogen bonding interactions.[145]

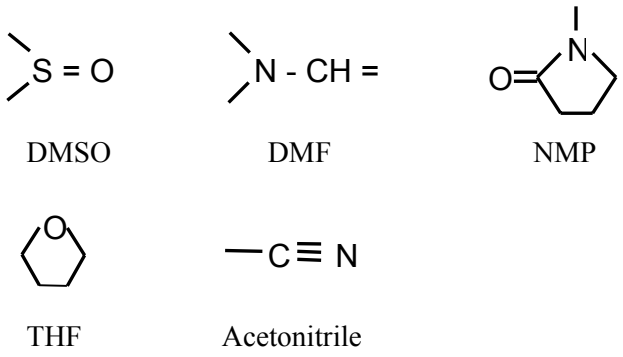

Figure 6.2. Molecular structure of selected solvents.

Dispersive or London dispersion interactions are attractive forces which occur between nonpolar molecules. Due to random fluctuations in electron density around the molecule, a nonpolar molecule can become temporarily polar. This temporary polarity can induce similar unequal electron distribution in another molecule thereby resulting in electrostatic

attractive forces. Polar interactions include permanent dipole-dipole or permanent dipole induced forces. Hydrogen bonding interactions are a subset of polar forces, but are treated separately by Hansen because the interaction is much stronger than typical polar interactions. Similarly, predictions of solubility of polymers in solvents can be made by closely matching the solvent parameter values with those of the polymer. In addition, the square root of the sum of the squares of the Hansen parameters is set equal to the Hildebrand parameter. This enables determination of all three Hansen parameters when two are measured.

The dielectric constant is a poor predictor for the solubility in this case. The dielectric constant of acetonitrile is similar to DMF and NMP. The polarity, as indicated by the dipole moment, appears to be relevant for predicting the fluorocarbon interaction. A minimum polarity may be required; however, water, the most polar solvent does not wet the fluorocarbon surface. Therefore, polarity alone is not an accurate predictor of the observed behavior. The Hildebrand parameter for THF and acetonitrile is fairly close to those of DMF and NMP. The Hildebrand parameter is a measure of total interaction; however, comparison of specific interactions is more accurate.

Hansen parameters account for individual types of interactions as mentioned previously. Although the data set is limited, there are some differences between the solvents. Acetonitrile has a dispersive strength similar to water. The Hansen polar and hydrogen bonding parameters for THF are lower than those of DMF, NMP and DMSO. Based on this small data set, it appears that both dispersive and polar interactions are important in

the observed delamination. This is consistent with the fact the fluorocarbon residue contains both a dispersive character from the carbon-carbon network as well as unshielded polar moieties such as CF and CF_3.

It is important to note the differences between the plasma deposited fluorocarbon residue and polytetrafluorethylene (PTFE). Although the carbon-fluorine bond is highly polar, the size and packing of fluorine atoms along the PTFE chains result in a perfectly shielded carbon backbone. The polar nature of the carbon-fluorine bond is not accessible to solvent molecules and therefore can not interact with solvent molecules. This results in a nonpolar surface. The etch residue surface differs from PTFE because there is a collection of CF_3, CF_2 and CF and CC moieties which prevent effective geometrical shielding of PTFE chains. Moieties such as CF and CF_3 are often exposed and contain strong dipoles providing interaction sites with polar molecules. Although water is polar, extremely strong hydrogen bonding prevents water from absorbing significantly into the fluorocarbon. In the next section, polar and dispersive interactions between the solvent and fluorocarbon are quantified.

6.2.2 Owens/Wendt/Fowkes method for determination of surface energy

Empirical observations suggest that both the polar and dispersive interactions are important parameters that indicate an ability of a solvent to wet the fluorocarbon residue surface. The Owens/Wendt two-component energy theory enables quantification of those individual contributions for both surfaces and solvents. This theory assumes that liquid/solid or liquid/surface interactions are composed of contributions from polar and dispersive interactions.[147,148] Originally this method utilized a variety of liquids with

varying polarities to characterize surfaces. Fowkes simplified the procedure for determination of surface energies by using only two probe liquids and a surface with a known surface energy.[149] Using probe liquids is ideal under these conditions where the solvents are known to strongly interact or absorb with (unknown) surfaces. A brief overview of the theory and methodology is given here; however, the reader is referred to specific references for a more complete discussion.[147,148,149,150]

The free energy, ΔG_i , associated with immersion of a solid into a liquid can be described by Equation 6.1 where γ_s is the air/solid interfacial free energy and γ_{sl} is the solid/liquid interfacial free energy. Upon immersion, the air/solid interface is replaced by a liquid/solid interface, and the free energy change between the two states is simply this difference as shown in Equation 6.2.

$$\Delta G_i = \gamma_{sl} - \gamma_s \qquad (6.2)$$

For simplification, the air/solid interfacial free energy will be referred to as the surface energy, air/liquid interfacial free energy will be refereed to as surface tension and solid/liquid interfacial free energy referred to as the interfacial energy. The most difficult parameter to determine is the solid/liquid interfacial energy. Immersion or wetting of a solid by a liquid is thermodynamically favorable if the free energy is negative. In addition, effective wetting is critical for dissolution of a solid in a liquid.[148] Furthermore, the magnitude of the free energy also indicates the strength of the liquid/solid interaction.

Young's equation describes the relationship between the solid surface energy, γ_s, the solid/liquid interfacial surface energy of a liquid, γ_{sl}, the air/liquid surface energy or surface tension, $\gamma_{l,}$ and the contact angle on a liquid drop on a surface, θ, as shown in Equation 6.2. Since there is typically little interaction between a liquid and air, the air/liquid interfacial energy can be thought of as the cohesive energy of the liquid (surface tension). Either the surface energy or the interfacial surface energy must be known for this equation to be applied to specific systems.

$$\gamma_s = \gamma_{sl} + \gamma_l \cos \theta \qquad (6.2)$$

Equation 6.2 can be described using a energy balance as shown in Figure 6.3. When a drop forms on the surface, two interfaces are important - the gas/liquid, liquid/surface. Cohesive forces (surface tension) within the liquid attempt to minimize thermodynamically unfavored interfaces and maximize the favored interfaces. If the surface has a high surface energy and can interact with the liquid, the surface energy overcomes cohesive energy and the drop spreads along the surface. For the liquid/air interface, a liquid almost always prefers to minimize this interface by forming a spherical shape which minimizes surface area to volume ratio.

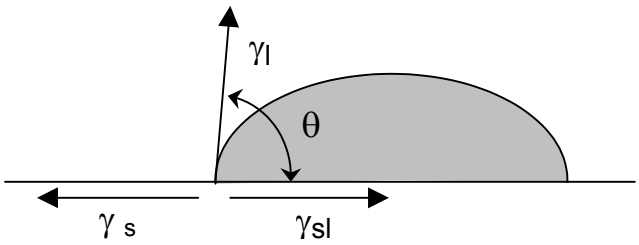

Figure 6.3. Force balance between surface tension, interfacial tension and surface energy.

Combining Equations 6.1 and 6.2, the relationship between the liquid contact angle and the free energy of immersion is described.

$$\Delta G_i = -\gamma_l \cos\theta \qquad (6.3)$$

This relationship is physically intuitive as contact angle measurements are commonly used to investigate the wetting behavior of a liquid on a solid surface. As the contact angle approaches 0°, the free energy becomes more negative and thus solvent/surface interactions become stronger. Contact angles above 90° lead to positive free energy values indicating unfavorable interactions.

To obtain surface energy information from contact angle measurements, the free energy from surface wetting, instead of complete immersion, needs to be determined. The free energy associated with the formation of a drop on a surface is given by Equation 6.4. The free energy change is related to the initial state of liquid and surface interfaces with

air. Upon liquid exposure, the interfacial surface energy replaces the initially separate liquid/air and surface/air interfacial energies.

$$\Delta G_{sl} = \gamma_{sl} - \gamma_s - \gamma_l \qquad (6.4)$$

In order for Equation 6.4 to be useful, two of the three interfacial energy values must be known. Generally, only the surface tension of the liquid, γ_l, is available. Good, based on empirical evidence and data fitting, assumed a relationship for the free energy, ΔG_{sl}, as a geometrical mean of polar and dispersive energy contributions shown in Equation 6.5 where the 'd' and 'p' superscripts denote dispersive and polar contributions, respectively.[150]

$$\Delta G_{sl} = -2\left[(\gamma_l^d \gamma_s^d)^{1/2} + (\gamma_l^p \gamma_s^p)^{1/2}\right] \qquad (6.5)$$

With this model, the free energy is always negative, thus always indicating favorable conditions for wetting. Since the initial state of the liquid is a drop surrounded by air, therefore; a liquid will almost always favor a solid surface interface versus an air interface (exceptions occur when contact angles are greater than 90°). It can also be shown that the free energy is minimized (maximum interaction and wetting) when the relative contributions of polar and dispersive forces for the surface and the liquid are equal. For example, if a polar contribution of the surface energy is 30% of the total, a liquid with a 30% polar contribution to the surface tension will minimize the free energy.

Combining Equations 6.4 and 6.5, the interfacial surface energy is a function of the surface tension and surface energy.

$$\gamma_{sl} = \gamma_s + \gamma_l - 2\left[(\gamma_l^d \gamma_s^d)^{1/2} + (\gamma_l^p \gamma_s^p)^{1/2}\right] \qquad (6.6)$$

Equation 6.2 can be substituted into Equation 6.6, to yield Equation 6.7, which relates the polar and dispersive contributions to the contact angle. This relationship is the basis for determination of the individual contributions.

$$(\gamma_l^d \gamma_s^d)^{1/2} + (\gamma_l^p \gamma_s^p)^{1/2} = \gamma_l(\cos\theta + 1)/2 \qquad (6.7)$$

In order to determine the dispersive and polar energy contributions, the solvents and surfaces are analyzed separately. For solvent characterization, the contact angle of the liquid is measured on a PTFE surface where the surface energy is known to be 18 mJ/m^2.[148] Since PTFE is capable of only dispersive interactions ($\gamma_s^d = \gamma_s = 18$, $\gamma_s^p = 0$), Equation 6.7 simplifies to Equation 6.8.[148]

$$\gamma_l^d = [\gamma_l(\cos\theta_{ptfe} + 1)]^2/72 \qquad (6.8)$$

6.2.3 Characterization of liquids

With the surface tension (γ_l) known for most liquids, the dispersive component of the liquid free energy can be determined by measuring the contact angle of the liquid on

PTFE. The polar component can be calculated by subtracting the dispersive component from the surface tension. This process was completed for the solvents used above and the results are shown in Table 6.2.

Table 6.2. Surface tension component results of selected solvents.

Solvent	Surface tension[145] (mJ/m^2)	Contact angle measured on PTFE	Dispersive component of surface tension, γ_l^d (mJ/m^2)	Polar component of surface tension, γ_l^p (mJ/m^2)
NMP	40.8	74.5°	37.1	3.7
DMSO	43.0	84.9°	30.5	12.5
DMF	37.1	74.1°	31.0	6.1
Acetonitrile	19.1	63.4°	10.6	8.5
THF	26.4	42.0°	29.4	-1.3
Diiodomethane	50.8	77.8°	52.8	-1.8
Water	72.8	113.9°	24.5	48.3

Contact angle measurements for the solvents ranged from 42° to 114° and the value for water matched closely with the literature value of 113.6°.[148] The negative values for the polar contributions for THF and diiodomethane are likely a result of error in measurement of the contact angle. Because the calculation is based on the cosine function, the error in surface energy values increases with contact angle measurements. For example, a 1° change in contact angle at 30° results in a 1% energy change, however, a 1° change in contact angle at 70° equates to a 5% change. Based on its molecular structure and its use as a basis for surface characterization, the polar contribution of the surface tension of diiodomethane should be zero.[148] The theoretical contact angle value required for zero polar contribution is 79°, which falls within the measurement error of diiodomethane as shown in Table 6.2. Dispersive values for THF and diiodomethane

will be assumed zero; since the following calculations prohibit negative values of the dispersive component.

The dispersive interaction contribution calculated from the Owens/Wendt/Fowkes method can be compared to the Hansen dispersive parameter. Each dispersive contribution is normalized by the appropriate parameter, i.e., the dispersive component of surface tension is divided by total surface tension and the Hansen dispersive parameter is divided by the Hildebrand solubility parameter. Results are plotted in Figure 6.4.

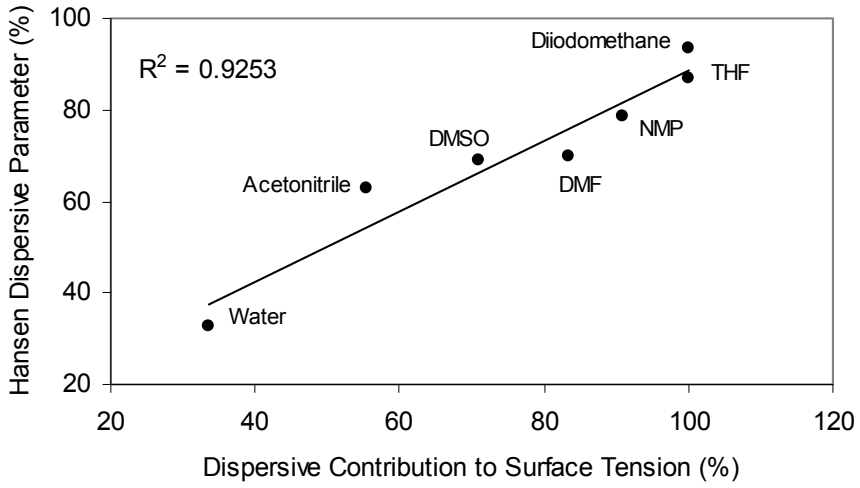

Figure 6.4. The percentage of the Hansen dispersion parameter is plotted versus the percent dispersive contribution of the surface tension determined by Owens/Wendt/Fowkes method.

For the limited data set, the correlation is good between the two theories, thereby justifying the procedure and results. The dispersive component of the surface tension also correlates with the number of CH_x moieties in each molecule (except for diiodomethane).

6.2.4 Characterization of surfaces

Similar to the above approach, dispersive and polar contributions of the energy for a surface can be characterized using the two probe liquids that have been characterized previously. Diiodomethane does not have a polar component of its surface energy simplifying Equation 6.5 to Equation 6.7 ($\gamma_l^d = \gamma_l = 50.8$). Therefore, only the contact angle of diiodomethane on the unknown surface is required to determine the dispersive component of the surface energy.

.

$$\gamma_s^d = \gamma_l (\cos \theta_{diiodomethane} + 1)^2/4 \qquad (6.7)$$

After the dispersive component is known, any other liquid with known contributions can be used to determine the polar component. With its strong polar contribution, water is typically used as the second probe liquid. From measurement of the contact angle of water on the unknown surface, every parameter in Equation 6.5 except the polar component of the surface energy, γ_l^p, is known. The polar and dispersive surface energies of various surfaces are shown in Table 6.3.

Table 6.3. Contact angle measurements and surface energy contributions for various surfaces.

Surface	Diiodo-methane contact angle	Water contact angle	Dispersive component of surface energy, γ_l^d (mJ/m^2)	Polar component of surface energy, γ_l^p (mJ/m^2)	Total surface energy, γ_s (mJ/m^2)
AP3-1	77°	92°	19.1	3.5	22.6
Reduced AP3-1 *	26°	49°	45.8	14.0	59.8
PTFE	74°	114°	20.7	0.07	20.7
Reduced PTFE *	57°	40°	30.3	27.9	58.2
Silicon wafer (SiO_2)	50°	51°	33.5	19.5	53.0

* Treated with 0.1 M sodium naphthalene for 1 minute

As expected, the surface energy of the model etch residue (AP3-1) is similar to that of PTFE with a low overall energy and high contribution from dispersive interactions. After defluorination by sodium naphthalene treatments, the total surface energy for both fluorocarbon surfaces increases significantly. The increases in total surface energy values imply that more energy is available for chemical interactions. In addition, the polar surface energy also increased significantly suggesting the introduction of polar surface moieties. From the energy balance described by Figure 6.3, as the interfacial surface energy, γ_{sl}, is reduced, the contact angle must decrease to balance the surface energy, γ_s. From XPS analysis of the treated surfaces, carbon-fluorine bonds are replaced with carbon-carbon or carbon-oxygen bonds, which are less polar; however, the overall surface became more polar. This is due to reduction of geometrical shielding caused by CF_2 and CF_3 moities similar to PTFE. Increased porosity and solvent accessibility to polar bonds result in the surface polar contribution increase. Incorporation of carbon-carbon double bonds also enhance dispersive interactions. Silicon dioxide surface analysis was included because the fluorocarbon model films are deposited on silicon wafers

6.2.5 Calculations of surface interaction energies

Calculation of the solid/liquid interfacial free energy is now possible using Equation 6.6. Results for each solvent/surface pair are shown in Table 6.4.

Table 6.4. Calculated interfacial energy (γ_{sl}) of solvent/surface pairs. Units of mJ/m^2.

	Model residue, AP3-1	Reduced model residue, AP3-1	PTFE	Reduced PTFE	Silicon wafer
NMP	3.0	3.8	7.1	11.6	6.3
DMSO	4.1	1.6	14.1	3.1	0.8
DMF	1.8	3.1	7.9	7.9	3.8
Acetonitrile	2.3	13.0	9.4	10.7	8.6
THF	4.1	16.7	0.8	28.1	19.9
Diiodomethane	11.1	14.1	8.3	30.6	21.3
Water	25.0	12.1	47.2	2.5	6.2

For each pair, the interfacial free energy describes the free energy available for interactions when the liquid is exposed to the solid surface. If little energy is available, this implies that the pair is strongly interacting. DMF has the lowest interaction energy, followed by acetonitrile. Interestingly, after the surfaces interactions become more polar as a result of defluorination, interactions with THF and acetonitrile become significantly weaker. Interactions with water, as expected, are stronger and interactions with NMP, DMSO and DMF are essentially unchanged. Similar trends are observed with PTFE and reduced PTFE surfaces.

The interfacial free energy still fails to account for differences observed with residue delamination by the solvents, although it is interesting to note that acetonitrile and THF do not interact as strongly with a silicon wafer surface (native SiO_2) as do DMF and DMSO. This interaction may enable or enhance wetting of the fluorocarbon/silicon substrate interface, and thus cause delamination. As discussed previously, the most favorable conditions for free energy minimization occur when the polar and dispersive

relative contributions of the solvent and solid surface match. These values are shown in Tables 6.5 and 6.6.

Table 6.5. Percent dispersive and polar contributions of the surface tension.

Solvent	Dispersive contribution (%)	Polar contribution (%)
NMP	91	9
DMSO	71	29
DMF	84	16
Acetonitrile	56	44
THF	100	0
Diiodomethane	100	0
Water	34	66

Table 6.6. Percent dispersive and polar contributions of the surface energy.

Surface	Dispersive contribution (%)	Polar contribution (%)
AP3-1	85	15
Reduced AP3-1*	77	23
PTFE	100	0
Reduce PTFE*	52	48

The relative contributions of NMP, DMSO and DMF are more similar to those of the model residue than those of THF and acetonitrile, a stronger interaction is therefore expected. Contributions for DMF match closely. Furthermore, calculation of the energy change associated with the formation of a drop on the surface, ΔG_{sl}, as described in Equation 6.5 indicates a similar trend. Results of the free energy calculations are shown in Table 6.7 for the residue surface.

Table 6.7. Free energy for formation of a drop on the model residue surface, ΔG_{sl}

Solvent	AP3-1 Surface
NMP	-60
DMSO	-62
DMF	-58
Acetonitrile	-39
THF	-45
Diiodomethane	-62
Water	-70

The value for water is particularly large because of the large value for surface tension compared to the other solvents. Clearly, surface wetting is more thermodynamically favorable for NMP, DMSO and DMF due to the closely matched values for dispersive and polar contributions.

6.2.6 Conclusions

The themodynamic analysis described above enables characterization of both polar and dispersive forces of solvents and surfaces using only contact angle measurements and two probe liquids. This method is simpler than determination of Hansen solubility parameters and can be applied to unknown surfaces and liquids quantitatively and rapidly. However, this method predicts liquid/solid wetting interactions, but cannot precisely predict whether a material will or will not dissolve in a specific solvent. While the ability to wet a surface is related to dissolution, properties such as geometrical packing, crosslinking and kinetics may reduce or exclude such interactions.

The closely matched polar and dispersive contributions between DMF, DMSO and NMP and the model residue surface is the most convincing evidence to explain film delamination from the silicon substrate. These solvents also interact more strongly with

the silicon surface than do THF and acetonitrile as evidenced by the lower interfacial free energy.

Finally, characterization of residue surfaces and underlying materials can improve the selection or development of cleaning chemistries for residue removal. Both wetting of small features and dissolution are important cleaning requirements. While NMP is the basis for several commercial cleaning formulations, solutions based on DMF or DMSO may improve effectiveness because of the better-matched polar and dispersive contributions with fluorocarbon residues.

6.3 Patterned Etch Residue Cleaning

6.3.1 Initial characterization of patterned etch residues

Model etch residues proved unsuitable for evaluation of electrochemically-generated radical anion solutions due to rapid delamination by solvent interaction. As an alternative, patterned etch residue samples, supplied by Novellus Systems Inc., were used to investigate residue removal. These samples are back-end-of-line processed samples with residue comparable to those that must be cleaned during commercial semiconductor processing. The as-received dual layer low-k stack, shown in Figure 6.5, emulates a dual-damascene structure.

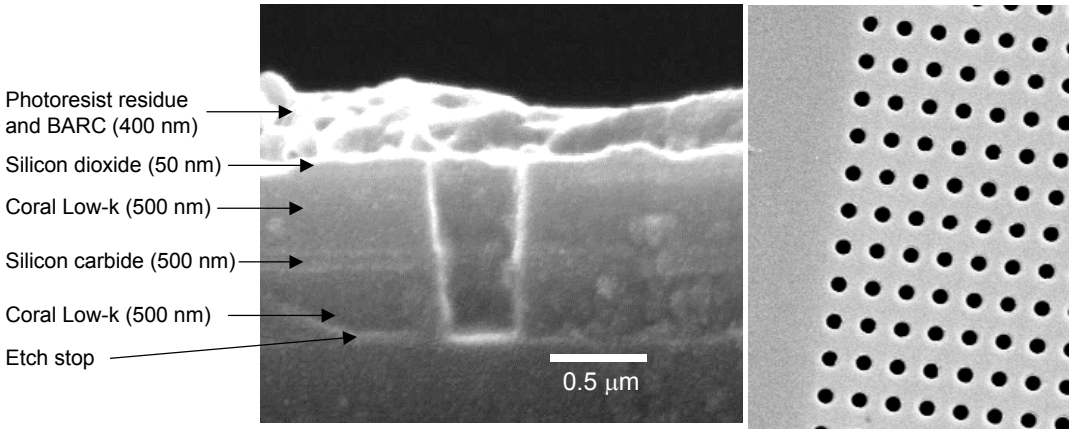

Figure 6.5. SEM micrograph of cross section(left) and top view (right) of patterned etch residue samples.

Coral is a plasma-deposited hydrocarbon doped silicon dioxide low-k dielectric material produced by Novellus Systems; for more details about Coral, see Chapter 3. The dielectric stack consists of a silicon carbide layer sandwiched between two Coral layers. This residue stack is coated with a 50 nm BARC (bottom anti-reflective coating layer)

used for patterning and a polyhydroxy styrene-based (PHOST/t-BOC) photoresist patterned with vias ranging in size from 130 to 1000 nm. The residue stack was etched using a proprietary C_4F_8-based plasma process. No cleaning or surface treatments were performed after etching. Throughout this section, the photoresist and plasma etch residue overlayer will be referred to as the etch residue.

The etch residue samples contain three different type of regions: open areas with no patterns, low-density vias and high-density spaced vias. An optical microscope image shows the three areas in Figure 6.6. Higher magnification images of the via regions are shown in Figure 6.7

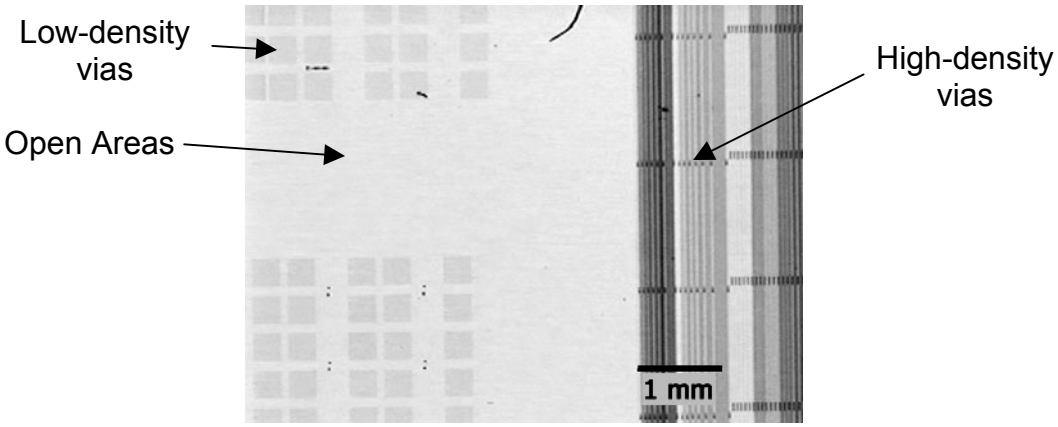

Figure 6.6 Optical microscope image of the three areas of the patterned etch residue samples.

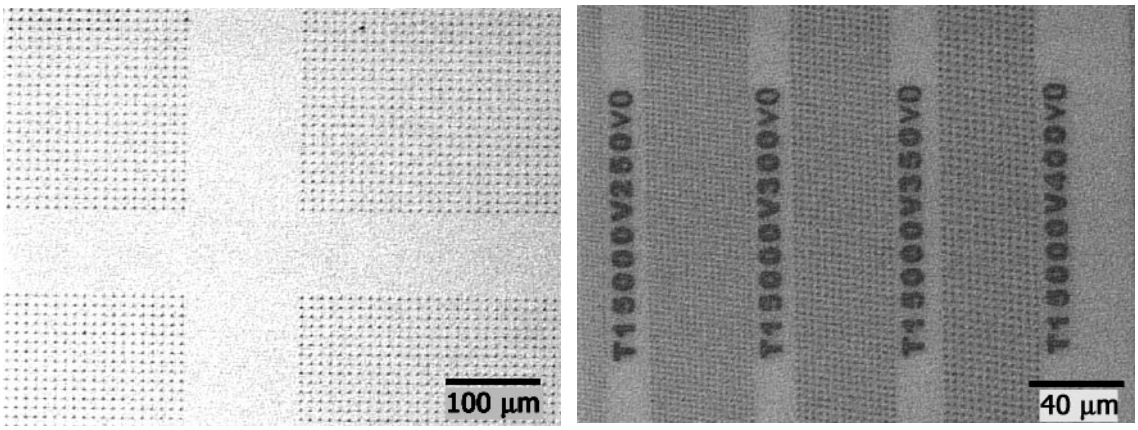

Figure 6.7 Optical microscope images of a low-density via region (left) and a high-density via regions (right).

The low-density via regions contain arrays of 500 nm-wide vias with a spacing or pitch of 10 microns. Each 35 x 35 array is separated by at least 120 microns. The high-density via regions contain tightly spaced arrays of vias ranging from 130 to 1000 nm in width. The pitch, or feature spacing, for each via ranges from one to three times the via width. Typically, via size and pitch are smallest at the lower metal layers and become larger as more metal layers are added. This patterned sample represents via sizes and pitches from a broad range of BEOL structures.

XPS surface compositional analysis of the different via regions differed by less than 0.5 at% for each element. The average atomic composition of the measurements was 59 at% carbon, 27 at% oxygen, 7 at% nitrogen and 7 at% fluorine. Angle resolved XPS analysis demonstrated only a slight gradient in the fluorine concentration. The surface fluorine concentration differed by 0.8 at% from the shallowest angle (60° with respect to normal)

to the deepest angle (25° with respect to normal). This suggests that the fluorocarbon or fluorine ions penetrate into the photoresist layer deeper than 50-75 angstroms. The high concentration of oxygen from the photoresist demonstrates that a fluorocarbon layer does not simply deposit on top of the photoresist, but becomes embedded or incorporated into the photoresist. Nitrogen is present from residual photolithographic developer which was tetramethylammonium hydroxide based. Cleaning was evaluated by analysis of optical and SEM images as well as XPS surface analysis.

Before etch residue samples were exposed the radical anion treatment, the effect of the electrochemical solvents was investigated. The following solvents were evaluated using both immersion and 'drop' techniques: acetonitrile, dimethylsulfoxide, dimethyformamide, n-methyl-2-pyrrolidone, tetrahydrofuran, isopropyl alcohol, acetone and DIW. The solvents were chosen because they are either standard electrochemical solvents, cleaning solvents (NMP) or are used for rinsing. No visual or chemical change was observed after exposure to isopropyl alcohol, acetone and DIW for 10 minutes. The remaining solvents, however, did cause swelling and partial removal of the residue. After immersion in NMP for five minutes, the samples were extensively swollen as shown in Figure 6.8. Samples were rinsed with IPA and dried with nitrogen after solvent exposure.

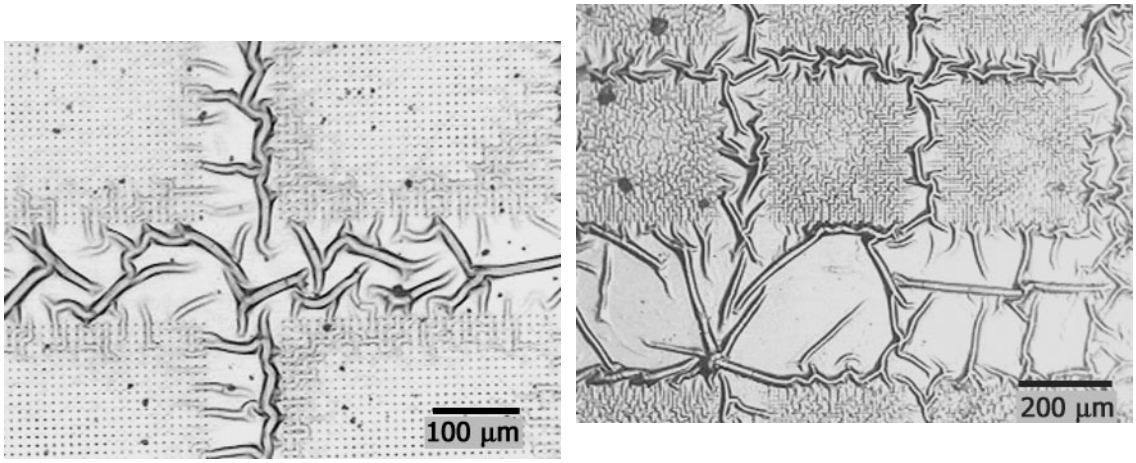

Figure 6.8. Optical microscope image of residue swelling after a five-minute exposure to NMP (left) and DMF (right).

Exposure to acetonitrile and tetrahydrofuran resulted in similar swelling, as well as partial removal of the photoresist and etch residue in the open areas of the sample. DMSO and DMF exposure resulted in more extensive swelling especially in-between vias. More consistent removal of the residue from the open areas was also observed with both DMSO and DMF. None of these solvent treatments were able remove the residue from either of the patterned via regions. Addition of tetrabutylammonium iodide to the solvents had no apparent effect on cleaning.

6.3.2 Patterned etch residue cleaning with electrochemically generated radicals

Initially the 'thin film' cell was used to expose residue samples to the electrochemically generated radical anions. Complete procedures and descriptions of the cell are detailed in Chapter 3. After naphthalene radical anions generated in DMF were brought into contact with the residue, partial removal was observed in the open and low-density via regions as shown in Figure 6.9. Film cracking and partial removal were inconsistently observed around via regions. In addition, removal was poor in the high density via region.

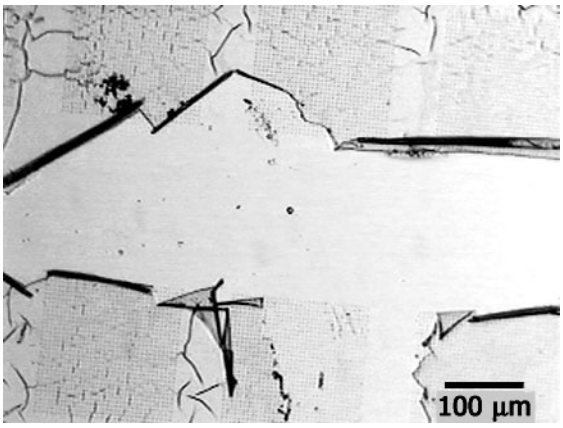

Figure 6.9. Partial residue removal following exposure to electrochemically generated radical anions using the thin film cell.

There are several limitations when using this particular cell for sample exposure. First, the area of the glass frit (1.25 cm^2) limits diffusion of ions which limits the maximum current and thus the generation rate of radical anions. Because the decay rate is finite, rapid generation is essential for reaching higher concentrations of radical anions. This cell design was limited to 4.8 mA regardless of the solvent, electrode area and background electrolyte concentration. Another issue is the decay of radical anions after the solution is transferred to the sample compartment of the cell. The samples are

exposed to a non-constant concentration and the exposure time is limited by the decay time. Finally, no agitation is possible during sample exposure.

To resolve these issues, sample exposure was completed using the larger UV-visible probe cell. The larger frit area (2.85 cm^2) allowed a maximum current of 19 mA. The probe was replaced with a clip which suspended the sample over the solution. To begin exposure, the sample can be lowered into the solution. During exposure, continued radical generation was possible to counteract the decay, thereby permitting constant concentration treatments. In addition, stirring provided solution agitation during sample exposure. Solution volume was nominally 2 mL using this method. For complete procedural details, see Chapter 3.

The effects of cleaning time and radical anion concentration were evaluated using the UV-vis probe cell. Concentrations were estimated using the model formulated in Chapter 5. Maximum current was applied to achieve the desired concentration value, and then the current was lowered to match the predicted decay rate at that concentration. Samples were exposed to solutions with concentrations of 5 mM and 20 mM. After 10 minute exposure of the 5 mM concentration solution, the residue was not removed in either of the via regions. With a 20 minute treatment time, the residue was completely removed in low-density via regions, but not removed from the high density via regions. An example of incomplete removal is illustrated in Figure 6.10. Similar results were observed after a 30 minute treatment at 5 mM.

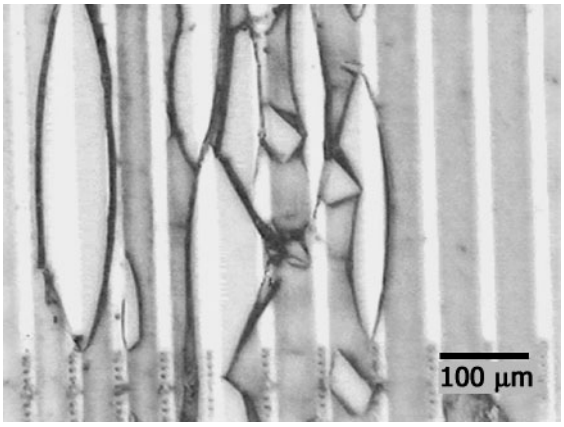

Figure 6.10. Example of incomplete residue removal in the high-density via region after a 30 minute - 5 mM naphthalene radical anion treatment.

Samples were also exposed to 20 mM concentrations of radical anions for various times. After a 10 minute treatment, residue in the low-density via regions was completely removed; however, residue remained in the high density regions. After a 20 minute treatment, residue in the high density regions was significantly reduced, but some residue still remained as shown in Figure 6.11. Even after a 45 minute treatment with 20 mM, some residue remained on the surface.

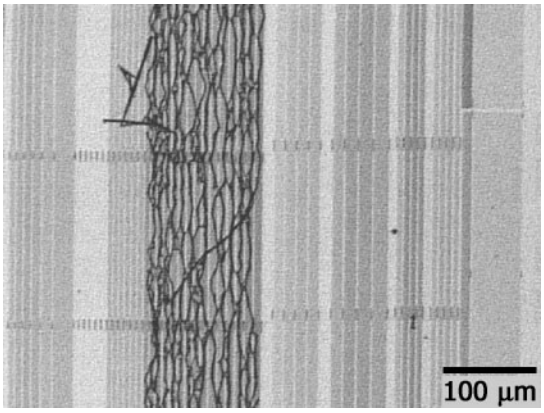

Figure 6.11. Incomplete residue removal in the high density via region after 20 minute radical anion treatment.

A maximum concentration was achieved by setting the current to its highest value for the entire exposure process (~20 mA). For a 20-minute exposure, the radical anion concentration was expected to be as high as 50 mM (near the end of the exposure time). Complete residue removal was achieved by samples treated for 20 minutes using this procedure. Completely cleaned vias are shown in Figure 6.12. To ensure that radical anions were responsible for removal, residue samples were treated with solutions after the radical anions completely degraded. Removal efficiency was similar to that by the pure solvent.

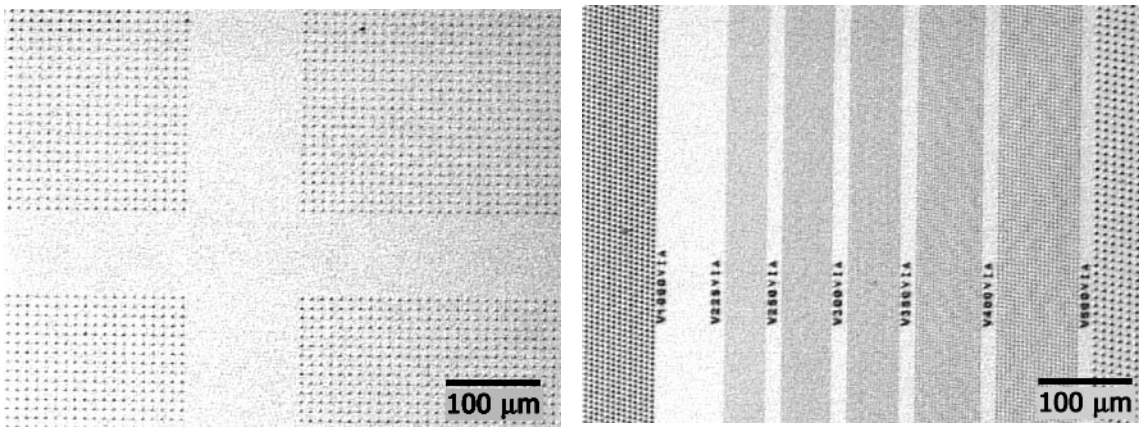

Figure 6.12. Patterned etch residue samples treated with concentration as high as 50 mM for 20 minutes. Residue is completely removed.

When incomplete residue removal was observed, samples were immersed in a variety of solvents, such as acetonitrile, isopropanol, acetone and methanol in an attempt to remove the remaining residue; however, these solvents could not remove the remaining residue. Occasionally, the mechanical action resulting from a rinse bottle did remove the remaining residue from the surface.

To confirm removal, cleaned samples were analyzed using XPS and SEM cross-sections. Conventional oxidative cleaning processes such as APM (ammonium hydroxide/ hydrogen peroxide) cleaned the residue and exposed the silicon dioxide capping layer on top of the etch stack. For completely cleaned samples, XPS surface composition is 25 at% silicon, 10 at% adventitious carbon and 65 at% oxygen.[151] For samples cleaned by the radical anion process, less than 1 at% silicon was detected on the surface indicating incomplete removal. SEM cross section analysis confirmed the incomplete residue

removal as shown in Figure 6.13. The thin roughened remaining layer is likely the bottom-anti-reflective coating (BARC) layer. XPS surface analysis indicates only 76 at% carbon, 19.9 at% and trace amounts of fluorine and nitrogen. Both inorganic and organic BARC materials exist, so it is reasonable to assume that this is indeed an organic BARC layer remaining on the surface, although no confirmation Novellus could be obtained. Without knowing the chemistry of the BARC material, it is difficult to speculate on the reason for incomplete removal.

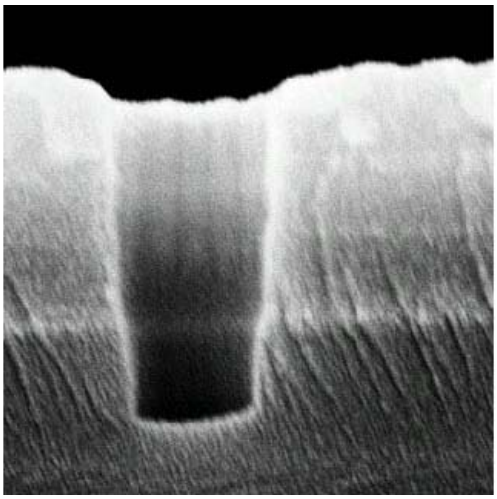

Figure 6.13. SEM Cross section indicating incomplete removal. The roughened surface is the remaining bottom antireflective coating

6.3.3 Sodium naphthalene and ozone exposure

Etch residues were exposed to 100 mM sodium naphthalene solutions for up to 45 minutes with agitation to emulate the conditions of the radical anion exposure. Little photoresist removal was observed; primarily surface wrinkling similar to results shown in Figure 6.8. XPS results indicate defluorination of the surface, but no other changes are detected. It is unclear why the sodium naphthalene radical has little success in cleaning the patterned residue. The most likely reason is related to the solvent. Even in its pure

form, DMF and DMSO were capable of removing some of the residue in the open areas of the samples. Pure THF, on the other hand, only caused wrinkling, but no removal. The synergistic combination of radical anions and solvents likely provided the results of effective photoresist removal, although the BARC remains on the surface.

To evaluate the effect of ozone on residue surfaces, samples were exposed to aqueous ozone for 10 minutes with and without a sodium naphthalene radical anion pre-treatment. In both cases, the ozone appeared to mildy oxidize the residue surface and incorporate oxygen (XPS analysis), but no visible cleaning or removal was observed as a result of the treatment. As mentioned previously, the low concentration of fluorine in the etch residue (7-8 at%) is significantly less than the APCI model etch residues where fluorine surface concentration ranged between 40-50 at%. With the low fluorine density, the concentration of double bonds that form is considerably less than that resulting from samples with higher fluorine density, making the ozone ineffective at removal. Without unsaturation generated in the residue, only short lifetime radicals are reactive, which by design, are minimized.

6.3.4 Owens/Wendt/Fowkes surface analysis on patterned etch residue

To understand the solvent/residue interactions, the patterned etch residue was analyzed using the Owens/Wendt/Fowkes procedure. In addition, the photoresist polymer (PHOST, 25% protected with t-BOC) and silicon dioxide were also analyzed by this method. Surface energy results for the analysis are shown in Table 6.8. Contact angle measurement on the patterned etch residue were completed in the uniform ‘open’ areas.

Table 6.8. Surface energy analysis of patterned etch residue and related surfaces.

Surface	Diiodo-methane contact angle	Water contact angle	Dispersive component of surface energy, γ_l^d (mJ/m^2)	Polar component of surface energy, γ_l^p (mJ/m^2)	Total surface energy, γ_s (mJ/m^2)
Patterned etch residue	61°	25°	27.9	38.5	66.4
PHOST	61°	46°	36.7	11.2	48.0
Silicon dioxide	48°	48°	35.2	19.6	54.8

The dispersive and polar character of the patterned etch residue surface is surprising. The conventional belief is that a fluorocarbon residue crust forms on the surface of the photoresist, which may prevent wetting of the underlying photoresist during cleaning. Compared to the PHOST polymer, the fluorocarbon plasma etch process significantly increased the polar surface energy. The etch residue surface does not resemble the model etch residue surface, AP3-1, which has a low overall surface energy and primarily dispersive contributions. Comparisons of the relative polar and dispersive contributions of surface and solvents are shown in Table 6.9; the interfacial energy is calculated in Table 6.10.

Table 6.9. Percent dispersive and polar contributions of the surface energy for etch residue and related surfaces.

Surface/Solvent	Dispersive contribution (%)	Polar contribution (%)
Patterned etch residue	42	58
PHOST	77	23
Silicon dioxide	64	36
NMP	91	9
DMSO	71	29
DMF	84	16
Acetonitrile	56	44
THF	100	0
Water	34	66

Table 6.10. Interfacial free surface energy, γ_{sl}, for surface/solvent pairs. Units are mJ/m^2.

Solvent	Patterned residue	PHOST	Silicon dioxide
NMP	18.9	2.0	6.3
DMSO	7.2	0.3	1.0
DMF	14.0	1.0	4.0
Acetonitrile	14.9	8.0	9.5
THF	38.5	12.0	20.3
Water	0.4	12.9	6.3

Recall that to maximize wetting, the interfacial energy should be low. Experiments show that films of the PHOST material dissolve in all the solvents listed above except water. Interfacial energies for the patterned etch residue are higher than for PHOST; however, wrinkling and wetting of the residue surface were also observed with the same solvents (except water). The larger values for THF with both the etch residue and silicon dioxide surface may explain why THF was least able to wrinkle or remove residue from the surface of the patterned etch residue. Based on this information, a removal mechanism will be proposed in the following section.

6.3.5 Residue removal mechanism

Although the entire residue is not removed from the surface, the photoresist portion of the residue can be reliably removed using electrochemically generated radical anions. Initially, it was thought that the fluorocarbon crust or layer is deposited and embedded into the photoresist surface while plasma etching. On the patterned etch residue samples analyzed, a fluorocarbon doped layer is detected on the photoresist following etching, but this layer does not have the hydrophobic properties of PTFE or the APCI model etch

residues analyzed in previous chapters. Indeed, incorporation of isolated CF moieties at the surface can actually enhance wetting via interactions polar interactions.

When the residue is removed conventionally, pieces of the residue visibly delaminate from the surface indicating that the photoresist residue is at least partially cross-linked. Owens/Wendt surface analysis and the solubility of PHOST in the solvents suggest that the residue can be wet, but the crosslinking prevents dissolution. Wetting of the silicon dioxide surface by the solvents is also energetically favorable. SEM and optical microscopy images show the results of surface and interface wetting which causes stress in the residue and delamination of the residue from the surface. These are observations are shown in Figure 6.14.

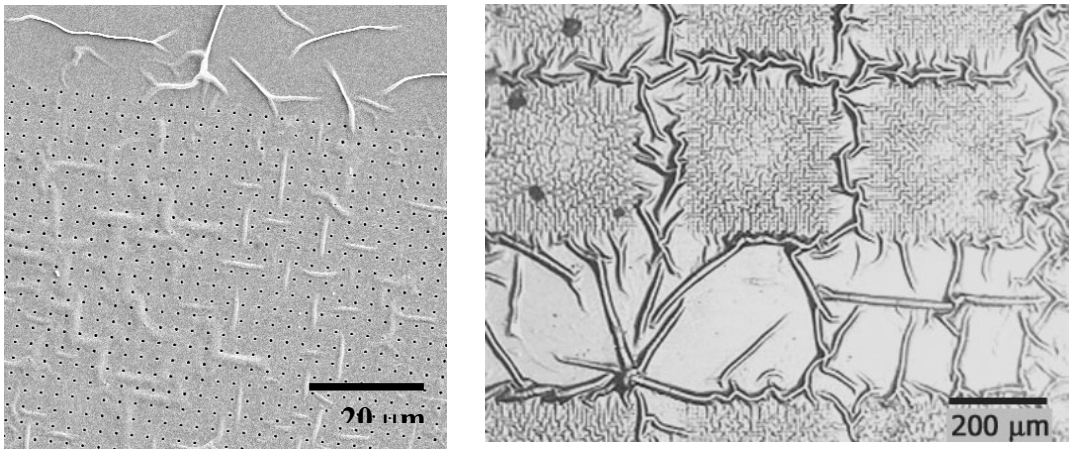

Figure 6.14. SEM micrograph (left) and optical micrograph (right) illustrating wetting, swelling and delamination of the residue from surface. Sidewall residue adhesion appears to prevent residue liftoff around vias.

In the regions between vias, visible delamination is observed; however, the sidewall residue prevents liftoff of the photoresist due to solvent exposure. The sidewall residue film is formed during the fluorocarbon plasma etching process primarily from reaction of fluorocarbon radicals and neutrals. The sidewall also experiences bombardment from species that result from physical sputtering at the bottom of the via during etching. These two processes result in a primarily fluorocarbon-based material with strong adhesion to the via sidewall that most likely resembles the composition of APCI 'model' film residue. As pictured in Figure 6.15, the sidewall prevents liftoff of the photoresist residue. Swelling of the residue can result in sufficient stress to fracture the sidewall film causing the loss of adhesion or delamination; however; the combined effect of the many vias prevents overall removal during solvent exposure. The effect of the vias is also demonstrated by the difference in time and concentration required for cleaning low density regions versus high density regions.

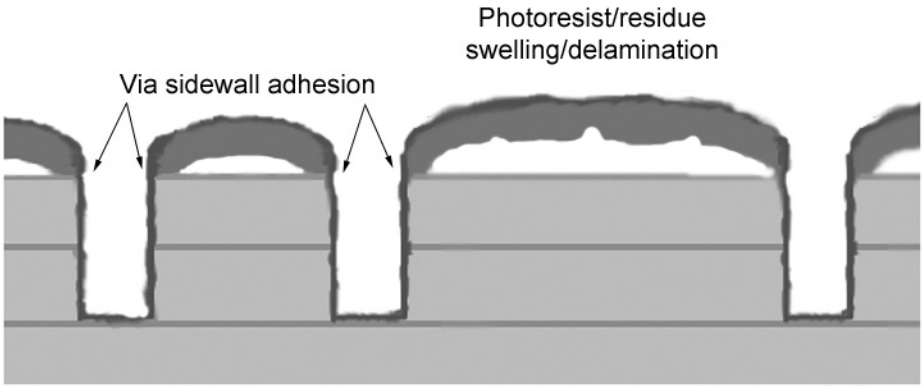

Figure 6.15. Illustration of residue swelling and via sidewall adhesion preventing removal.

The radical anion cleaning process may aid in residue removal via two mechanisms. Radical anions have demonstrated defluorination of fluorocarbon residues which enhance

their propensity to absorb solvent which results in film stress. With the APCI model residues however, the radical anion did not need to penetrate through the film due to delamination. Second, defluorination of the sidewall allows solvent molecules access to the interface with the underlying film. If the interface is wetted, stress can build up and result in bond fracture and subsequent residue removal. While the exact mechanism is not clear, the radical anion cleaning process offers an enhancement to traditional wetting and swelling by solvents for cleaning processes.

CHAPTER 7

INTEGRATION

7.1 Overview

In this chapter, issues relating to industrial integration are discussed including chemical compatibility, equipment and chemical safety. Semiconductor device and process compatibility of the radical anion cleaning process has been evaluated using blanket films of a plasma deposited low-k material (Coral™) and a spin-on low-k material (methysilsesquioxane). No chemical modification or etching was observed upon a standard exposure (20 °C, 20 min, 40 mM) with either low-k material. In addition, a design for a radical anion-based residue stripping reactor suitable for single-wafer processing, is suggested. Toxicity data of DMF and DMSO are compared to those of NMP, a solvent commonly used industrially. Possible fabrication schemes that utilize the IC compatible defluorination treatment to pattern fluoropolymer surfaces are suggested.

7.2 Semiconductor Compatibility

Chemical compatibility of new IC processes must be evaluated extensively if they are to be considered for industrial integration. With shrinking feature sizes, BEOL cleaning processes must not decrease the printed feature dimension by more than 2.5%.[9] In addition, cleaning processes must avoid modification of the electrical or mechanical properties of the material. The ITRS roadmap permits a dielectric constant modification of only 2% as a result of processing. Although rigorous electrical and reliability testing of current ICs subjected to these cleaning processes is required prior to implementation or

perhaps even before industrial consideration, several tests can be used to assess preliminary compatibility. No reports have demonstrated process or device compatibility limitations with silicon-dioxide low-k materials and NMP-based cleaners, which are commonly used in the IC industry. DMF and DMSO have similar solvent properties to those of NMP; therefore, it is expected that the radical anion cleaning processes, based on DMF, should also be compatible.

Two representative interlevel dielectric materials were used to evaluate IC compatibility of both radical anion and ozone processes. As discussed previously, the ozone process may or may not be required depending upon the nature of the residue. The two interlevel dielectric materials studied were Coral™ and methylsilsesquioxane. Coral™ is a commercial methyl-doped silicon dioxide low-k material developed by Novellus Systems, Inc with a dielectric constant of 2.6-2.7. Thin films of Coral are deposited by plasma enhanced chemical vapor deposition (PECVD) using tetramethylsilane and siloxane precursors. The material is both non-porous and amorphous. The dielectric constant of Coral™ is lower than that of silicon dioxide due to a reduction in the overall polarizability of the material which is achieved by replacement of silicon-oxygen bonds with less polar silicon-carbon bonds and the incorporation of nonpolar methyl groups. Coral™ samples were provided by Novellus Systems, Inc. Methylsilsesquioxane (MSQ) is a porous spin-on silicon dioxide-based material with a dielectric constant of approximately 2.6 and an average pore size of 2.8 nm.[151] The silicon-oxygen network forms a cage-like structure with methyl side groups as shown schematically in Figure 7.1. Replacement of silicon-oxygen bonds with silicon-carbon bonds and the addition of

porosity result in a reduction of the dielectric constant compared to that of silicon dioxide.

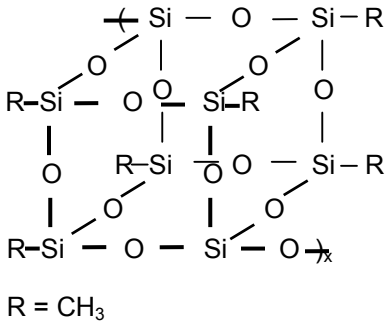

Figure 7.1. 'Cage' structure of porous methylsilsesquioxane.

One-centimeter square samples of each material were individually exposed to both the reductive radical anion and aqueous ozone treatments using standard processing conditions. Radical anion treatments of 20 minutes with a maximal electrolysis current (20 mA) produced radical anion concentrations as high as 50 mM. These conditions resulted in effective cleaning of the industrially-generated plasma etch residues. Ozone treatments were conducted using an ozonated DIW solution (approximately 0.30 mM) for 10 minutes. In order to scavenge hydroxyl radicals, tertiary-butanol was added to the solution at a ratio of 1:5 (t-butanol:DIW) by volume.

IC compatibility was evaluated by the measurement of etch rates and changes in surface and bulk chemical composition. Etch rates were evaluated by performing film thickness measurements before and after chemical exposure. Changes in the bulk film composition were determined using Fourier-transform infrared spectroscopy (FTIR) in transmission mode. Surface composition and bonding structure changes were evaluated using high-

resolution XPS surface analysis. Changes in the refractive index of the film, which indicate dielectric property modification, were also determined.

After the radical anion treatment, film thickness, surface composition and bulk composition were measured; results are shown in Table 7.1. The film thickness changed by less than 1 nm and the refractive index changed by less than 1% for both Coral and MSQ. The silicon to oxygen ratio of the MSQ and Coral surface changed by less than 1.5% and 7%, respectively. Because the ratio in Coral increased, this is likely due to measurement variability or contamination as opposed to chemical oxidation. Clearly, these film properties were essentially unchanged by the radical anion treatment.

Table 7.1. Thickness and chemical composition changes after exposure to the radical anion cleaning process.

	Coral™ Untreated	Coral™ Treated	MSQ Untreated	MSQ Treated
Thickness (nm)	493.0	492.3	396.7	397.4
Refractive index (600 nm)	1.4109	1.4105	1.3139	1.3114
XPS surface composition				
Silicon (at%)	24.7	25.5	25.9	26.5
Oxygen (at%)	50.2	48.3	54.7	55.2
Carbon (at%)	25.1	26.2	19.4	18.3

In addition, neither XPS nor FTIR analyses was able to detect significant changes in the surface or bulk bonding structures. Since no etching or compositional changes were detected within the film, the residue cleaning process shows initial compatibility with the two low-k dielectric materials evaluated. However, measurement of electrical properties such as dielectric constant, breakdown field and leakage current are necessary for a

complete evaluation. Unfortunately, the small area of treated samples prevented fabrication of the capacitor structures required for electrical testing.

IC compatibility of the aqueous ozone process with both low-k materials was evaluated using the techniques described above. Again, no thickness or chemical change was observed with the Coral™ film after a 10 minute exposure. Although, silicon-carbon bonds may be susceptible to oxidation by hydroxy or hydroperoxy radicals, either the low concentration of the species or low film reactivity apparently prevented significant oxidation. Unfortunately, the porous MSQ film was oxidized after exposure to the aqueous ozone. The O:Si ratio increased by 13%, likely a result of the formation of Si-OH bonds. In an attempt to decrease the radical concentration, a radical scavenger (t-butanol) was added to the aqueous ozone solution. After addition of the scavenger (20 vol%), no chemical change in the surface composition of the MSQ was observed by XPS or FTIR analysis, and thickness changes for both films were less than 1 nm after a 10 minute ozone exposure. Nevertheless, this aqueous/t-butanol solution was still capable of removing the defluorinated layer.

7.3 Proposed Equipment for Integration

The electrochemical cell used for prelimiary studies described above would not be suitable for the scale and requirements of manufacturing processes. Batch reactors require a setup time and the radical anion concentration is not well-controlled. Furthermore, the electrochemical solution in both compartments must be refreshed or replaced regularly. Possible equipment design for continuous and, thus better controlled

and manufacturable single-wafer cleaning approach using electrochemically-generated radical anions is shown in Figure 7.2.

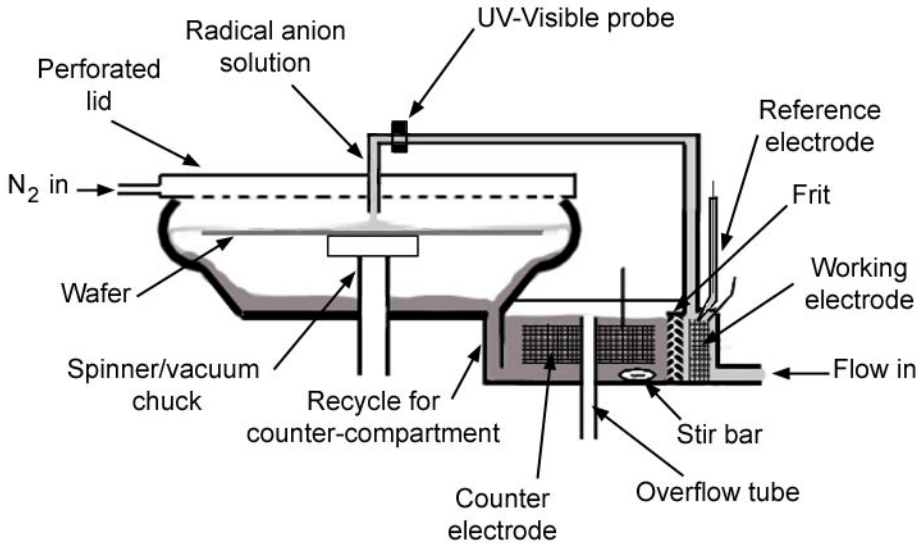

Figure 7.2. Schematic of proposed equipment for single-wafer electrochemical-based residue removal.

A flow of dried and deaerated solvent with naphthalene and a background electrolyte must be pumped into the working electrode compartment (pictured on the right). This segment of the process could be accomplished by passing the solvent through a nitrogen bubble column and a molecular sieve column. The radical anion can then be generated continuously at the working electrode. The radical anion solution is continuously pumped through a delivery tube and dispensed onto the spinning wafer. A UV-visible probe and spectrometer enable monitoring and feedback control of the radical anion concentration and a perforated lid forms a blanket of dry nitrogen over the wafer to prevent protonation of the radical anion by atmospheric water vapor. Dispensed cleaning fluid is collected in the bottom of the bowl and is recycled into the working cell

compartment, wherein mixing can be performed with a magnetic stir bar. Iodine (I_2) molecules formed during the electrochemical reaction can be reduced by unreacted radical anions, thereby regenerating the counter-electrode solution; this procedure will extend the working lifetime of the solutions. Finally, the volume of solution in the counter electrode compartment is controlled by an overflow tube.

This continuous configuration is clearly superior to a batch reactor system. The radical anion concentration is established under steady state conditions consistent and the wafer is always cleaned with fresh solution. In addition, the solution is recycled into the counter electrode compartment thereby reducing the need for constant solution replacement. Used cleaning solution may require filtering prior to recycling in order to eliminate polymeric residues removed from the wafer. Agitation provided by wafer spinning will aid in undercutting and thus detaching and transporting the residue from the wafer surface.

The primary design challenge with the proposed configuration is the achievement of a sufficiently large enough electrolysis current to maintain an adequate concentration of radical anions to ensure high rate cleaning. In the batch configuration, the medium porosity (10-15 μm) glass frit limited the electrolysis current. With an area of 2.85 cm^2 in the larger (dip probe) cell, the maximum electrolysis current was 20 mA in both DMF and DMSO. With a typical dispense rate of 1 mL/s and 10 mM concentration of radical anions, a current of 0.965 A is required. Assuming a linear relationship with area, a frit area of 137 cm^2 and large electrodes are needed. This is not an unreasonable frit size;

however, a more porous frit would improve diffusion rates and reduce the required area. A more porous frit, however, also increases the rate of diffusion of radical anions from the compartment.

Treatment of surfaces by dispensing solutions onto a spinning substrate is superior to immersion into a bath. Therefore, improved uniformity and process control is achieved using this modified configuration; in addition, a reduction in cross-contamination that can occur in batch equipment or baths will also be achieved.

From a safety perspective, DMF and DMSO are similar to NMP which is used industrially as a solvent for stripping photoresist. Important chemical and physical properties of the materials are compared in Table 7.2.

Table 7.2. Comparison of chemical and physical properties of solvents.[152]

	DMF	DMSO	NMP
Flash Point	58	95	91
Vapor pressure (Torr @ 20 °C)	2.6	0.42	0.29
LD50 (mg/Kg Rat)	2800	14500	3914
TLV (ppm)	10	Not established	100
NFPA: Health rating	2	1	2
NFPA: Flammability	2	2	2
NFPA: Reactivity	0	0	0
Carcinogen	No	No	No

DMF is slightly more toxic and has a much lower flash temperature than DMSO and NMP; however, the differences are not sufficient to prevent its use. Solvents such as acetone and isopropyl alcohol that are more flammable than DMF are used regularly in

manufacturing. Physical effects due to inhalation or skin contact from DMSO and DMF are comparable to NMP which include irritation, redness and discomfort to mucous membranes. Based on these comparisons, safety concerns about these solvents should not prevent their use in the IC industry. Of course, any use of such solvents in processing equipment requires adequate ventilation in order to limit solvent exposure.

There are strong efforts to reduce solvent use in IC fabrication facilities; however, a cleaning process based on radical anions may be capable of replacing multiple stripping or photoresist removal processes, thereby reducing overall chemical usage. Furthermore, special consideration will be given to effective cleaning solutions because of the need for compatibility with low-k materials.

7.4 Surface Modification Applications

The proposed radical anion treatment can also be used to dehalogenate halocarbon surfaces. Previous reports have demonstrated defluorination of fluoro- and chloropolymer surfaces, thus increasing the surface energy and enabling adhesion of inks or additional coatings.[67] The radical anion treatment is most effective with saturated fluoropolymers. While sodium-naphthalene solutions are capable of defluorinating surfaces, sodium is incompatible with IC process sequences; however, electrochemically-generated radical anion solutions are compatible with IC materials. In surface modification for adhesion improvement, a penetration depth of less than 5 nm is sufficient. With naphthalene radical anion chemistry, this requires only low concentrations (<10 mM) and short exposure times (<5 seconds). Nevertheless, effective

and efficient processes demand uniformity and process control, so that new approaches similar to the continuous process described above are needed.

Two possible schemes that can be envisioned to pattern fluoropolymer surfaces using radical anion treatments; these are detailed in Figure 7.3. In either scheme, the first step is defluorination of the surface via a short exposure to the radical anion. Without this step, photoresist will not uniformly coat or adequately adhere to fluoropolymer surfaces.[153] If necessary, an additional step to apply an adhesion promotor can be involked. The fluoropolymer surface can then be processed using conventional photolithographic patterning.

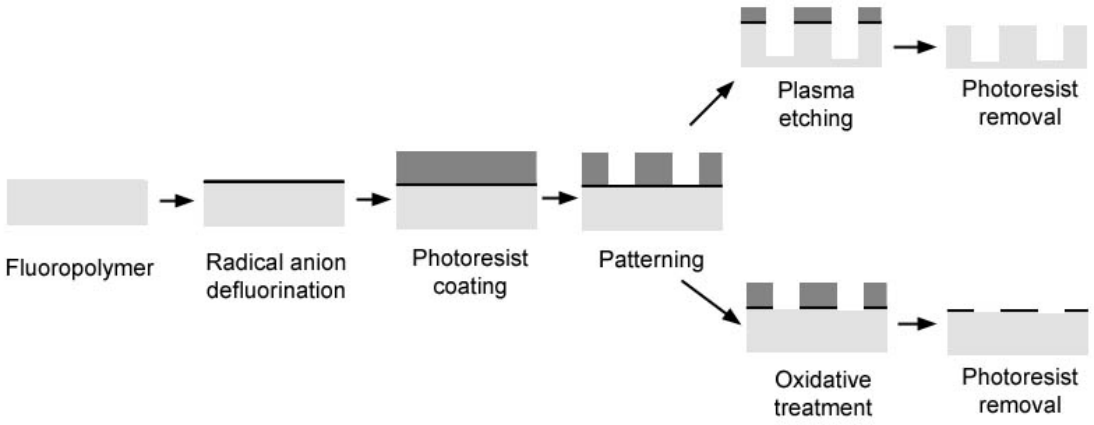

Figure 7.3. Patterning of fluoropolymers using radical anion surface modification and photolithography.

After patterning, the defluorinated layer can be removed using an oxidative treatment followed by photoresist removal with an appropriate solvent. This process will result in selective wetting (defluorinated regions) of the fluoropolymer surface. Alternatively, the

patterned surface can be etched using an anisotropic plasma process to form features in the fluorocarbon surface.

Fluoropolymer patterning can be valuable in a variety of areas. The advantage of this process versus sodium-naphthalene is the lack of alkali metal contamination; therefore, only applications sensitive to alkali metal would benefit from this technique. Patterns of wetted and non-wetted regions can be exploited using aqueous self-assembled monolayers or seeding chemistry. Aqueous or aqueous-based liquids will preferentially accumulate in defluorinated regions, but should avoid fluorinated areas. In IC or MEMS processing, this approach may be particularly useful with fluoropolymer coatings. Fluoropolymer or fluorocarbon films are advantageous because of their high thermal stability, chemical resistance and low moisture absorption. Although fluorocarbons have not proved useful in BEOL IC processing because of thermal limitations, their use in microsystem or module packaging could be promising. This radical anion process could offer an approach to pattern fluorocarbon layers or modify surfaces to enable the selective deposition of metal layers.

7.5 Conclusions

No changes in the bonding structure or thickness of blanket low-k dielectric samples were observed after the radical anion cleaning treatment. Electrical testing is required to complete semiconductor compatibility evaluation; however, the small sample size in this study inhibited (~3x5 mm) fabrication of capacitor structures required for testing. The chemical toxicity of the two primary solvents, DMF and DMSO, is comparable to NMP

which already used widely in device manufacturing. Two fabrication schemes utilizing radical anions for fluorocarbon surface modification have been proposed to facilitate the use of fluoropolymers in IC and MEMS processing.

CHAPTER 8

SUMMARY AND FUTURE WORK

8.1 Dissertation Summary

Fluorocarbon plasma-deposited films were provided by Air Products and Chemicals, Inc to serve as model residues for fluorocarbon post-plasma etch residues. These residues were deposited in an environment similar to that used in the plasma etching of silicon-based dielectrics for IC manufacturing. Plasma etching parameters were varied to investigate the effect of the plasma environment on the composition of the residue that forms. Carbon double bonds in the fluorocarbon etch feedgas caused high residue deposition rates, likely due to the propensity to form radical species by electron impact collisions in the plasma. Inclusion of oxygen in the feedgas suppressed the high deposition rate and increased the degree of crosslinking in the deposited polymer (residue). In some cases, samples were positioned vertically in the plasma etcher in an attempt to simulate formation of residues formed on the sidewalls of features; those depositions produced extremely thin films, but with similar bonding structure to those of the horizontally positioned samples. Modification of plasma parameters resulted in observable compositional differences in the residues; however, the differences did not appear to affect cleaning chemistry effectiveness.

After characterization of the residues, chemistries capable of reacting with the fluorocarbon residue were identified. Sodium-naphthalene radical anion reductive chemistries have been shown to abstract fluorine from fluoropolymers under relatively

mild conditions (room temperature and atmospheric pressure). In addition to a chemical attack of the fluorocarbon residue, the reductive nature of the fluorocarbon reaction mechanism was expected to be compatible with emerging low-k materials that are susceptible to oxidative degradation. Preliminary experiments demonstrated that sodium naphthalene radical anion solutions were capable of defluorinating the fluorocarbon residue; however, removal was incomplete. With longer exposure times, the radical anion solution penetrated into the film, forming a clearly discernable defluorinated layer. Characterization of the carbonaceous defluorinated layer indicated that carbon-carbon (~5 at%) formed as a result of the reductive treatment. To complete the removal of this layer, an aqueous ozone treatment was used to selectively cleave carbon-carbon double bonds, likely forming short soluble oligomers. After the ozone treatment, the underlying fluorocarbon layer was detected. Unselective oxidation by the aqueous ozone solution was inhibited by the addition of t-butanol, a known radical scavenger.

This two-step residue removal process was used to investigate the penetration rate of the sodium-naphthalene radical anion solution into the residue surface by varying the exposure time and measuring the remaining film thickness after completion of the two steps. An average penetration rate of 27 nm/min was observed and the rate became diffusion-limited in less than 5 seconds. A quasi-steady model was developed to describe the process. Knowledge of two of the three model parameters (the diffusion coefficient, reaction constant) allowed determination of the third parameter (partition coefficient). The surface reaction constant was estimated by modifying a previously reported bulk reaction rate constant for the defluorination reaction of PTFE by sodium naphthalene.

The diffusion coefficient was estimated based on the diffusion of benzene of polyethylene and a correlation that related benzene and naphthalene diffusion coefficients. A partition coefficient of 0.26 was determined using these estimates and subsequent fitting of the experimental data to the model.

Although, the sodium naphthalene radical anion solution demonstrated effective defluorination of the model residue films, sodium is a known contaminant in integrated circuit processing. Use of sodium or any alkali metal in semiconductor processing is unacceptable; two methods were identified to remove sodium from the sodium-naphthalene radical anion solution. An ion-exchange reaction was invoked to replace the sodium counter ion with a tetraalkylammonium ion, which would be IC compatible. Unfortunately, weak ionization of the tetraakylammonium salt (tetrabutylammonium chloride) in the solvent (THF) resulted in degradation of the radical anion in solution. The reaction, determined by identification of reaction products using ^{1}H NMR, was identified as a Hoffman elimination via protonation of the radical anion by the tetrabutylammonium salt. Weak ionization by the tetrabutylammonium salt in the solvent was the likely cause of the reaction. Experiments with other salts and solvent combinations were performed; however, similar results were observed.

A second method of sodium-free radical anion generation utilized electrochemical methods. Although many polycyclic aromatic hydrocarbon-based radical anions have been previously generated, few studies have described their generation with naphthalene. Custom electrochemical cells were fabricated to generate naphthalene radical anions

using a platinum working electrode and a separated compartment configuration. This approach allowed naphthalene radicals to be generated; however, the radical lifetime was short ($t_{1/2}$ ~ 200 sec). In order to quantify the concentration during electrolysis, the degradation rate was determined. Using a UV-visible dip probe and spectrometer, the molar absorptivity for naphthalene was measured. Next, the degradation rate of the radical was measured and a model for the concentration as a function of electrolysis current was determined. The radical anion degraded by a fractional reaction order, indicating a combination of different mechanisms; however, the most likely is radical protonation by trace contaminants (water vapor) in the dry box. With the generation and degradation, characterized, specific radical anion concentrations could be maintained for controlled residue exposure.

Unfortunately, exposure of model etch residue films to electrochemically generated radical anions resulted in delamination of the film from the substrate. This was also observed with exposure to pure electrochemical solvents (DMSO, DMF and NMP). The interaction between the solvents and the model residue were evaluated using the Owens/Wendt/Fowkes procedure where the dispersive and polar contributions of the surface energy are determined. In addition, dispersive and polar contributions of the solvents were also measured. These results matched well with respective Hildebrand parameters. The percent contributions of the solvents that caused delamination matched closely with the percent contributions of the residue indicating strong interactions or wetting behavior. This interaction leads to absorption and interfacial wetting which causes delamination. While this behavior prevents a detailed study of the penetration

rates, the interfacial wetting and delamination are advantageous for cleaning processes. Indeed, matching of dispersive and polar contributions of solvents and residues could aid in the development of novel cleaning technologies.

Post-plasma etched residue samples, from Novellus, Inc., were exposed to electrochemically generated radical anion solutions. Photoresist and top surface residue removal were evaluated using optical and scanning electron microscopy. The effect of treatment time and concentration were found to be important for complete residue removal. Radical anion concentrations as high as 50 mM and exposure times as long as 20 minutes were required for effective removal. The photoresist layer was completely removed; however, SEM and XPS analyses indicated that a rough carbonaceous layer remaining on the silicon dioxide capping layer which is likely the bottom anti-reflective coating. During removal, residue fragments were observed in the solution indicating that residue dissolution is not the removal mechanism. Liftoff due to interfacial wetting and solvent absorption in the residue appear to cause removal. While solvent exposure alone removed the residue in open areas, the radical anion was required in areas of densely-spaced vias. The radical anion cleaning process appears to attack sidewall fluorocarbon residues, which makes them susceptible to wetting, swelling or liftoff, thereby enabling complete residue removal.

Finally, semiconductor compatibility was evaluated using two low-k candidate materials (MSQ and Coral™). As expected, chemical composition changes and etching of the low-k materials by the radical anion treatment were negligible. Electrical testing, however, is

required to confirm complete compatibility. In addition, aqueous ozone treatments caused surface oxidation of MSQ films; however, addition of t-butanol, a known radical scavenger, to the aqueous solution prevented this reaction. The aqueous ozone treatments had no effect on removal of post plasma etch residues from industrial samples following a defluorination treatment. In order to implement such a radical anion scheme for residue removal, issues such as safety and equipment must be considered. DMF and DMSO are not significantly more toxic than NMP, which is currently used industrially as a residue stripper. For more controlled and uniform exposure, single wafer tools are recommended which generate the radical anion continuously. Also, solvent recycling can reduce solvent consumption in this configuration. Patterning of fluoropolymer films, enabled by radical anion surface defluorination, may be another useful application in the IC industry.

8.2 Recommendations for Future Work

The radical anion-based cleaning process is capable of removal of both model fluorocarbon residues and residue from post-plasma etched (patterned) samples. The solvents, DMF or DMSO, strongly interact and enhance the removal process, inhibiting attempts to determine the exact role of the defluorination reaction. Indeed, mechanistic studies of removal were hampered by delamination of films from substrates upon exposure to the electrochemical solvents. The solvents absorbed into or diffused through the model fluorocarbon residues causing delamination; however, a similar phenomenon was not observed with post-plasma etch sidewall residues. This likely indicates that stronger interfacial bonds are formed between sidewall residues and the underlying dielectric material. It would be useful to investigate this interface by plasma deposition

of fluorocarbon films onto low-k materials and copper surfaces. By studying the strength of the interface as a function of plasma parameters such as feedgases, ion density and ion bombardment energy, suitable model films, which more accurately represent sidewall films, could be generated. In addition, fluorocarbon interfaces that prevented delamination would enable mechanistic studies of the role of the radical anion chemistry.

Patterned samples that contain copper, visible sidewall residue and inorganic contamination would enable improved evaluation of the radical anion cleaning capability. Sidewall residues were not observable by SEM cross-sections of patterned samples used in this work. Furthermore, the exact material chemistry of the film stack as well as the exact etching and photolithographic processing conditions of theses samples were not supplied by Novellus. This information would improve analysis of the cleaning solution interaction and aid in understanding the incomplete removal of the bottom-later anti-reflective coating. Obtaining or generating patterned residues with known materials and processing conditions is clearly needed.

A synergistic effect involving solvent penetration and radical anion defluorination was required to remove residues from industrially-generated samples. Radical anion solutions generated in THF with sodium were not successful at residue removal. Owens/Wendt analysis indicated poor compatibility between THF and the residue. Only the most common electrochemical solvents were used for generation; however, a similar analysis (Owens/Wendt) indicated nearly ideal compatibility (dispersive and polar contributions matching) between those solvents and the fluorocarbon residue. Other solvents or

background electrolytes may provide enhanced cleaning, more rapid generation or decreased degradation. If generation and accumulation of radical anions was achieved in NMP, it would be particularly attractive to the semiconductor industry because of its familiarity and known effectiveness. Effective rinsing is required to remove all ammonium salts from the surface. Analysis of rinsing effectiveness using secondary ion mass spectroscopy should be performed.

A study to evaluate the effect of the reaction rate and surface penetration rate on the solvent, counter cation and temperature of the radical anion would supply additional understanding of this process. Unfortunately, no suitable film/substrate combinations have been found that are resistant to delamination by DMF. Plasma deposited fluorocarbons on silicon and aluminum substrates, and Teflon AF on copper all delaminated when exposed to radical anions in DMF or DMSO for more than 10-20 seconds. Reaction rates of radical anions with PTFE could be determined using a method reported previously; however, precise penetration depth measurement into PTFE surfaces has been unsuccessful.[129] PTFE surface roughness, due to machining, prevents measurement of penetration depth by profilometry.

Finally, modifications to the electrochemical cell would enable improved analysis of processing parameters. Although a flow cell described in Chapter 7 would be ideal for sample treatment, it may not be practical for laboratory experimentation. The batch-style split cell design could be improved to enable study of temperature effects as well as allow larger samples to be treated. A one-piece split cell could be fabricated with an outer

jacket to enable temperature control and solution heating. It is expected that increased temperature would enhance the cleaning capability of the solution by increasing the reactivity of the radical anions. A more porous frit could allow fast generation of radical anions; however, hydrostatic pressure between compartments must be balanced. A schematic of an improved electrochemical cell design is shown in Figure 8.1. The cell is thin with a small volume, but allows treatments of larger samples and solution agitation. The sample can be lowered into the solution when the desired concentration is reached. A bulb at the bottom of the working electrode compartment should be large enough to accommodate a stir bar without significantly increasing the compartment volume. The new cell should have an air-tight lid and be purged with dry nitrogen (using improved drying techniques) to reduce radical anion degradation. The ability to process larger samples would allow electrical testing of low-k materials as well as fluoropolymer patterning described in Chapter 7.

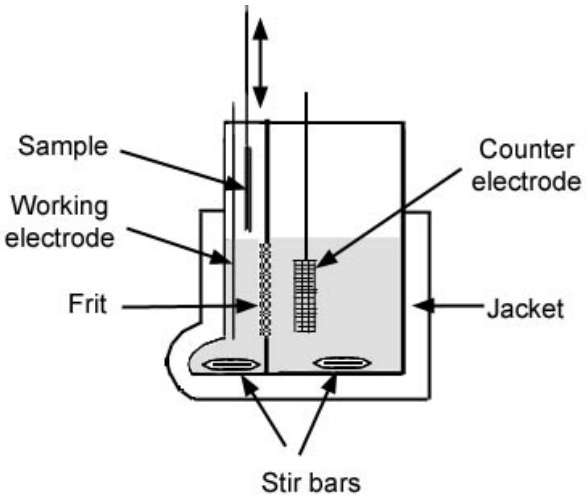

Figure 8.1. Improved electrochemical split cell for treatment of larger samples. (Reference electrode not shown)

APPENDIX A

In the following appendix, results of high resolution XPS surface analysis on the first set of fluorocarbon residue films provided by Air Products and Chemicals, Inc.

Sample 1: 12 sccm C4F6, 24 sccm O2

Overall composition (at%)

Carbon	Oxygen	Fluorine	Silicon
48	11	36	6

Carbon (1s)

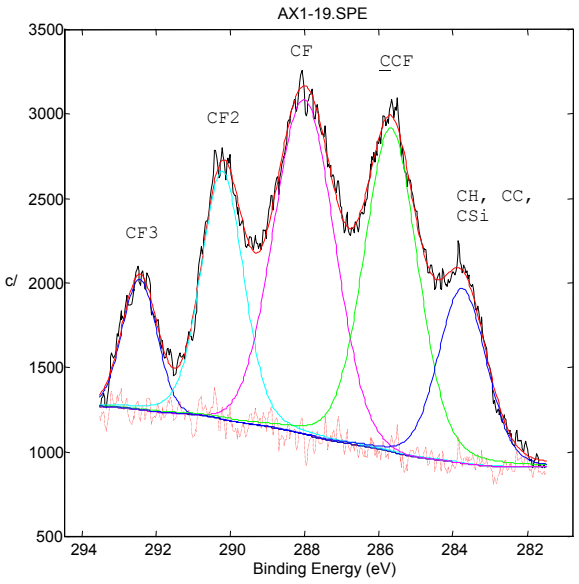

Band	Pos	Delta	B_FWHM	G_FWHM	Height	Area	%Gauss	%Area
5	283.75	0.00	1.52	1.52	1033	1801	84	14.03
4	285.66	1.92	1.69	1.69	1918	3788	80	29.51
3	288.00	4.25	1.92	1.92	1983	4059	100	31.61
2	290.20	6.45	1.34	1.34	1467	2289	80	17.83
1	292.42	8.68	1.10	1.10	771	902	100	7.02

ChiSquared: 0.313

Oxygen (1s)

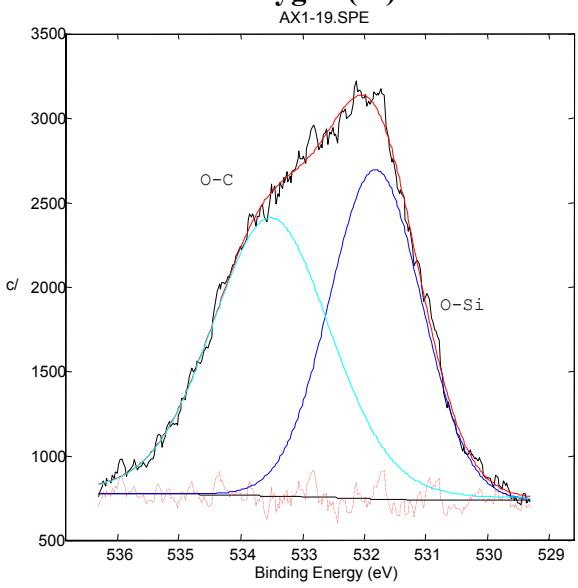

Band	Pos	Delta	B_FWHM	G_FWHM	Height	Area	%Gauss	%Area
1	531.80	0.00	1.76	1.76	1950	3676	98	46.27
2	533.50	1.70	2.27	2.27	1646	4270	84	53.73

Chi Squared: 0.361

Silicon (2p)

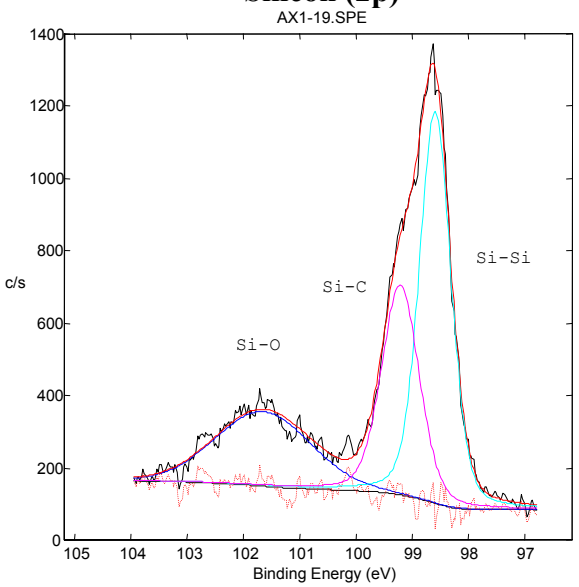

Band	Pos	Delta	B_FWHM	G_FWHM	Height	Area	%Gauss	%Area
2	98.58	0.00	0.66	0.66	1084	857	74	46.36
3	99.20	0.62	0.78	0.78	581	542	74	29.34
1	101.64	3.06	1.99	1.99	206	449	94	24.30

Chi Squared: 0.380

Fluorine (1s)

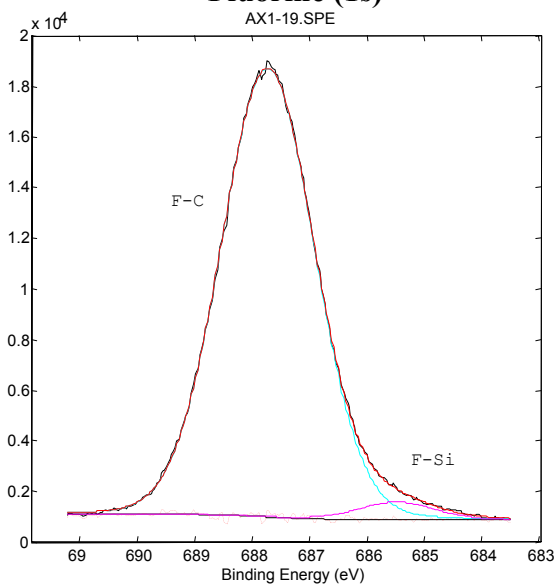

Band	Pos	Delta	B_FWHM	G_FWHM	Height	Area	%Gauss	%Area
2	685.47	0.00	1.57	1.57	707	1288	81	3.36
1	687.72	2.25	1.91	1.91	17715	37027	94	96.64

Chi Squared: 0.381

Key: Pos: Position (eV), B_FWHM: Band Full width at half max, G_FWHM: Gaussian full width at half max, Height (counts/s)

Sample 2: 12 sccm C4F6, 0 sccm O2

Overall composition (at%)

Carbon	Oxygen	Fluorine	Silicon
54	5	42	0

Carbon (1s)

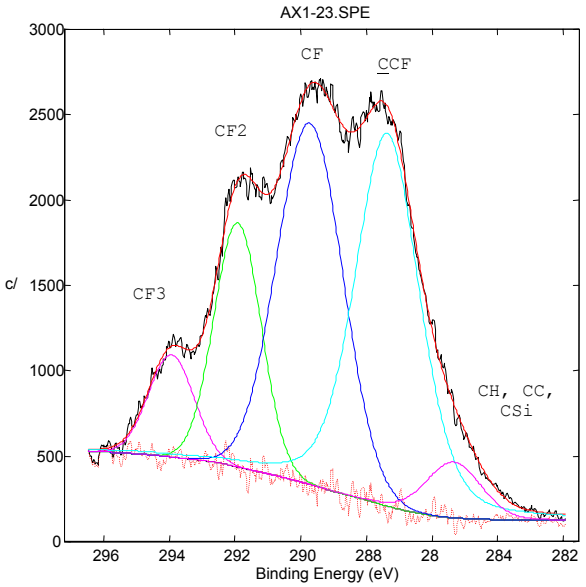

Band	Pos	Delta	B_FWHM	G_FWHM	Height	Area	%Gauss	%Area
5	285.34	0.00	1.97	1.97	324	712	90	4.50
4	287.36	2.02	2.30	2.30	2182	6154	68	38.91
3	289.72	4.38	2.38	2.38	2114	5346	100	33.80
2	291.92	6.58	1.69	1.69	1430	2566	100	16.22
1	293.93	8.60	1.63	1.63	600	1040	100	6.57

ChiSquared: 0.348

Oxygen (1s)

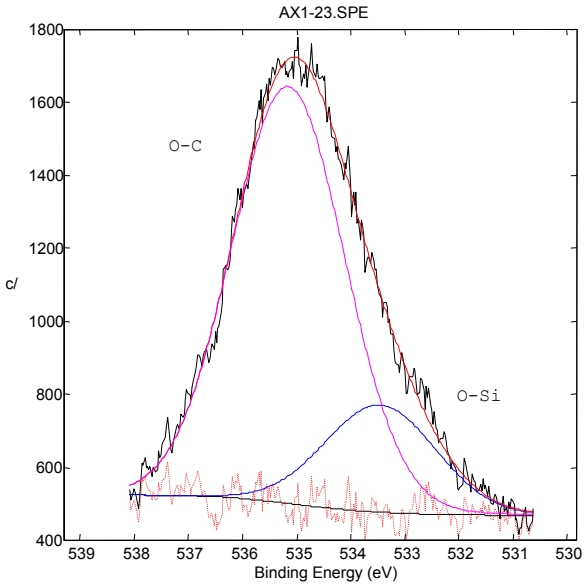

Band	Pos	Delta	B_FWHM	G_FWHM	Height	Area	%Area
1	533.45	0.00	2.42	2.42	294	757	20.01
2	535.15	1.70	2.46	2.46	1143	3027	79.99

ChiSquared: 0.311

Silicon (2p)

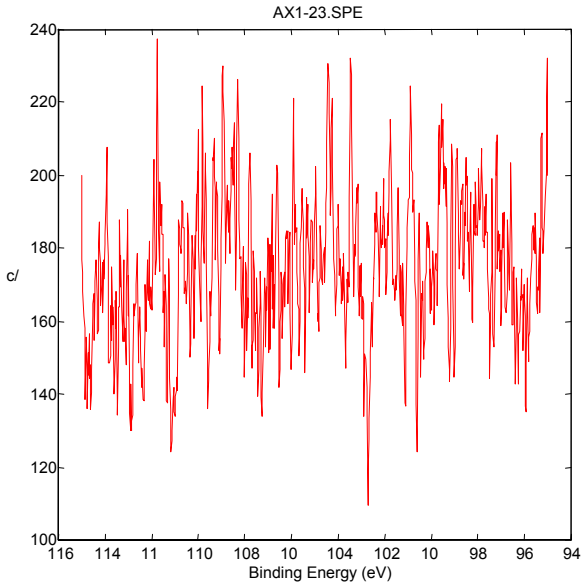

Fluorine (1s)

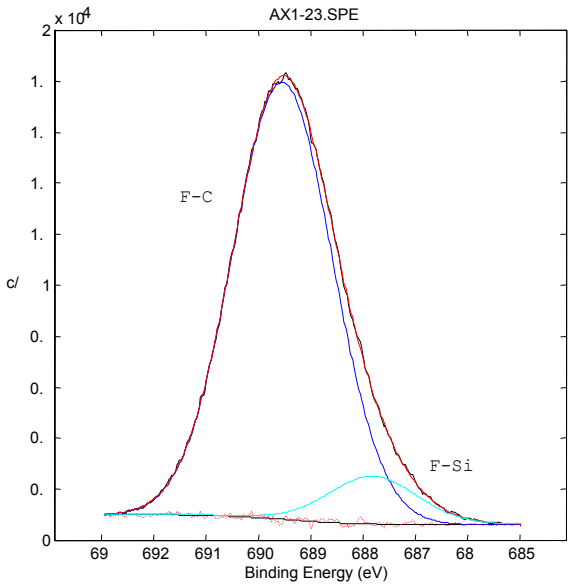

Band	Pos	Delta	B_FWHM	G_FWHM	Height	Area	%Gauss	%Area
2	687.57	0.00	1.80	1.80	1453	2935	89	6.52
1	689.50	1.93	2.28	2.28	17361	42057	100	93.48

ChiSquared 0.291

Sample 3: 12 sccm C4F8, 6 sccm O2

Overall composition (at%)

Carbon	Oxygen	Fluorine	Silicon
37	20	23	20

Carbon (1s)

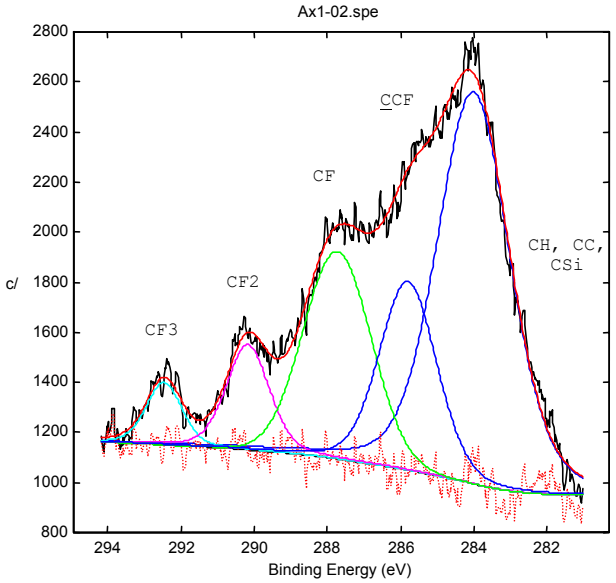

Band	Pos	Delta	B_FWHM	G_FWHM	Height	Area	%Gauss	%Area
1	284.01	0.00	2.34	2.34	1565	4385	73	49.04
5	285.80	1.79	1.84	1.84	751	1593	82	17.81
4	287.73	3.71	2.18	2.18	828	1921	100	21.48
3	290.17	6.15	1.38	1.38	420	699	72	7.82
2	292.45	8.44	1.15	1.15	249	344	72	3.85

ChiSquared: 0.332

Oxygen (1s)

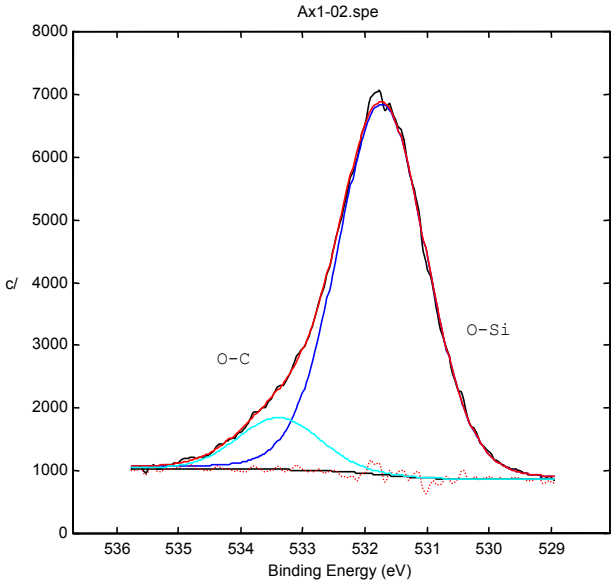

Band	Pos	Delta	B_FWHM	G_FWHM	Height	Area	%Gauss	%Area
1	531.72	0.00	1.68	1.68	5912	11071	90	88.78
2	533.38	1.66	1.55	1.55	822	1399	94	11.22

ChiSquared: 0.233

Silicon (2p)

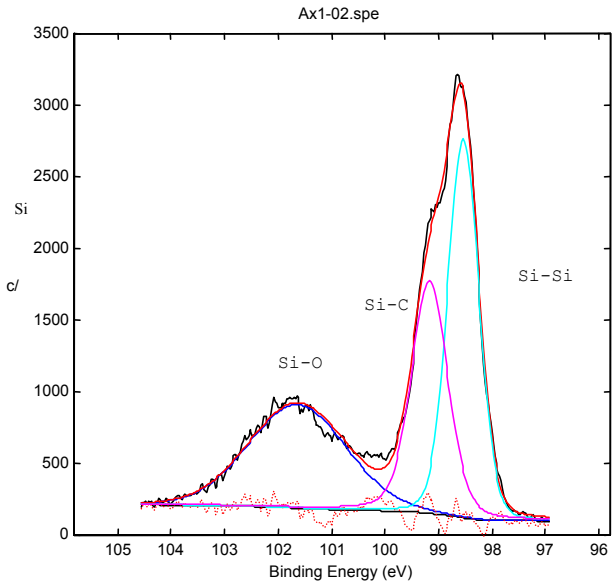

Band	Pos	Delta	B_FWHM	G_FWHM	Height	Area	%Gauss	%Area
2	98.53	0.00	0.69	0.69	2650	2044	88	38.56
3	99.17	0.63	0.80	0.80	1625	1552	74	29.29
1	101.63	3.10	2.15	2.15	721	1704	94	32.15

ChiSquared: 0.755

Fluorine (1s)

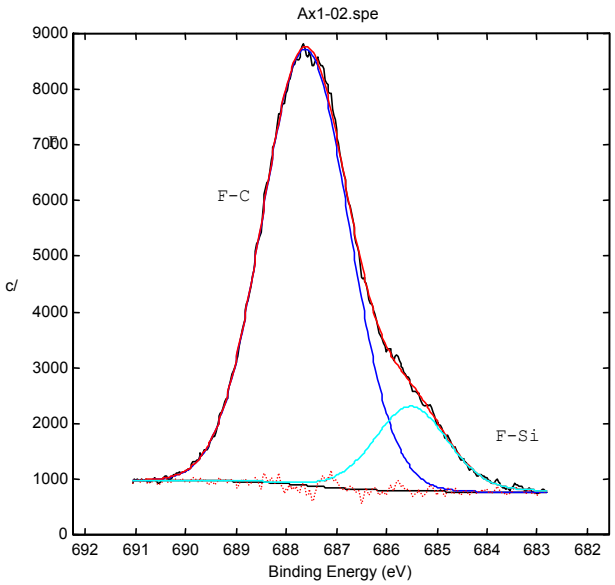

Band	Pos	Delta	B_FWHM	G_FWHM	Height	Area	%Gauss	%Area
2	685.51	0.00	1.72	1.72	1516	2988	84	14.96
1	687.61	2.10	2.04	2.04	7837	16989	100	85.04

ChiSquared: 0.279

Sample 4: 12 sccm C4F8, 0 sccm O2

Overall composition (at%)

Carbon	Oxygen	Fluorine	Silicon
44	5	46	5

Carbon (1s)

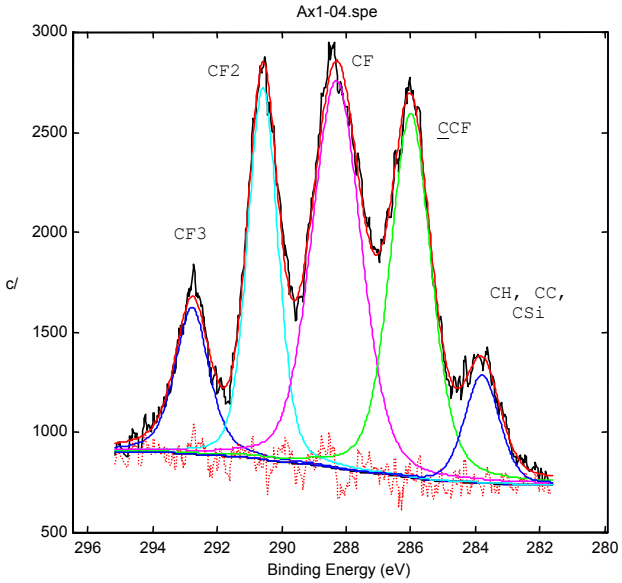

Band	Pos	Delta	B_FWHM	G_FWHM	Height	Area	%Gauss	%Area
5	283.78	0.00	1.26	1.26	531	794	76	6.65
4	286.01	2.22	1.48	1.48	1803	3421	57	28.65
3	288.30	4.52	1.80	1.80	1931	4168	74	34.90
2	290.58	6.80	1.09	1.09	1838	2409	74	20.17
1	292.78	9.00	1.24	1.24	715	1150	54	9.63

ChiSquared: 0.382

Oxygen (1s)

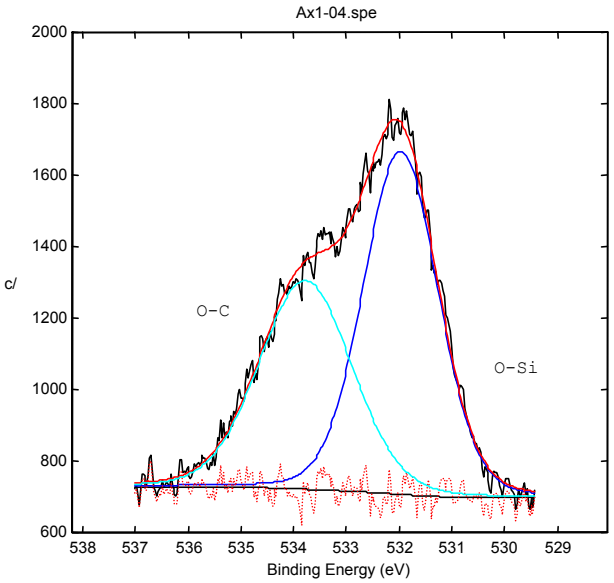

Band	Pos	Delta	B_FWHM	G_FWHM	Height	Area	%Gauss	%Area
1	531.97	0.00	1.67	1.67	961	1814	86	57.00
2	533.77	1.80	2.07	2.07	584	1368	86	43.00

ChiSquared: 0.191

Silicon (2p)

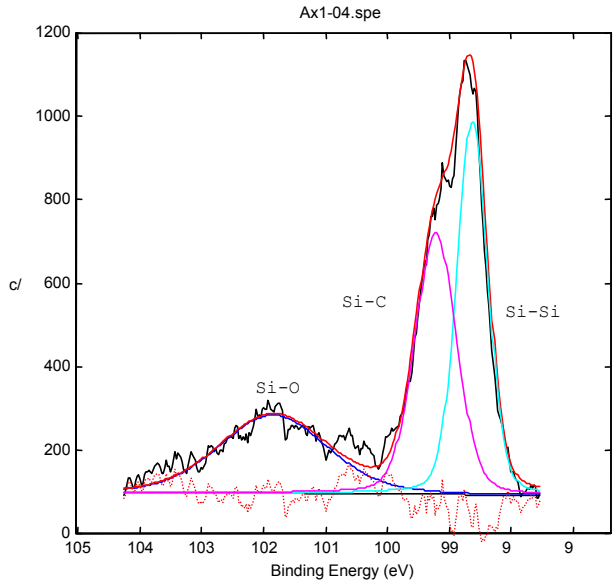

Band	Pos	Delta	B_FWHM	G_FWHM	Height	Area	%Gauss	%Area
2	98.63	0.00	0.59	0.59	895	612	81	37.62
3	99.22	0.59	0.78	0.78	626	570	81	35.05
1	101.85	3.22	2.05	2.05	187	445	81	27.33

ChiSquared: 0.836

Fluorine (1s)

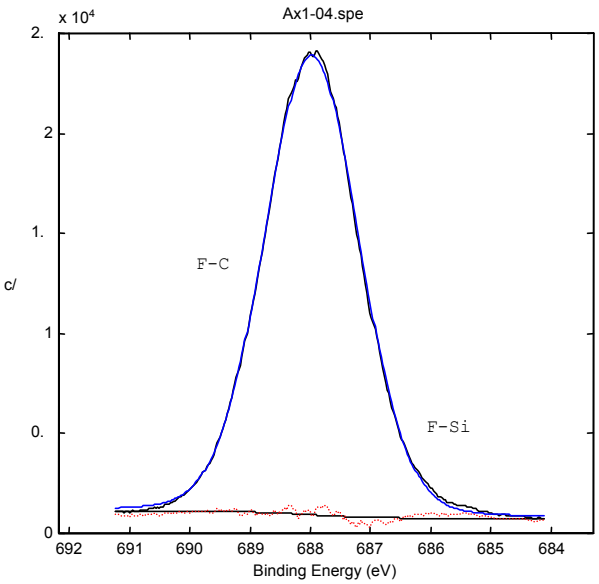

Band	Pos	Delta	B_FWHM	G_FWHM	Height	Area	%Gauss	%Area
1	687.97	0.00	1.85	1.85	22968	47268	91	100.00

ChiSquared: 2.047

Sample 5(V): 12 sccm C4F8, 6 sccm O2

Overall composition (at%)

Carbon	Oxygen	Fluorine	Silicon
28	31	11	30

Carbon (1s)

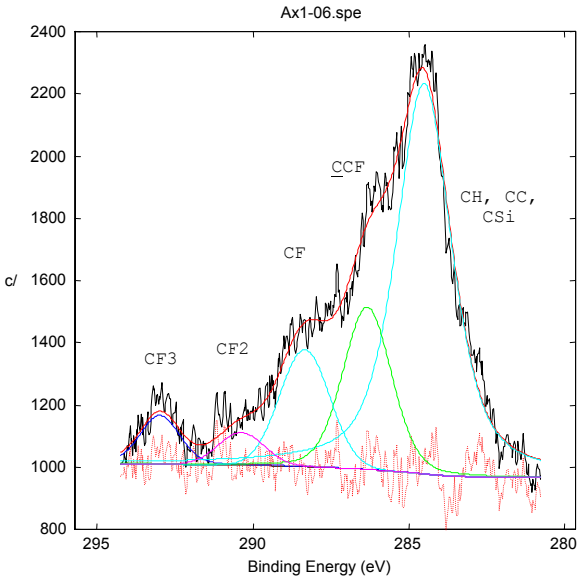

Band	Pos	Delta	B_FWHM	G_FWHM	Height	Area	%Gauss	%Area
2	284.52	0.00	2.10	2.10	1255	3609	40	60.71
3	286.34	1.82	1.83	1.83	522	1110	80	18.68
4	288.34	3.82	1.90	1.90	376	758	100	12.75
5	290.37	5.86	1.73	1.73	105	193	100	3.24
1	292.98	8.47	1.50	1.50	157	275	80	4.62

ChiSquared: 0.456

Oxygen (1s)

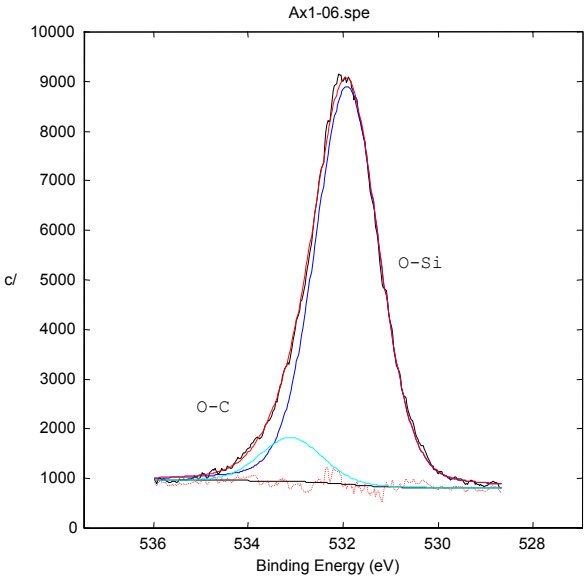

Band	Pos	Delta	B_FWHM	G_FWHM	Height	Area	%Gauss	%Area
1	531.92	0.00	1.59	1.59	8019	14660	83	90.76
2	533.10	1.19	1.52	1.52	880	1492	90	9.24

ChiSquared: 0.629

Silicon (2p)

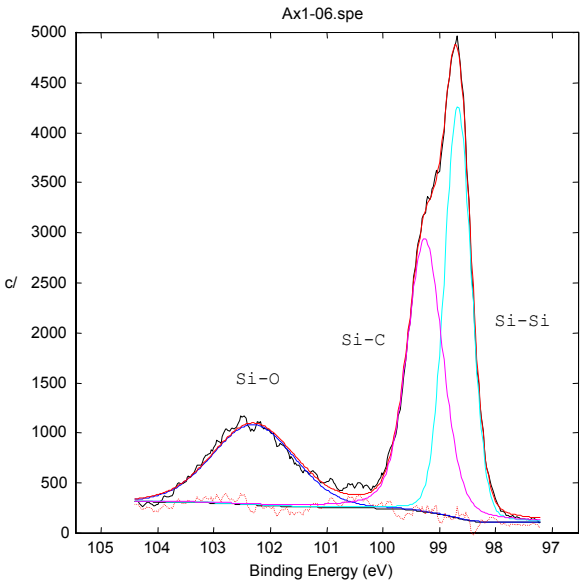

Band	Pos	Delta	B_FWHM	G_FWHM	Height	Area	%Gauss	%Area
2	98.67	0.00	0.56	0.56	4110	2587	89	39.23
3	99.26	0.59	0.74	0.74	2730	2464	70	37.37
1	102.29	3.63	1.72	1.72	803	1543	90	23.40

ChiSquared: 1.024

Fluorine (1s)

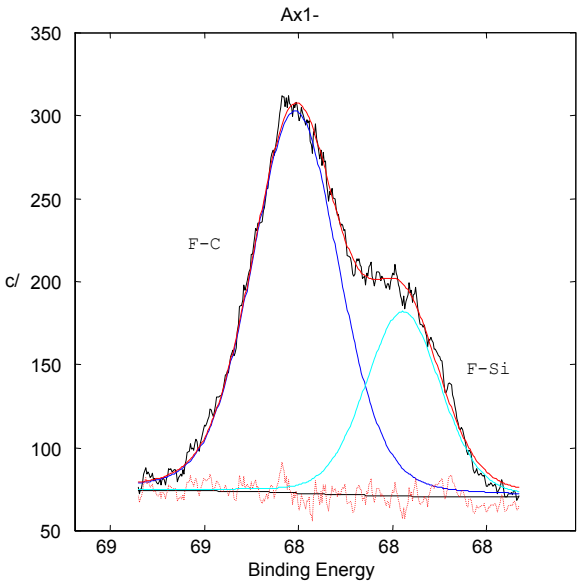

Band	Pos	Delta	B_FWHM	G_FWHM	Height	Area	%Gauss	%Area
2	685.77	0.00	1.88	1.88	1113	2435	80	29.55
1	688.06	2.29	2.16	2.16	2303	5806	80	70.45

ChiSquared: 0.429

Sample 6(V): 12 sccm C4F6, 24 sccm O2

Overall composition (at%)

Carbon	Oxygen	Fluorine	Silicon
29	27	14	29

Carbon (1s)

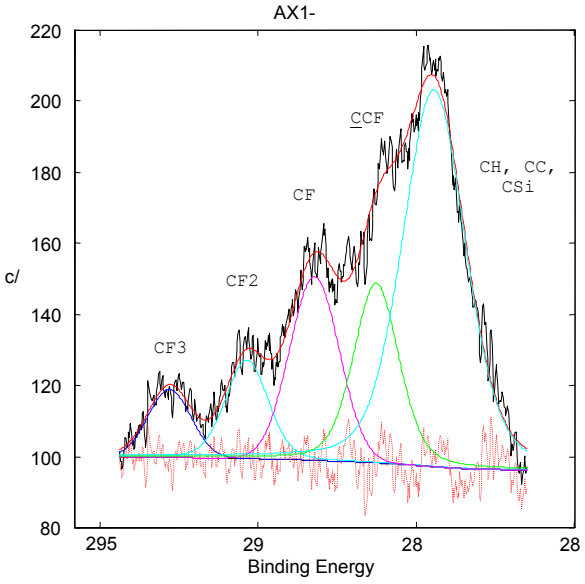

Band	Pos	Delta	B_FWHM	G_FWHM	Height	Area	%Gauss	%Area
5	284.42	0.00	2.36	2.36	1059	3038	70	51.25
4	286.25	1.83	1.69	1.69	505	1039	70	17.53
3	288.20	3.78	1.85	1.85	516	1016	100	17.14
2	290.35	5.93	1.59	1.59	277	512	80	8.64
1	292.80	8.38	1.59	1.59	191	322	100	5.44

ChiSquared: 0.336

Oxygen (1s)

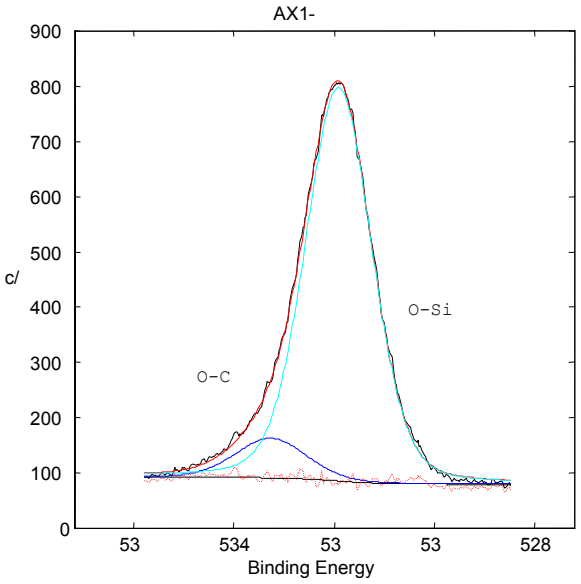

Band	Pos	Delta	B_FWHM	G_FWHM	Height	Area	%Gauss	%Area
2	531.91	0.00	1.56	1.56	7119	12940	80	90.39
1	533.26	1.35	1.65	1.65	716	1376	80	9.61

ChiSquared: 0.580

Silicon (2p)

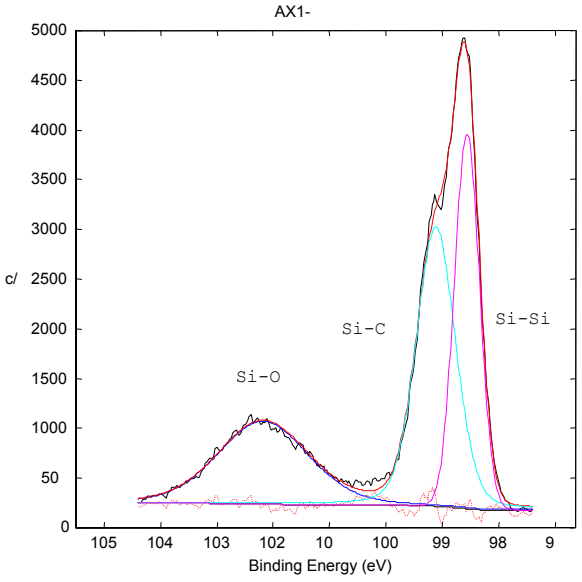

Band	Pos	Delta	B_FWHM	G_FWHM	Height	Area	%Gauss	%Area
3	98.56	0.00	0.52	0.52	3766	2104	100	31.80
2	99.11	0.55	0.82	0.82	2812	2678	80	40.48
1	102.18	3.62	1.89	1.89	833	1834	80	27.72

ChiSquared: 0.749

Fluorine (1s)

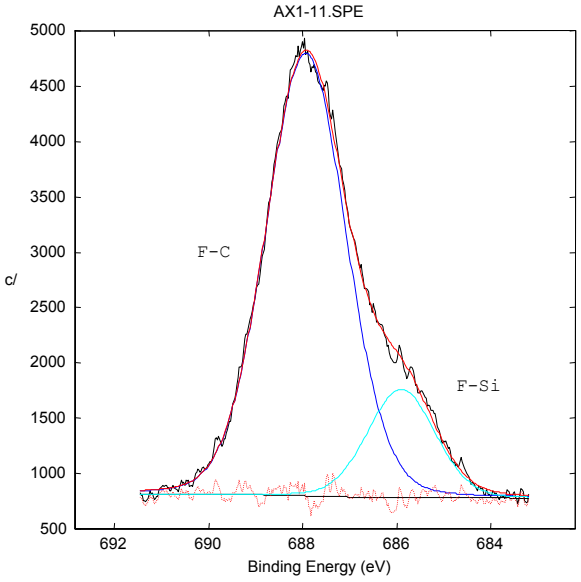

Band	Pos	Delta	B_FWHM	G_FWHM	Height	Area	%Gauss	%Area
2	685.90	0.00	1.69	1.69	977	1840	90	17.13
1	687.93	2.03	2.00	2.00	3993	8899	90	82.87

ChiSquared: 0.389

Sample 7(V): 12 sccm C5F8, 15.6 sccm O2

Overall composition (at%)

Carbon	Oxygen	Fluorine	Silicon
32	27	16	25

Carbon (1s)

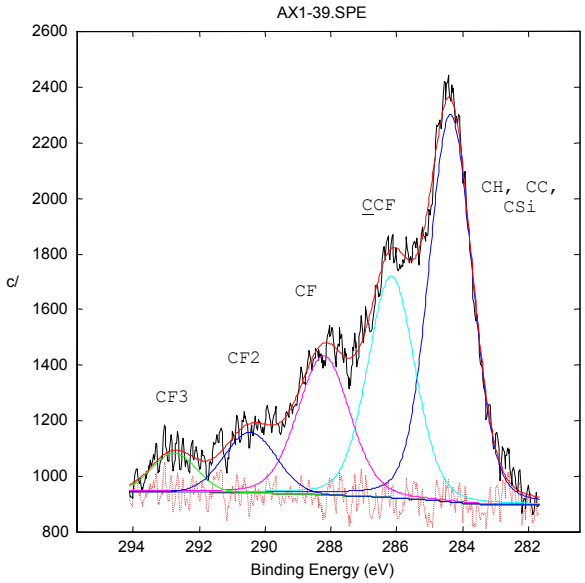

Band	Pos	Delta	B_FWHM	G_FWHM	Height	Area	%Gauss	%Area
1	284.36	0.00	1.54	1.54	1393	2503	80	43.18
2	286.15	1.79	1.67	1.67	797	1554	80	26.80
3	288.21	3.85	1.86	1.86	498	1079	80	18.61
5	290.45	6.09	1.86	1.86	217	428	100	7.39
4	292.75	8.39	1.58	1.58	138	233	100	4.02

ChiSquared: 0.303

Oxygen (1s)

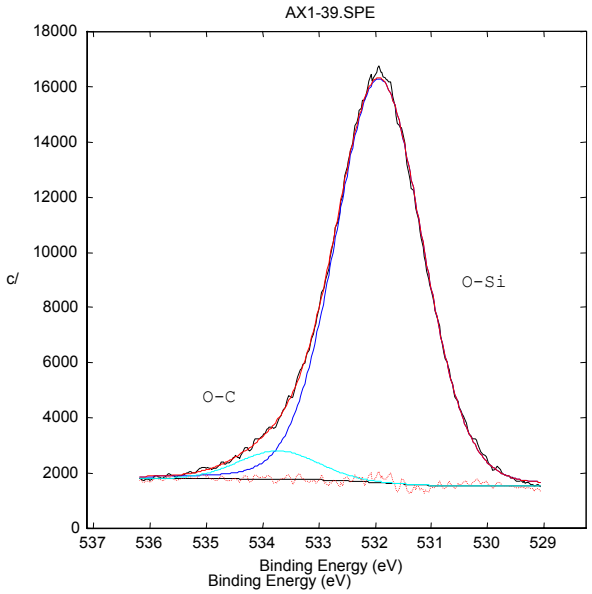

Band	Pos	Delta	B_FWHM	G_FWHM	Height	Area	%Gauss	%Area
1	531.92	0.00	1.82	1.82	14637	29660	90	94.36
2	533.72	1.80	1.65	1.65	1010	1774	100	5.64

ChiSquared: 0.571

Silicon (2p)

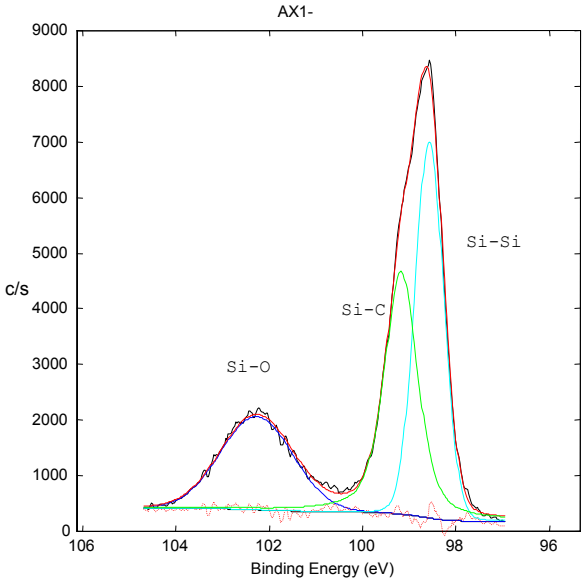

Band	Pos	Delta	B_FWHM	G_FWHM	Height	Area	%Gauss	%Area
2	98.57	0.00	0.72	0.72	6760	5295	96	39.65
3	99.18	0.60	0.84	0.84	4364	4803	50	35.97
1	102.27	3.70	1.82	1.82	1677	3257	100	24.39

ChiSquared: 0.959

Fluorine (1s)

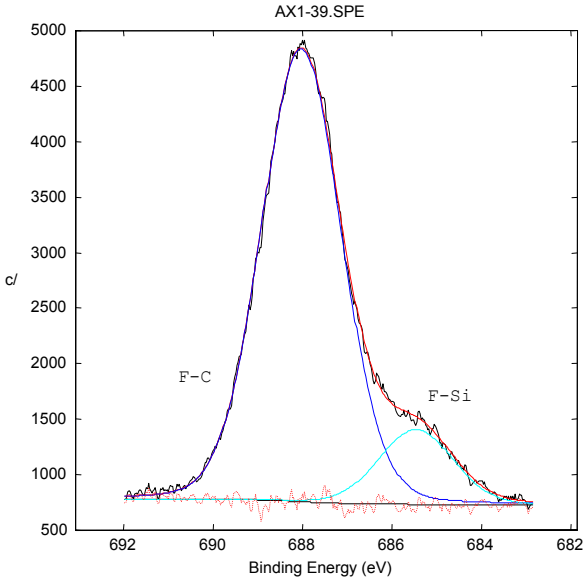

Band	Pos	Delta	B_FWHM	G_FWHM	Height	Area	%Gauss	%Area
2	685.48	0.00	1.96	1.96	680	1485	90	13.52
1	688.04	2.56	2.08	2.08	4087	9499	90	86.48

ChiSquared: 0.250

Sample 8: 12 sccm C5F8, 15.6 sccm O2

Overall composition (at%)

Carbon	Oxygen	Fluorine	Silicon
43	19	20	17

Carbon (1s)

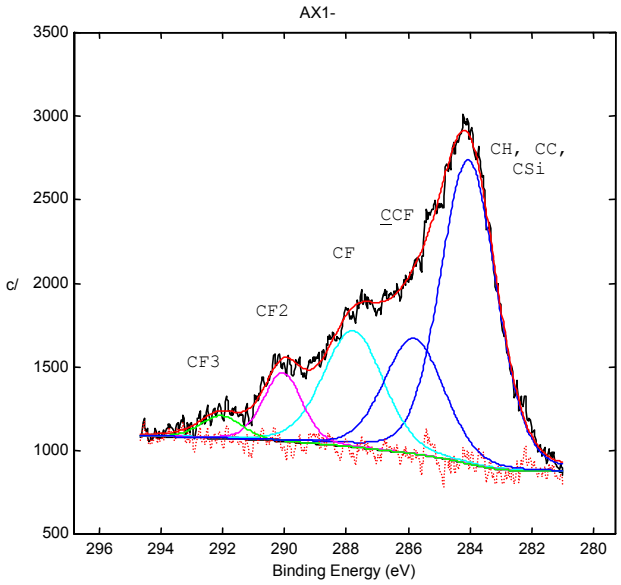

Band	Pos	Delta	B_FWHM	G_FWHM	Height	Area	%Gauss	%Area
1	284.05	0.00	2.14	2.14	1818	4530	80	49.38
5	285.80	1.76	2.28	2.28	693	1840	80	20.06
2	287.77	3.72	2.28	2.28	698	1845	81	20.12
3	290.05	6.00	1.48	1.48	411	708	80	7.72
4	292.02	7.98	1.58	1.58	135	250	80	2.73

ChiSquared: 0.293

Oxygen (1s)

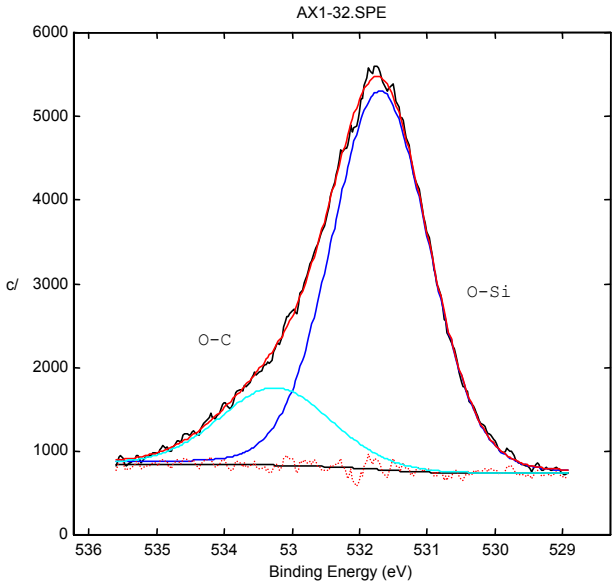

Band	Pos	Delta	B_FWHM	G_FWHM	Height	Area	%Gauss	%Area
1	531.69	0.00	1.68	1.68	4527	8495	90	81.05
2	533.24	1.55	1.92	1.92	926	1986	90	18.95

ChiSquared: 0.275

Silicon (2p)

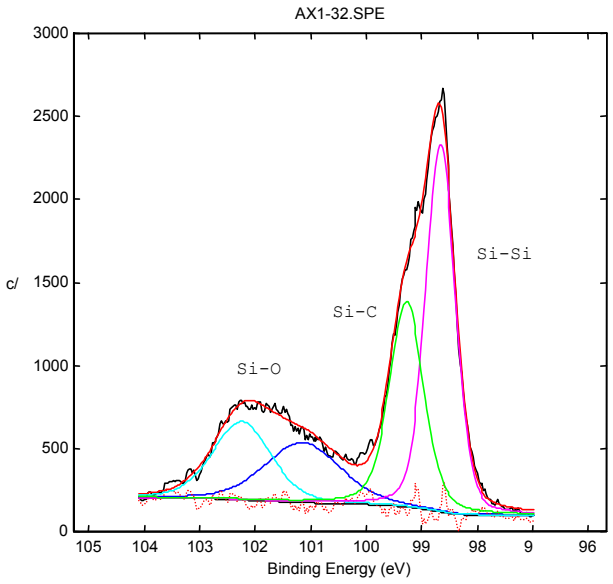

Band	Pos	Delta	B_FWHM	G_FWHM	Height	Area	%Gauss	%Area
3	98.66	0.00	0.63	0.63	2210	1639	77	39.70
4	99.27	0.61	0.72	0.72	1236	1100	66	26.64
1	101.14	2.48	1.60	1.60	361	686	76	16.63
2	102.24	3.58	1.24	1.24	472	703	72	17.03

ChiSquared:0.546

Fluorine (1s)

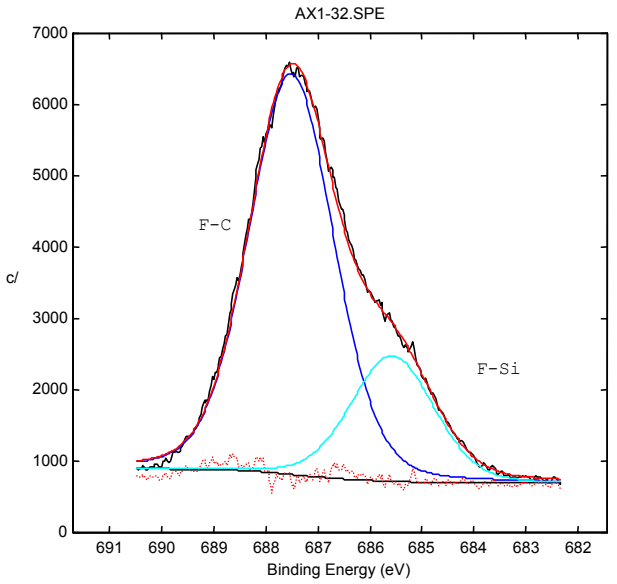

Band	Pos	Delta	B_FWHM	G_FWHM	Height	Area	%Gauss	%Area
2	685.57	0.00	1.89	1.89	1760	3835	82	23.55
1	687.51	1.94	1.91	1.91	5635	12447	82	76.45

ChiSquared:0.611

Sample 9: 12 sccm C5F8, 0 sccm O2

Overall composition (at%)

Carbon	Oxygen	Fluorine	Silicon
52	4	43	0

Carbon (1s)

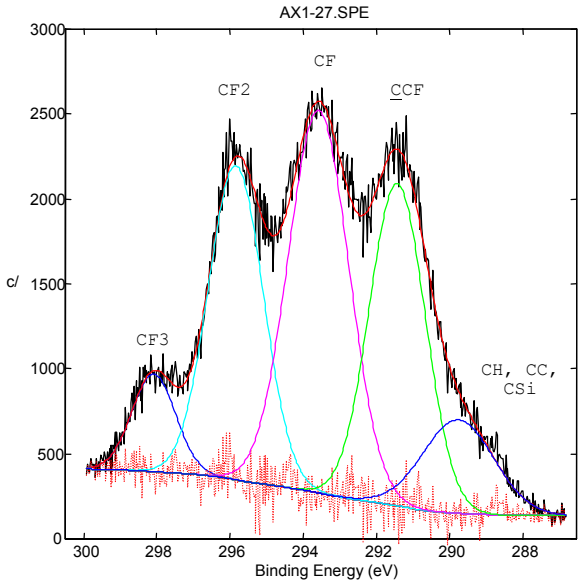

Band	Pos	Delta	B_FWHM	G_FWHM	Height	Area	%Gauss	%Area
5	289.85	0.00	2.39	2.39	601	1531	100	10.94
4	291.35	1.51	1.59	1.59	1739	2969	98	21.21
3	293.54	3.69	2.26	2.26	2239	5388	100	38.48
2	295.91	6.06	1.66	1.66	1796	3251	94	23.22
1	298.07	8.22	1.40	1.40	580	862	100	6.157

ChiSquared: 1.090

Oxygen (1s)

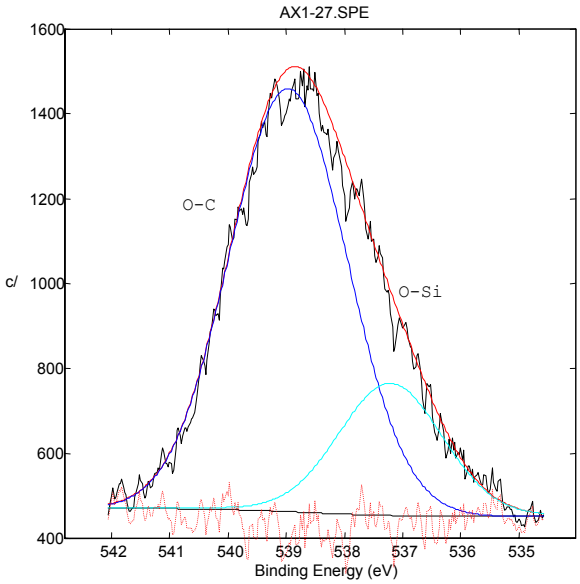

Band	Pos	Delta	B_FWHM	G_FWHM	Height	Area	%Gauss	%Area
2	537.21	0.00	2.10	2.10	297	680	94	21.99
1	538.96	1.75	2.37	2.37	955	2413	100	78.01

ChiSquared: 0.266

Silicon (2p)

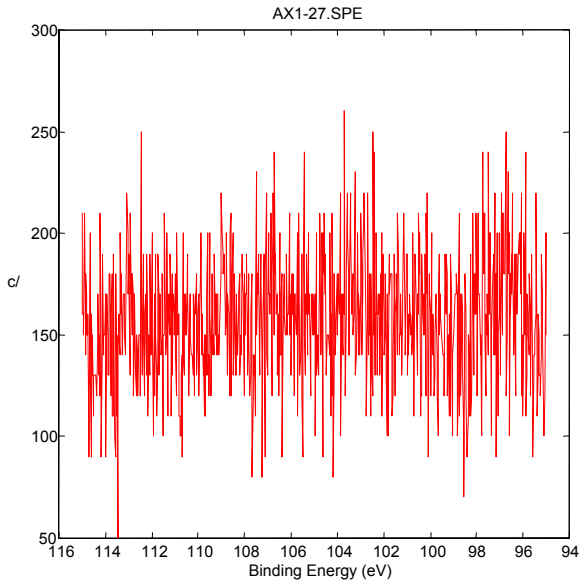

Fluorine (1s)

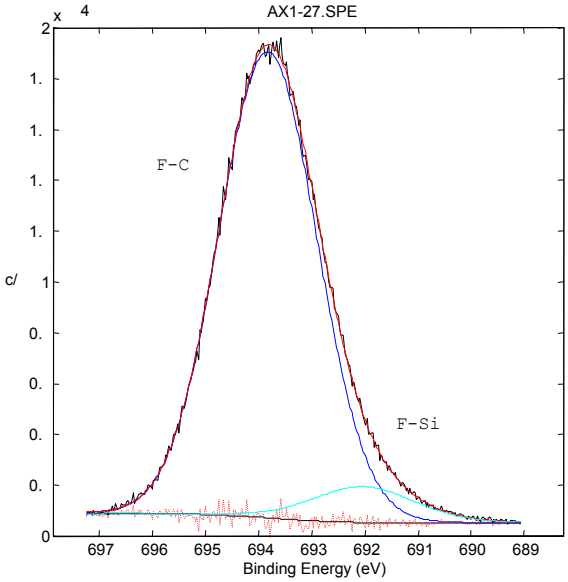

Band	Pos	Delta	B_FWHM	G_FWHM	Height	Area	%Gauss	%Area
2	692.04	0.00	2.28	2.28	1410	3665	85	7.90
1	693.82	1.78	2.17	2.17	18344	42740	98	92.10

ChiSquared: 1.157

APPENDIX B

Appendix B contains proton NMR data from products generated by the reaction of 0.1 M sodium naphthalene and tetrabutylammonium chloride in THF. Samples were prepared in deuterated DMSO. Data from reaction products of sodium naphthalene intentionally quenched with DIW is also included for comparison. Proton NMR shifts were determined from proton NMR measurements of individual reaction and simulated proton shifts generated from ChemOffice software (Cambridgesoft). Expected shifts are shown below.

Naphthalene

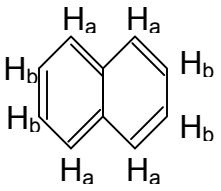

H_a - 7.67
H_b - 7.32

1-4, Dihydronaphthalene

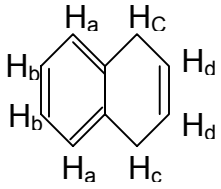

H_a - 6.95
H_b - 6.94
H_c - 3.35
H_d - 5.98

1-2, Dihydronaphthalene

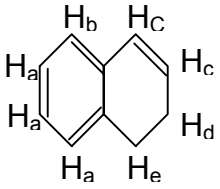

H_a - 7.03-7.09
H_b - 7.25
H_c - 6.62-5.8
H_d - 2.29
H_e - 2.6

Tetrabutylammonium chloride

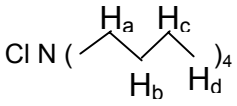

H_a - 3.24
H_b - 1.73
H_c - 1.33
H_d - 0.96

Tributylamine

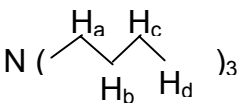

H_a - 2.36
H_b - 1.39
H_c - 1.33
H_d - 0.96

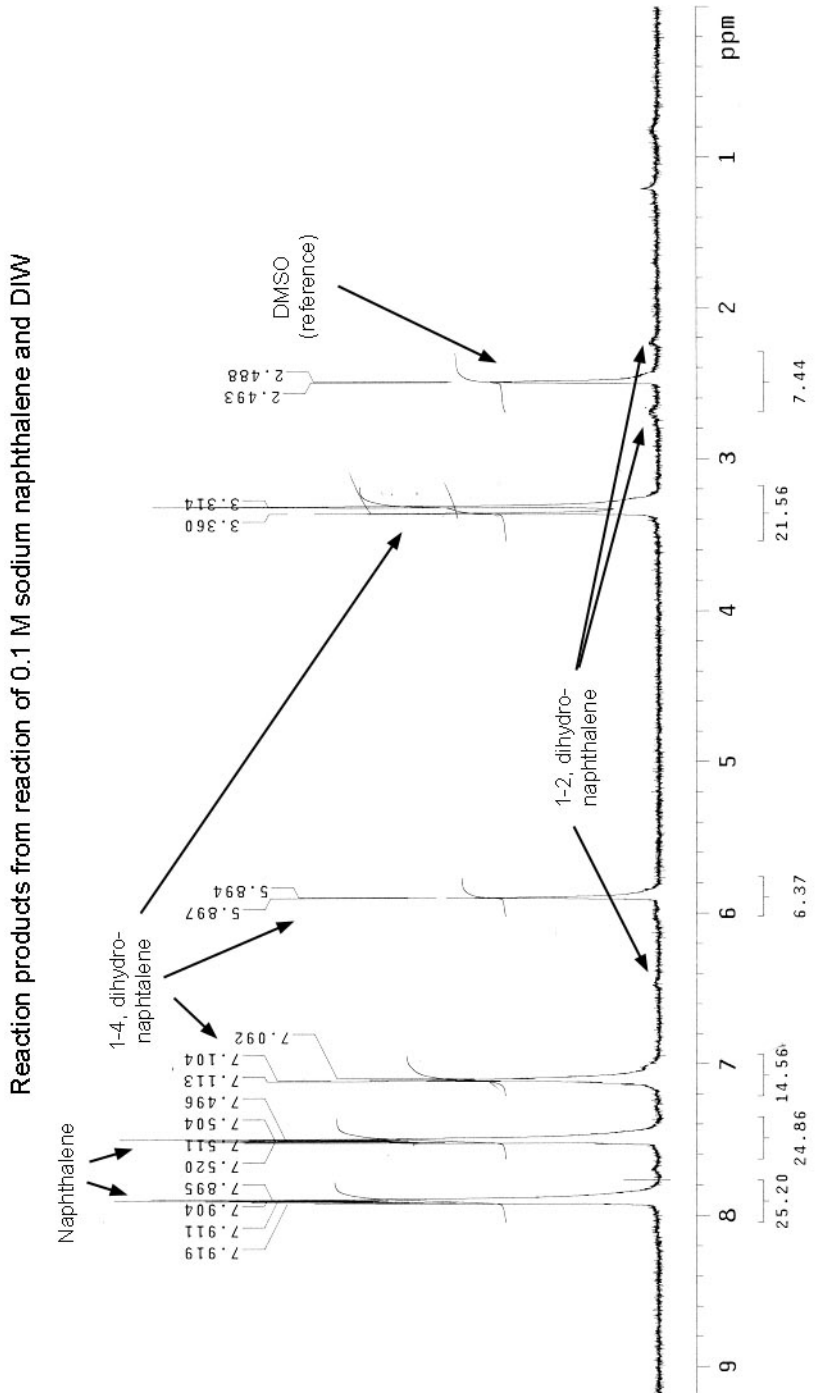
Reaction products from reaction of 0.1 M sodium naphthalene and DIW
Naphthalene
1-4, dihydro-
naphtalene
DMSO
(reference)
1-2, dihydro-
naphthalene
7.919
7.911
7.904
7.895
7.520
7.511
7.504
7.496
7.113
7.104
7.092
5.897
5.894
3.360
3.314
2.493
2.488
ppm
25.20
24.86
14.56
6.37
21.56
7.44

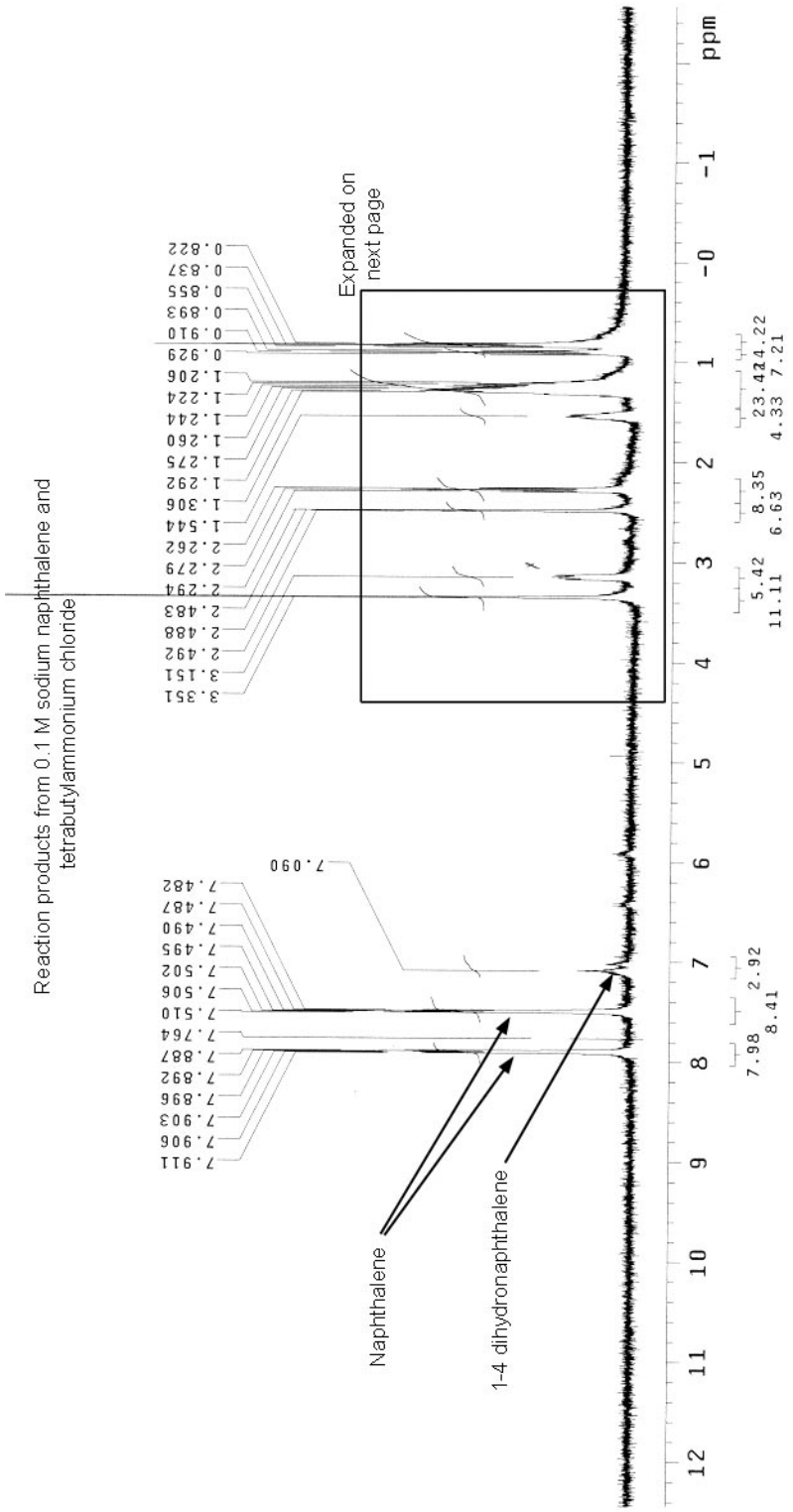
Reaction products from 0.1 M sodium naphthalene and tetrabutylammonium chloride
Expanded on next page
Naphthalene
1-4 dihydronaphthalene
ppm

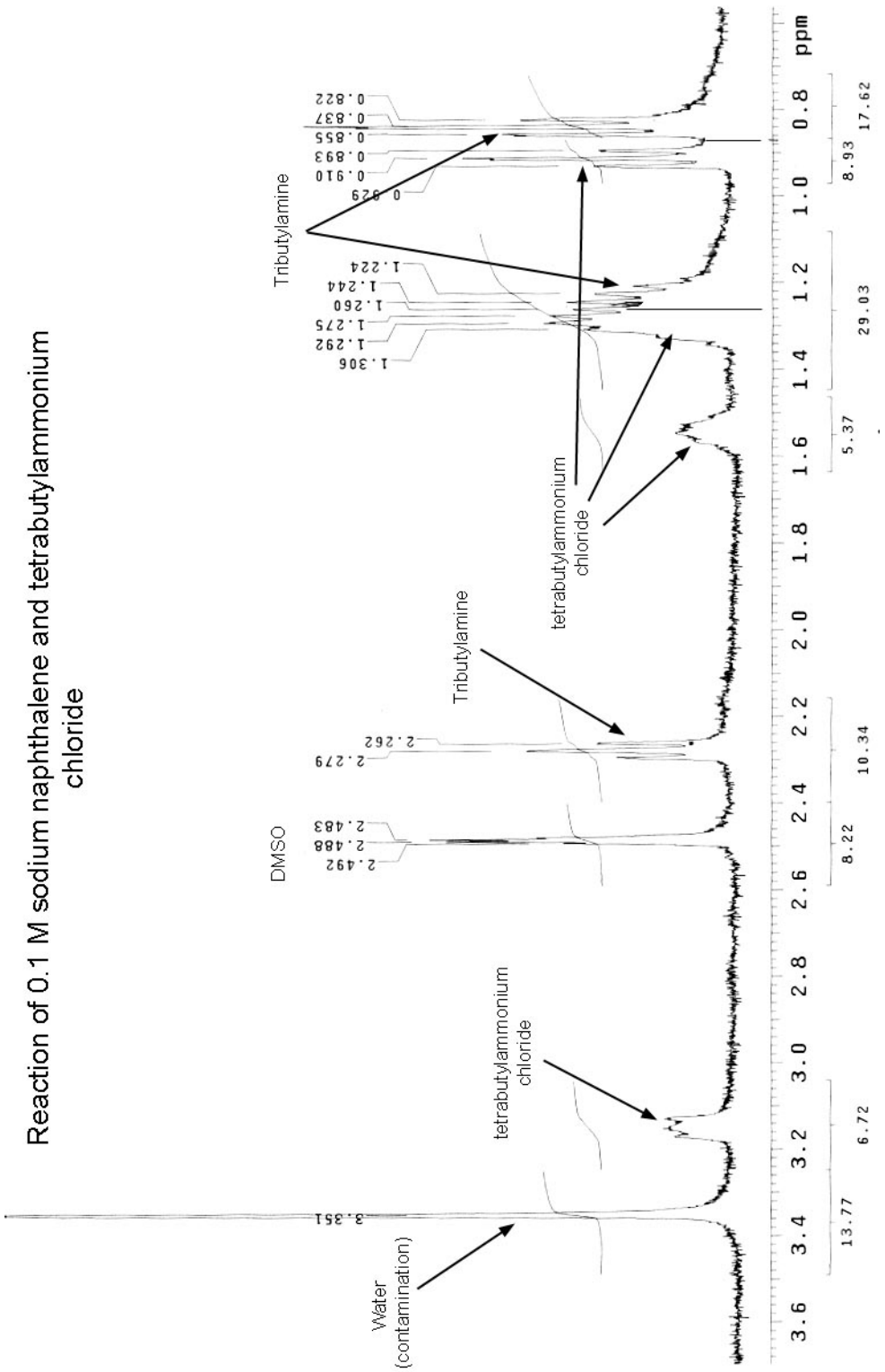
Reaction of 0.1 M sodium naphthalene and tetrabutylammonium chloride
Water (contamination)
tetrabutylammonium chloride
Tributylamine
DMSO
tetrabutylammonium chloride
Tributylamine
3.351
2.492
2.488
2.483
2.279
2.262
1.306
1.292
1.275
1.260
1.244
1.224
0.929
0.910
0.893
0.855
0.837
0.822
3.6
3.4
3.2
3.0
2.8
2.6
2.4
2.2
2.0
1.8
1.6
1.4
1.2
1.0
0.8
ppm
13.77
6.72
8.22
10.34
5.37
29.03
8.93
17.62

REFERENCES

1 Online source: http://www.icknowledge.com/history/1950s.html

2 Online source: 'History of the Transistor', http://www.pbs.org

3 G.E. Moore, Electronics **38**, 8 (1965)

4 Online source: Intel web site data: http://www.intel.com/research/silicon/mooreslaw.htm

5 S. Jeng, R. Havemann, M. Chang, 'Advanced Metallization and Interconnect Systems for ULSI Applications, Mat. Res. Soc. Proc. **337**, 25 (1996)

6 S. Verhaverbeke, S. Kuppurao, C. Beaudry and J. Truman, Semi. Interntl. **25,** 91 (2002)

7 A. Braun, "Photoresist Stripping Faces Low-k Challenges," Semiconductor Intl., October 1999

8 P. D. Agnello, IBM J. Res. & Dev. **46**, 317 (2002)

9 ITRS 2003 edition, available online at http://public.itrs.net

10 S. Jeng,. et al., Material Research Society Proceedings **337**, 25 (1996)

11 Staff Writer, "Much Hype, Little Reality in Low-k," Semiconductor International, Electronic News, 6/2/04

12 J. Chappell, "Can't Keep a Good FSG Down," Semiconductor International, Electronic News, 5/26/2004

13 S. Hwang, G. Lee, J. Min, S. Moon, Electrochem. Sol-State Letters **6**, G12 (2003)

14 N. Posseme, T. Chevolleau, O. Joubert, L. Vallier and P. Mangiagalli, J. Vac. Sci. Technol. B **21**, 2432 (2003)

15 D. Fuard, O. Joubert, L. Vallier, M. Assous, P. Berruyer, R. Blanc, J. Vac. Sci. and Tech. **19**, 2223 (2001)

16 G. Oehrlein, T. Standaert, P. Matsuo, Solid State Technol. **43**, 125 (2000)

17 D. Manos and D. Flamm, eds., An Introduction to Plasma Etching. Academic Press: San Diego, Ca

18 M. Schaepkens and G. S. Oehrlein, J. Electrochem. Soc. **148**, C211 (2001)

19 A. Hynes, M. Shenton and J. Badyal, Macromolecules **29**, 18 (1996)

20 T. Standaert, C. Hedlund, E. Joseph, G. Oehrlein and T. Dalton, J. Vac. Sci. Technol. A **22**, 52 (2004)

21 S. Imai, H. Motomura and K. Tachibana, J. Vac. Sci. Technol. B **20**, 1482 (2002)

22 Xi Li, Xuefeng Hua,Li Ling, G. Oehrlein, M. Barela and H. Anderson, J. Vac. Sci. Technol. A **20,** 2052 (2002)

23 M. Jaso and G. Oehrlein, J. Vac. Sci. Technol. A **6**, 1397 (1988)

24 M. Mastsui, T. Tatsumi and M. Sekine, J. Vac. Sci. Tech. A **19**, 1282 (2001)

25 R. Luginbuhl, M. Garrison, et al., Am. Chem. Soc. Symp. Series 787 (2001)

26 Y. Kim, M. Baklanov, T. Conard, S. Vanhaelemeersch and W. Vanderworst, Solid State Phen. **65-66**, 291 (1999)

27 R. Chatterjee, S. Karecki, R. Reif, V. Vartanian and T. Sparks, J. Electrochem. Soc. **149**, G276 (2002)

28 A. Sankarana and M. Kushner, Appl. Physics Let. **82**,1824 (2003)

29 S. Fonash, J. Electrochem Soc. **137**, 3885 (1990)

30 G. Oehrlein, R. Tromp, J. Tsang, Y. Lee and E. Petrillo, J. Electrochem Soc. **132**, 1441 (1985)

31 G. Potter, G. Morrison, P. Charvat and A. Ruoff, J. Vac. Sci. Technol. B **10**, 2398 (1992)

32 S. Verhaverbeke, S. Kuppurao, C. Beaudry and J. Truman, Semiconductor Intl. **25**, 91 (2002)

33 D. Louis, C. Peyne, E. Lajoinie, D. Valessi, D. Homes, D. Maloney and S. Lee, Microelectronic Eng. **46**, 307 (1999)

34 W. Kern, J. Electrochem. Soc. **137**, 1887 (1990)

35 A. Somashekhar, H. Ying, P. Smith, D. Aldrich and R. Nemanich, J. Electrochem. Soc. **146**, 2318 (1999)

36 H. Cerva, E. Mohr and H. Oppolzer, J. Vac. Sci. Tech. B **5** (2) 590 (1997)

37 J. Simko and G. Oerhlein, J. Electrochem. Soc. **138**, 277 (1991)

38 G. Saunders, Angew. Chem. Int. Ed. Engl. **35,** 2615 (1996)

39 A. Braun, "Photoresist Stripping Faces Low-k Challenges," Semiconductor Intl., October 1999

40 P. Matsuo, T. Standaert, S. Allen, G. Oerhlein and T. Dalton, J. Vac. Sci Tech. B **17**, 1435 (1999)

41 R. Donaton, B. Coenegrachts, et al., MRS Symp. Proc. **612**, D5.14 (2000)

42 S. Vitale and H. Sawin, J. Vac. Sci. Technol. A **20**, 651 (2002)

43 C. Waldfried, O. Escorcia, Q. Han and P. B. Smith, Electrochem. and Solid-State Lett. **6** G137 (2003)

44 D. Shamiryan, M. Baklanov, S. Vanhaelemeersch, and K. Maex, J. Vac. Sci. Tech. B **20,** 1923 (2002)

45 O. Louveau, D. Louis, M. Assous, R. Blanc, P. Brun, S. Lamy and E, Lajoinie, Microelectronic Eng. **61**, 867 (2002)

46 C. Waldfried, O. Escorcia, Q. Han, P. Smith, Electrochem. Sol-State Letters **6**, G137 (2003)

47 D. Shamiryan, M. Baklanov, S. Vanhaelemeersch, K. Maex, J. of Vac. Sci. Tech. B **20**, 1923 (2002)

48 Y. Wang and R. Kumar, J. Electrochem. Soc. **151,** F73 (2004)

49 G. Asai, Y. Muraoka, K. Saito, I. Mizobata, T. Iwata, K. Masuda, K. Iijima, T. Yoshikawa, D. Peters, Diff. Defect Data B **92**, 297 (2003)

50 S. Myneni, D.W. Hess, J. Electrochem. Soc. **150**, G744 (2003)

51 A. Sehgal,M. Yalamanchili, C. Millet, A. Danel, F. Tardif, Diff Def Data B **92,** 301 (2003)

52 B. Moslehi, Micro **22**, 65 (2004)

53 M. Spuller, D.W. Hess, J. Electrochem. Soc. **150**, G476 (2003)

54 L. Rothman, R. Robey, M. Ali, D. Mount, IEEE Intl Symp. Semi. Manuf. Conf. Proc. 372 (2002)

55 J. Burdeniue, B. Jedlicka and R. Crabtree, Chem. Ber/Recueil **130**, 145 (1997)

56 G. Saunders, Angew. Chem. Int. Ed. Engl. **35,** 2615 (1996)

57 J. Marsella, A. Gilicinski, A. Coughlin and G. Pez, J. Org. Chem. **57**, 2856 (1992)

58 J. Lukas, L. Lochmann and J. Kalal, Ange. Makromol. Chemie **181**, 183 (1990)

59 R. Harrison and T. Richmond, J. Am. Chem. Soc. **115**, 5303 (1993)

60 B. Bennet, R. Harrison and T. Richmond, J. Am. Chem. Soc., **116**, 11165 (1994)

61 D. Clark and D. Hutton, J. Polym. Sci. A **25**, 2643 (1987)

62 I. Noh, K. Chittur, G. Krishnan, S. Goodman and J. Hubbell, J. Polym Sci A **35**, 1499 (1997)

63 S. Tasaka, K. Narushima and K. Teranishi, J. Appl. Polym. Sci. **83**, 340 (2002)

64 C. Lin, W. Hsu and B. Hwang, J. Adhesion Sci. and Technol. **14**, 1 (2000)

65 V. Boittiaux, F. Boucetta, C. Combellas, F. Kanoufi, A. Thiebault, M. Delamar and P. Bertrand, Polymer **40**, 2011 (1998)

66 Acton manufactures a commercial PTFE etchant: Fluoroetch based on sodium naphthalene in diglyme

67 C. Costello and T. McCarthy, Macromolecules **20**, 2819 (1987)

68 K. Ha, S. McClain, S. Suib and A Garton, J. Adhesion **33**, 169 (1991)

69 V. Boittiaux, F. Boucetta, C, Combellas, F. Kanoufi, A. Thiebault, M. Delamar and P. Bertrand, Polymer **40**, 2011 (1999)

70 B. Belzung, K. Brace, C. Combellas, M. Delamar, F. Kanoufi, M. Shanahan and A. Thiebault, Polymer **39**, 4867 (1998)

71 K. Lee and T. McCarthy, Macromolecules **21,** 2318 (2318)

72 H. Bickford,et al. International Business Machines, US Patent 5,800,858

73 M. Berthelot, Justus Liebags Ann. Chem. **143,** 97 (1867)

74 W. Schlenk, J. Appenrodt, A. Michael and A. Thal, Chem. Ber. **47**, 473 (1914)

75 W. Schlenk, J and E. Bergmann, Justus Liebags Ann. Chem. **464**, 1 (1928)

76 N. Holy, Chem. Rev. **74**, 243 (1974)

77 S. Pederson, T. Christensen, T. Thomasen and K. Daasbjerg, J. Electroanal. Chem. **454**, 123 (1998)

78 N. Bauld, Radical Anion Chemistry Overview, Online: http://www.cm.utexas.edu/bauld/unit6_anrad.htm

79 H. Sakuri, Y. Kubo, M. Shiotani, H. Yahiro and Y. Okuda, J. Appl. Polym Sci. **74,** 286 (1999)

80 S. Bank and D. Jucket, J. Amer. Chem. Soc. **98**, 7742 (1976)

81 K. Hofelmann, J. Jagur-Grodzinski and M. Szwarc, J. Amer. Chem. Soc. **91**, 4645 (1969)

82 E. de Boer, A. Grotens and J. Smid, J. Amer. Chem. Soc. **92** 4742 (1970)

83 P. Chang, R. Slates and M. Szwarc, J. Phys. Chem. **70**, 3180 (1966)

84 T. Hogen-Esch and J. Smid, J. Amer. Chem. Soc. **88**, 307 (1966)

85 A. Shatenshtein, E. Petrov and E. Yakoleva, J. Polym. Sci. C **16** 1729 (1967)

86 K. Suga and S. Aoyagui, Bull. Chem. Soc. Jpn. **55,** 358 (1982)

87 P. Chang, R. Slates and M. Szwarc, J. Phys. Chem. **70**, 3180 (1966)

88 S. Bank and B. Bockrath, J. Amer. Chem. Soc. **93**, 430 (1971)

89 W. Armarego and C. Chai, Purification of Laboratory Chemicals, Elsevier Science, MA, 2003

90 H. Zieger, I. Angres and D. Mathisen, J. Amer. Chem. Soc. **98**, 2580 (1976)

91 S. Bank and D. Jucket, J. Amer. Chem. Soc. **97,** 567 (1975)

92 M. Fox, Chem. Rev. **79**, 253 (1978)

93 A. Shatenshtein, E. Petrov and E. Yakovleva, J. Polym. Sci. C **16**, 1729 (1967)

94 S. Pederson, T. Lund, K. Daasbjerg, M. pop, I. Fussing and H. Lund, Acta Chemica Scand. **52**, 657 (1998)

95 F. De Smedt, S. De Gendt, M. Heyns and C. Vinckier, J. Electrochem Soc. **148,** G487 (2001)

96 E. Bergman, M. Melli, M. Magrin and M. Source, Europ. Semicond. **22,** 25 (2000)

97 B. Smith and J. March, *Advanced Organic Chemistry,* Wiley Interscience, New York, (2001)

98 R. Atkinson and W. Carter, Chem. Rev **84,** 437 (1984)

99 Y. Ku, W. Su and W. Shen, Ind. Eng. Chem. Res. **35,** 3369 (1996)

100 E. Reisz, W. Schmidt, H. Schuman and C. Von Sonntag, Environ. Sci. Technol. **37,** 1941 (2003)

101 A. Nemes, I. Fabian and R. van Eldik, J. Phys. Chem A **104,** 7995 (2000)

102 F. De Smedt, H. Vankerckhoven and C. Vinckier, Ozone Sci. and Eng. **25,** 445 (2003)

103 G. Wittmann, I. Horvath and A. Dombi, Ozone Sci and Eng. **24,** 281 (2002)

104 R. Flyunt, A. Leitzke, G. Mark, E. Mvula, E. Reisz, R. Schick and C. von Sonntag, J. Phys. Chem. B **107,** 7242 (2003)

105 G. Buxton, C. Greenstock, W. Helman, A. Ross, J. Phys. Chem. Ref. Data **17,** 513-886 (1998)

106 T. Ohmi, T. Isagawa, M. Kogure and T. Imaoka, J. Electrochem. Soc. **140,** 804 (1993)

107 T. Hattori, T. Osaka, A. Okamoto, K. Saga and H. Kuniyasu, J. Electrochem. Soc**. 145,** 3278 (1998)

108 M. Heyns, P. Mertens, T.Bearda, S. Mertens, I. Cornelissen, M. Meuris, S. Degendt, M. Schaekens, K. Wolke, IBM J. Res. Dev. **43,** 339 (1999)

109 I. Kashkoush, R. Matthews and R. Novak, Proceedings of the 5th Internation Symposium on Cleaning Technology in Semiconductor Device Manufacturing, 471 (1997)

110 F. Desmdt, H. Vankerekhoven and C. Vinckier, Ozone Sci. and Eng. **25,** 445 (2003)

111 W, Kleetmeier and V. Graham, Solid State Phen.: Diff. And Def. Data B **65-66,** 143 (1999)

112 J. Jeon, B. Ogle, M. Baeyens, P. Mertens, Solid State Phen.: Diff. And Def. Data B **65-66,** 119 (1999)

113 S. Nelson, Solid State Tech. **42** 107 (1999)

114 H. Vankerckhoven, F. De Smedt, M. Claes, S. De Gendt, M. Heyns, M. Vinckier, Solid State Phen.: Diff. And Def. Data B **92,** 101 (2003)

115 F. De Smedt, H. De Gendt, S. Heyns and H. Vankerckhoven, , Solid State Phen.: Diff. And Def. Data B **92,** 215 (2003)

116 H. Abe, H. Iwamoto, T. Toshima, T, Iino and G. Gale, IEEE Transactions of Semiconductor Manufacturing, **16,** 401 (2003)

117 S. De Gendt, J. Wauters and M. Heyns, Solid State Tech. **41,** 57 (1998)

118 M. Miyamoto, I. Oya, S. Noda and M. Kuzumoto, Solid State Phen.: Diff. And Def. Data B **76-77,** 219 (2001)

119 G. Gale, T. Toshima, N. Shindo, T Iino, S. Kitahara and K. Taguchi, Solid State Phen.: Diff. And Def. Data B **92,** 227 (2003)

120 *XPS Users Handbook*, Physical Electronics Inc. (1994)

121 H. Tompkins and W. McGahan, *Spectroscopic Ellipsometry and Reflectometry: A User's Guide*, John Wiley & Sons: New York, 1999

122 Ellipsometry Cauchy model

123 D. Harris, *Quantitative Chemical Analysis 5th ed.,* W. H. Freeman and Company: New York, 1998

124 ChemOffice v. 8.0 software, produced by CambridgeSoft

125 PCI Ozone Control Systems manual for Model G-2 (1980)

126 N. Mackie, N. Dalleska, D. Castner and E. Fisher, Chem. Mater. **9**, 349 (1997)

127 E. Hagen, Plaste und Kautschuk **14**, 565 (1967)

128 Rice and Netzer, *Handbook of Ozone Technology and Applications* Vol 1, Ann Arbor, Science Publishers, 1982.

129 K. Ha, S. McClain, S. Suib, A. Garton, J. Adhesion. **33**, 169 (1991)

130 S. Middleman, *An Introduction to Heat and Mass Transfer*, John Wiley & Sons: New York (1997)

131 Plasma deposited films of pentafluoroethane deposited in our lab

132 Online data: http://www.diffusion-polymers.com

133 K. Gustafson and R. Dickhut, J. Chem. Eng. Data, **39**, 281 (1994)

134 Y. Yamamoto, S. Nishida, X. Ma and K. Hayashi, J. Phys. Chem. **90,** 1921 (1986)

135 J. Dubois, A. Monvernay and P. Lacaze, Electrochimica Acta, **15**, 315 (1970)

136 N. Connelly and W. Geiger, Chem. Rev. **96**, 877 (1996)

137 A. Bard and L. Faulkner, *Electrochemical Methods: Fundamentals and Applications 2nd ed.,* John Wiley & Sons: New York 2000

138 J. Dubois, A. Monvernay and P. Lacaze, Electrochimica Acta **15,** 315 (1970)

139 A. Bard and L Faulkner, *Electrochemical Methods: Fundamentals and Applications:* Wiley: New York 2000

140 B. Jensen and V. Parker, J. Amer. Chem. Soc. **97,** 5211 (1975)

141 S. Shurmer, T. Christensen, T. Thomasen and K. Daasbjerg, J. Electroanal. Chem., **454,** 123 (1998)

142 S. Bank and B. Bockrath, J. Amer. Chem. Soc, **93**, 430 (1971)

143 S. Bank and B. Bockrath, J. Amer. Chem. Soc, **94**, 6076 (1972)

144 Posistrip® EKC830™ is a commercial photoresist remover from EKC technology that consists primarily of NMP

145 I. Smallwood, *Handbook of Organic Solvents Properties*, Halsted Press: New York 1996

146 Dippr physical property database, American Institute for Chemical Engineers

147 D. Owens and R. Wendt, J. Appl. Polym. Sci. **13,** 1741 (1969)

148 C. Rulison, Augustine Scientific Inc, Ohio, Application Note 401 and 403

149 F. Fowlkes, Industrial and Eng. Chem. **56** 12 (1964)

150 R. Good and L. Girifalco, J. Phys. Chem. **64**, 561 (1960)

151 S. Myneni, 'Fluorocarbon residue removal using CO2-based fluids,' Thesis, Georgia Tech 2004

152 Sigma-Aldrich online MSDS database, www.sigmaaldrich.com

153 Experiments performed in lab: spin coating commercial resists on PTFE and Teflon AF™ surfaces